ABSTRACT

Title of Dissertation: CARDIAC MITOCHONDRIAL FUNCTION AND EXERTIONAL TOLERANCE IN A RAT MODEL OF PRESSURE-OVERLOAD INDUCED HEART FAILURE

Harry Zichen Li, Doctor of Philosophy, 2022

Dissertation directed by: Assistant Professor Sarah Kuzmiak-Glancy, Department of Kinesiology

Heart failure (HF) is characterized by the inability of the heart to provide adequate cardiac output to meet their body's demand for fuel and oxygen, particularly during periods of exertion. In fact, a hallmark characteristic of HF is exertional intolerance where performing activities brings about, or exacerbates, symptoms of dyspnea and/or fatigue. This exercise intolerance has been attributed to altered cardiac and skeletal muscle function.

The myocardium of the heart is reliant upon cardiac mitochondria to generate sufficient ATP to fuel this highly metabolically active tissue. Therefore, reduced mitochondrial ATP production may play a role in myocardial dysfunction and contribute to reduced cardiac output in HF. Mitochondria react to intracellular signals to respond to energetic demands, and therefore, mitochondrial function is a product of both the mitochondria itself and the environment in which it resides. Intracellular Ca^{2+} and Na^{+} are of particular interest as they play a role in regulating mitochondrial function and the intracellular concentrations are elevated in ventricular myocytes

in HF. Therefore, a goal of these investigations was to evaluate how altered Na^+ and Ca^{2+} can impact the ability of cardiac mitochondria to respond to an increase in demand in mitochondria isolated from young healthy rat hearts, as well as rats with pressure-overload induced HF. A second goal of these investigations was to determine if pressure-overload induced heart failure altered exercise capacity, as well as *in vivo* and *ex vivo* skeletal muscle strength.

In the first study, mitochondria were isolated from the ventricular tissue of young, healthy male rats, and oxygen consumption and mitochondrial activation by Ca^{2+} was assessed in the presence of elevated Na^+ to mimic the cellular environment of HF. Ca^{2+} effectively activated mitochondrial ATP production, despite elevated Na^+, suggesting that the ionic conditions of HF ventricular myocytes alone are not sufficient to disrupt mitochondrial function. In the second study, mitochondrial function was assessed under the same ionic conditions as the previous study, however, mitochondria were isolated from male rats with pressure-overload induced hypertrophy or sham-operated controls. Ca^{2+} was able to activate mitochondrial function regardless of Na^+ concentration in both HF and sham mitochondria; however, failing mitochondria exhibited depolarized mitochondrial membrane values across these respiration rates, implicating an impaired potential for ATP production in failing ventricular mitochondria. In the third study, HF and sham male and female rats were evaluated for their exertional tolerance, and the results indicated that HF rats tolerated treadmill running and showed no deficits in grip exercise; however, solei muscle from female heart failure rats exhibited diminished contractile capacity, suggesting female skeletal muscle may respond differently than male skeletal muscle to heart failure. These findings indicate that failing mitochondria may be intrinsically dysfunctional regardless of an altered ionic environment and that there may be sexual dimorphism in the skeletal muscle function and its role in exercise intolerance in HF.

CARDIC MITOCHONDRIAL FUNCTION AND EXERTIONAL TOLERANCE IN A RAT MODEL OF PRESSURE-OVERLOAD INDUCED HEART FAILURE

by

Harry Zichen Li

Dissertation submitted to the Faculty of the Graduate School of the
University of Maryland, College Park, in partial fulfillment
of the requirements for the degree of
Doctor of Philosophy
2022

Advisory Committee:
Assistant Professor Sarah Kuzmiak-Glancy, Chair
Professor James M. Hagberg
Professor Steven J. Prior
Assistant Professor Sushant Ranadive
Professor Byung-Eun Kim

Dedications

This dissertation is dedicated to my wife, Dr. Keziah C. Morrison, who has been a constant source of love, support, and encouragement during the challenges of graduate school and life. Thank you for being the best partner in my life. This work is also dedicated to my parents, Marilyn and Lumin, and my sister, Lisa, who have always loved me unconditionally and offered support at every turn. Lastly, I would like to dedicate this dissertation to my late grandfathers, Hanying Zhang and Zhenkui Li. Their stories of strength and determination during a time of tremendous change and uncertainty were humbling and awe-inspiring.

Acknowledgements

I have been so fortunate to be surrounded by an academically passionate community that has supported me during my graduate career. There are many who have helped me during my time here at the University of Maryland.

I would like to thank the members of the Department of Laboratory Animal Resources for the care and attention they provided to the well-being of the animals used in this dissertation.

I am grateful to Jackson Durbin, Sigmund Tejada, and Chris Dagdag, for their contributions to our research and for their friendships.

I deeply appreciate the camaraderie and support of my fellow graduate students. I would like to especially thank Yuan Liu for being a great partner in the laboratory, for helping me when I was indisposed, and for being so humble about Alabama football.

To all the distinguished professors that have helped me to this point, I am truly thankful for their tremendous wisdom and counsel, both academically and personally.

Lastly, I could not have undertaken this journey without my advisor, Dr. Sarah Kuzmiak-Glancy, and her unwavering support, guidance, and mentorship. This endeavor would not have been possible without her tutelage, in the laboratory, classroom, and life. She has my utmost respect and admiration.

Table of Contents

This Table of Contents is automatically generated by MS Word, linked to the Heading formats used within the Chapter text.

List of Tables

List of Figures

List of Illustrations

List of Abbreviations

ACE – angiotensin-converting enzyme

AF – atrial fibrillation

ANT – adenine nucleotide translocase

ARB – angiotensin II receptor blockers

BNP – B-type natriuretic peptide

BSA – bovine serum albumin

Ca^{2+} – Calcium

CK – creatine kinase

CKD – chronic kidney disease

CS – citrate synthase

D – distance

DH – dehydrogenase enzyme

ECG – electrocardiogram

EDL – extensor digitorum longus

EDV – end diastolic volume

EF – ejection fraction

ESV – end systolic volume

ETC – electron transport chain

F – force

G – glutamate

HF – heart failure

HFpEF – heart failure with preserved ejection fraction

HFrEF – heart failure with reduced ejection fraction

IACUC – Institutional Animal Care and Use Committee

J_O – oxygen consumption

L – conductance

LA – left atrium

LV – left ventricle

LVEF – left ventricular ejection fraction

M – malate

MCU – mitochondrial calcium uniporter

mi-CK – mitochondrial creatine kinase

MRA – mineralocorticoid receptor antagonists

MRI – magnetic resonance imaging

MRS – magnetic resonance spectroscopy

Na^+ – sodium

NCE – sarcolemmal Na^+/Ca^{2+} exchanger

NCX_m – mitochondrial sodium calcium exchanger

NHE – sarcolemmal Na^+/H^+ exchanger

NHX – mitochondrial Na^+/H^+ exchanger

NT-proBNP – N-terminal-pro hormone B-type natriuretic peptide

PCR – phosphocreatine

RM – respiration media

ROS – reactive oxygen species

RV – right ventricle

RyR – ryanodine receptor

SD – Sprague-Dawley

SERCA – sarcoplasmic/endoplasmic reticulum calcium ATPase

SGLT2 – sodium-glucose co-transporter 2

SR – sarcoplasmic reticulum

TAC – transverse aortic constriction

TCA – tricarboxylic acid

TnI – cardiac troponin I

TnT – cardiac troponin T

W – work

ΔG – Gibbs free energy

ΔG_{ATP} – Gibbs free energy of ATP

ΔG_{redox} – Gibbs free energy of redox potential

$\Delta G_{\Delta\Psi}$ – Gibbs free energy of membrane potential

$\Delta\Psi$ – membrane potential

Chapter 1: Review of Literature

1.1 Heart Failure

1.1.1 Significance & Overview

Heart failure (HF) affects approximately 6 million people in US and at least 26 million people worldwide, and the prevalence is expected to increase by 46% over the next decade[1]. Half of patients with heart failure die within 5 years of diagnosis[2,3].

Heart failure is a remarkably complex clinical syndrome characterized by dyspnea and fatigue that are often due to cardiac dysfunction. In individuals with HF, the heart is unable to provide adequate blood to the body to meet the demands. HF has a diverse etiology, with left ventricular (LV) dysfunction, right ventricular (RV) dysfunction, valve disease, or pericardial disease[4] as common precursors, however, the mechanism and differential development remains largely a mystery.

When the heart contracts, oxygenated blood is pumped out of the left ventricle and distributed to the tissues of the body via the vasculature. When the heart relaxes, the left ventricle fills with oxygenated blood to be pumped out during the next contraction. The percentage of the blood in the ventricle that is ejected per beat is known as left ventricular ejection fraction (LVEF) and is usually between 50-75% in healthy individuals. Traditionally, HF has been associated with a reduced LVEF; in other words, a lower percentage of blood from the ventricular chamber leaves per contraction, and is classified as heart failure with reduced ejection fraction (HFrEF). Current treatments for HFrEF aim pharmacological treatments to reduce blood volume

and blood pressure (ACE inhibitors, β-blockers, and diuretics), as well as the use of inotropic agents in order to increase myocardial contractility and improve LVEF.

A second classification of HF is heart failure with preserved ejection fraction, or HFpEF. Individuals with HFpEF do not demonstrate a reduced LVEF upon echocardiographic assessment, however they do manifest the clinical presentations of HF. Interestingly, many patients with HFpEF demonstrate normal stroke volume (SV) at rest but exhibit a blunted rise in SV with exertion. Importantly, reduced LVEF is not the cause of symptoms in individuals with HFpEF, and there are currently no pharmacological treatments that improve outcomes or prognosis in HFpEF[5,6].

1.1.2 Clinical Presentations of Heart Failure

Patients with HF often have physical manifestations related to excessive fluid accumulation and inadequate hemodynamic supply. Symptoms related to fluid accumulation include dyspnea, orthopnea, edema, hepatic congestion pain, and abdominal distention[4]. Insufficient cardiac output has been thought to be related to fatigue and weakness, which can be exacerbated with exertion. Both categories of symptoms, however, are related to each other[4]. The inadequate cardiac output lends to fluid retention issues, which is often mediated, at least in part, by changes in renal function. More specifically, there may be greater activation of the renin-angiotensin-aldosterone axis lending to greater sodium retention and a greater sympathetic nervous system activation. Because deficits in hemodynamic supply appear to have their own physical manifestations and influence those related to fluid accumulation, the heart has traditionally been the target for investigation and therapeutic intervention.

1.1.3 Clinical Diagnosis of Heart Failure and Classification

There is no single test to diagnose HF. A patient's history, physical examination, laboratory data, and imaging data are used collectively to make the diagnosis of HF. The recommended blood tests for identifying HF include B-natriuretic peptide (BNP) levels, cardiac troponin T (TnT) or I (TnI) levels, complete blood count, serum electrolyte levels, blood urea nitrogen, creatinine, liver function, and fasting blood glucose. BNP levels are frequently elevated in patients with HFrEF but may be normal in many patients with HFpEF. Therefore, an elevated BNP would strongly suggest the presence of HF, but a normal level does not exclude it. Elevated TnT and/or TnI represent markers of myocardial injury and would help indicate the severity of the HF in the patient. The current method of HF diagnosis can be complex and is dependent on the aggregation of several clinical results.

Once a HF diagnosis has been made, the disease can then be classified into one of three categories in accordance with LV ejection fraction (LVEF). As described above, LVEF is the proportion of blood that leaves the LV chamber per contraction. More specifically, it is the quotient of stroke volume (SV) and end-diastolic volume (EDV). When LVEF is <40% in patients with HF, these individuals are classified as having HF with reduced ejection fraction (HFrEF). HF with LVEF between 41 and 49% is HF with mid-range ejection fraction (HFmrEF). Lastly, HF with LVEF >50% is known as HF with preserved ejection fraction (HFpEF). While these are the current categories for HF, these classifications will probably stratify further as more is discovered about the disease in the future.

1.2 Heart Failure with Preserved Ejection Fraction

1.2.1 Prevalence & Demographics

The number of patients being diagnosed with HFpEF is increasing in number[7,8]. The Framingham Heart Study and the Cardiovascular Health Study reported that the incidence of HFrEF has decreased over two decades and the incidence of HFpEF increased by 45% over the same period[9]. HFpEF is now the dominant form of HF among older adults in the United States, representing 65 to 77% of prevalent cases according to the Atherosclerosis Risk in Communities (ARIC) study[10]. HFpEF was thought to be a disease of aging, but many patients of HFpEF are under 65 years old[11]. When adjusted for age and other risk factors, the prevalence with HFpEF is similar between men and women in many community-based studies[12–16]. However, women have a greater prevalence of HFpEF than men in general, and in a report of at least 100,000 hospitalizations, patients with HFpEF were more likely to be older, female, hypertensive, and less likely to have a prior acute cardiac event and in-hospital mortality[17].

Many comorbidities and risk factors are shared between HFpEF and HFrEF, such a hypertension, diabetes, and kidney disease. Hypertension carries the highest risk for the development of HF in the general population[18,19] and more than doubles the probability of developing HFpEF than with HFrEF[20]. Similarly, patients with HFpEF have hypertension as the most common cardiovascular risk factor, at a prevalence of 55-85%[21].

Because HFpEF is generally regarded as a disease of age, it is believed that this sex disparity may be due to greater longevity and lower mortality in women with HFpEF. This allows females more time to develop the HFpEF condition as well as lower the available comparisons due to survivability[22]. In contrast, most patients with HFrEF are male, possibly due to the greater prevalence of coronary disease among men[17]. The sex disparity suggests the development of HFpEF may be different between males and females and may require different therapeutic interventions.

1.2.2 Signs & Symptoms

The symptoms of HFpEF are generally indistinguishable from other forms of HF[23–25]. Patients with clinically diagnosed HFpEF have or had at least one symptom of HF. Dyspnea and fatigue are the most common symptoms of HFpEF[26]. Hypertension is a common condition found alongside HFpEF that increases LV wall stress, which can impede proper ventricular relaxation thereby elevating pulmonary venous pressures[27]. As a result, patients with HFpEF may have associated physical signs of HF such as jugular vein distention, respiratory rattling, and edema of the legs. Additionally, many patients with HFpEF exhibit chest pain on or during exertion[28,29].

A critical characteristic of HFpEF, and other forms of HF, is exertional intolerance. Patients with HFpEF have difficulty tolerating exertion or exercise but the mechanisms behind this intolerance are not fully understood. Physical activity is one of the most common stresses encountered by these patients because it requires an increase in cardiac output to meet the increasing demands of the body[30]. Patients with HFpEF participating in physical activity are unable to tolerate an increase in venous return, afterload, and tachycardia and further experience greater left atrial (LA) and

pulmonary venous pressures[31,32]. As a result, patients exhibit dyspnea, reduced aerobic capacity, and increased risk of death[33–35].

1.2.3 Tests & Evaluation

Initial evaluation of patients suspected with HF commonly include a chest radiograph and electrocardiogram (ECG). The chest radiograph is used to identify pulmonary edema and potential causes of dyspnea as well as signs of an enlarged heart. Unfortunately, patients with HFpEF often have a normal chest radiograph[36]. Results of the ECG often can be nonspecific but have the capacity to identify myocardial ischemia or previous infarction. More importantly, an ECG can be used to identify atrial fibrillation (AF), which is strongly indicative of HFpEF if the patient demonstrates normal LVEF and dyspnea[37].

Echocardiography and serum natriuretic peptide levels are also used to help diagnose suspected HFpEF. Echocardiography can evaluate if the LVEF is preserved and LV volume is normal. It can also identify issues to exclude the diagnosis of HFpEF, such as valvular and pericardial diseases. Doppler measurements during echocardiography can also provide estimates of LV diastolic filling pressure[38,39]. Serum measures of natriuretic peptides of BNP or NT-proBNP can be used to help diagnose HFpEF but are generally more useful for prognosis[40,41]. While normal levels of natriuretic peptides does not exclude HFpEF, elevated levels provide more evidence for the presence of HFpEF[37] and can be used to predict adverse cardiovascular event in patients with HFpEF[42].

1.3 Treatment of HFpEF

1.3.1 General Management

The current goals of treatment for patients with HFpEF are to increase patient function, reduce HF symptoms, and decrease risk for hospitalization. After being diagnosed with HFpEF, routine evaluation is recommended to monitor changes in symptoms, blood pressure measurements, conditions of comorbidities, and medication tolerance[43]. Adoption of lifestyle changes such as participation in exercise programs, cardiac rehabilitation, and dietary interventions are generally safe and can result in small improvements in exertional tolerance and functional status[43]. However, there are no therapies at present that have been proven to consistently reduce the risk of mortality in patients with HFpEF[5,6].

1.3.2 Management of Comorbidities

Hypertension is thought to be one of the main contributors to the development of HFpEF, so pharmacological therapies targeting hypertension have been at the forefront of HFpEF treatment. The choice of antihypertensive medication depends on the kinds of comorbid conditions and the severity of the hypertension present in the patient. Diuretics and mineralocorticoid receptor antagonists (MRAs) are generally used to initially treat hypertension and if there are no other compelling treatments for specific comorbid conditions present[44,45]. Importantly, MRAs appear to improve quality of life and reduce rates of hospitalization in patients with HFpEF[45–47]. The primary goals of these antihypertensive drugs are to reduce the symptoms of HF and hospitalization while preventing hypotensive reactions.

Diabetes and chronic kidney disease (CKD) are comorbidities that complicate the treatment of HFpEF. Sodium-glucose co-transporter 2 (SGLT2) inhibitors have been recommended when type 2 diabetes and/or CKD are present. Like MRAs, SGLT2 inhibitors have demonstrated improvements in quality of life and reduced hospitalization[48–50]. Unfortunately, neither SGLT2 inhibitors nor MRAs reduce the rate of mortality in patients with HFpEF[46–50]. When SGLT2 and MRAs are contraindicated for a patient, then angiotensin-converting enzyme (ACE) inhibitors and angiotensin II receptor blockers (ARB) are often used. Unfortunately, these medications do not appear to reduce hospitalization or mortality in patients with HFpEF[51–53].

Several other pharmacological agents used to treat cardiac conditions associated with HF have generally been ineffective. Beta blockers are used to control heart rate in AF and to treat hypertension but do not appear to reduce mortality rates[54]. Likewise, digoxin, which is used in the management of AF, does not appear to lower rates of hospitalization nor mortality[55]. Phosphodiesterase-5 inhibitors and nitrates have been investigated as potential pharmacological agents to improve hemodynamic responses with exertion; however, neither appear to improve exercise tolerance[56,57] and may even reduce physical activity levels[58]. Overall, there does not appear to be a pharmacological therapy that is effective at lowering the mortality burden in the population with HFpEF.

1.3.3 Prognosis

Morbidity is similar between patients with HFpEF compared to patients with HFrEF; however, it is unclear if mortality is similar between patients with HFpEF or HFrEF given that there are no effective therapies for the former. The rate and frequency

of hospitalizations, symptomatic status, 6-minute walking distance, and quality-of-life measures are similar between HFrEF and HFpEF[17,59–62]. Data from hospitalized patients suggest that mortality rates are similar between patients of HFpEF and HFrEF[60,63]. Conversely, meta-analysis of community-based studies and trials seem to indicate that mortality is lower in patients with HFpEF compared to HFrEF[64]. The cause of death, whether cardiovascular or non-cardiovascular, for patients with HFpEF is varied. In population[65] and community-based[66] studies, the rate of non-cardiovascular deaths is greater perhaps due to greater frailty and complications from comorbidities. However, in the I-Preserve trial, mortality in patients with HFpEF was twice as likely to be due to cardiovascular reasons than non-cardiovascular[67]. Overall, HFpEF may present as a less severe form of HF compared to HFrEF; however, the lack of effective therapies for HFpEF may make this a more problematic form of HF.

1.4 Pathophysiology of HFpEF

1.4.1 Abnormal Cardiovascular Structure & Function

HFpEF is often associated with structural remodeling that adversely affects the myocardium and connective tissue. A common characteristic of HFpEF is concentric left ventricular hypertrophy, a thickening of the LV wall with a reduction in LV chamber volume, which is thought be a result of elevated afterload and hormones (e.g. aldosterone, angiotensin II, and/or catecholamines)[68,69]. Adverse cardiac remodeling may lend itself to diastolic dysfunction such that the heart is unable to fill properly[70], which is often believed to be the main contributor to reduced stroke volume and cardiac output in patients with HFpEF during periods of elevated activity.

HFpEF exhibits very different structural alterations than in HFrEF. Patients with HFpEF often exhibit concentric LV hypertrophy with normal end diastolic volume (EDV) at rest and increased wall thickness[71–78]. Conversely, patients with HFrEF most frequently exhibit eccentric LV remodeling with an increase in EDV and little to no increase wall thickness[76]. These differences at the organ level correspond to the differences seen at the cellular level. Cardiomyocytes from HFpEF demonstrate greater diameter with no change in length, paralleling the increase in LV wall thickness with the lack of change in LV chamber volume. Conversely, cardiomyocytes from HFrEF exhibit greater length with no change in diameter, paralleling the increase in LV chamber volume with no change in LV wall thickness[76]. Both HFpEF and HFrEF demonstrate stark differences in the development of their structural abnormalities, yet both still exhibit inadequate cardiac output during elevated workloads.

Collagen deposition and development of myocardial fibrosis may contribute to myocardial stiffness[79,80], a contributing component of diastolic dysfunction in HFpEF. Patients with HFpEF can exhibit slightly more fibrosis compared to age-matched healthy counterparts; however, many patients may not present with any fibrosis[81]. Conversely, patients with HFrEF may demonstrate degradation of collagen during early stages of HFrEF that can change into an overall increase in collagen deposition and fibrosis development during late stage HFrEF[73,75,76]. Although collagen deposition and fibrosis may contribute to diastolic dysfunction in HFpEF, they do not appear to be a requirement.

Several abnormalities in diastolic function can occur in HFpEF. These can include impairments to myocardial relaxation, impaired LV filling, greater LV filling from atrial contraction, increased passive stiffness of the LV, reduced LV relaxation capacity during exercise, and greater diastolic chamber and pulmonary venous pressures at rest and during exercise[72,74,76,82–84]. Any one of these symptoms would result in reduced capacity for the LV to stretch appropriately and elevate diastolic pressure. Furthermore, these would result in lower LV filling rate and volume, shifting the burden of ventricular filling towards atrial contraction. Due to the increased importance of the atrial contraction, patients with HFpEF are more sensitive to tachycardia and alterations in atrial pacing. An increase in heart rate, such as during exercise, shortens the diastole period and restricts diastolic filling in patients with HFpEF[32,85–88]. In healthy individuals during exercise, increased heart rate and cardiac output require faster LV filling, which is accomplished by faster LV relaxation and lowering the LV diastolic pressure to create a greater LA-LV pressure gradient[32]. Patients with HFpEF or diastolic dysfunction in general have an impaired LV relaxation, which reduces LV filling, and greater dependence on LA pressure, which increases the risk for pulmonary congestion during exertion or exercise[89].

1.4.2 Skeletal Muscle Abnormalities

Although exertional intolerance in individuals with HFpEF has been well documented[90–94], it is still largely unknown whether central or peripheral factors play a greater role in this problem. Recently, it has been discovered that cardiac function does not correlate well with the development of exercise intolerance in patients with HFpEF[90,95]. Conversely, skeletal muscle dysfunction has shown a greater association

with exercise intolerance compared to diastolic dysfunction.[45,95–99], but the specific mechanism is still unknown. Therefore, interventions targeting skeletal muscle may have a greater impact on combating exertional intolerance in patients with HFpEF.

Patients with HFpEF have exhibited skeletal muscle changes that may impact their ability to tolerate exertion. Magnetic resonance imaging (MRI) of thighs in patients with HFpEF demonstrated that skeletal muscle and fat composition may have an association with exercise intolerance[100]. More specifically, patients with HFpEF exhibited lower skeletal muscle/thigh compartment ratio and higher intermuscular fat/skeletal muscle ratio compared to healthy controls[100]. These results suggest an occurrence of muscular atrophy as well as an increased fat deposition potentially associated with adipose-related dysfunction. Moreover, biopsy samples from patients with HFpEF demonstrate greater number of Type II fibers and less Type I fibers compared to controls suggesting greater fatigability in the disease[98]. Capillary density was also lower in biopsy samples from patients with HFpEF than controls suggesting diminished skeletal muscle perfusion[98]. Functionally, patients with HFpEF had lower VO_2 peak, peak workload, and 6-minute walking distance compared to controls[98,100]. Altogether, abnormal skeletal muscle composition and adiposity may be involved with the exertional intolerance seen in HFpEF.

Several skeletal muscle alterations have been reported in rat models of HFpEF. Skeletal muscle extracted from aortic-banded rats have demonstrated lower muscle mass, slow twitch fiber proportion, and capillary density compared to sham controls[101]. Solei of salt-sensitive Dahl rats, a hypertension-based model of HF, have exhibited greater fatigability and greater slow-twitch fiber atrophy than controls[102].

Similarly, solei and extensor digitorum longus (EDL) extracted from the ZSF1 obese rat, a hypertension and obesity-based model of HF, was reported to have greater fiber atrophy, lower capillary density, and lower force production than controls[103]. These findings suggest that HF can elicit histological changes in skeletal muscle that could contribute to muscle weakness implicated in the exertional intolerance characterizing the disease or that the impairments in skeletal muscle could contribute to the development of HF.

1.4.3 Potential Mechanism Leading to the Development of HFpEF

It is not entirely clear what the specific mechanisms are that lead to cardiac, vascular, and peripheral dysfunction seen in HFpEF; however, hypertension appears to have a significant impact on the development of this condition. Hypertension carries the greatest risk for the development of HFpEF[18,19,21]. Chronic increase in LV afterload as seen in hypertension may lead to concentric remodeling and hypertrophy that are commonly featured in HFpEF[104]. Arterial hypertension induces vascular remodeling and arterial stiffness[105] further increasing PVR and LV afterload. Importantly, however, antihypertensive medications may prevent the development of HFpEF[106–109] but do not appear to effectively reverse the condition or improve mortality once developed[109]. This suggests that while hypertension is important in the development of HFpEF, it is not the singular mechanism behind this condition.

1.5 Animal Models of HFpEF

A commonly used small animal model for HFpEF is the salt-sensitive Dahl rat[102,110,111]. These animals were selectively bred from Sprague-Dawley rats that were

hypersensitive to Na^+ and exhibited the highest blood pressure[110]. When fed a high sodium diet, these animals develop ventricular hypertrophy, diastolic impairment, pulmonary congestion, and hypertension[102], all of which are symptoms of HFpEF. Additionally, solei of salt-sensitive Dahl rats appear to demonstrate greater fatiguability, slow-twitch fiber atrophy, and lower citrate synthase (CS) activity than controls[102]. However, these rats have not been confirmed to demonstrate a key characteristic of HF, exertional intolerance. When given free access to wheel-running, salt-sensitive Dahl rats ran an average of 10 km/day[111] while Sprague-Dawley rats ran a similar 9 km/day[112]. While the salt-sensitive Dahl rat may not recapitulate the exertional intolerance seen in HFpEF, it may still be a suitable model for a subset population of HFpEF.

Another rat model of HFpEF based on the comorbidities of hypertension and metabolic syndrome, the ZSF1 obese rat, also demonstrates functional and histological deficits. The obese ZSF1 rat exhibits exertional intolerance manifesting as lower VO_2 peak[113,114] and running distance[114] compared to normotensive lean controls. These animals also exhibit greater fiber atrophy, lower capillary density, and lower force production in the soleus and extensor digitorum longus (EDL) than controls[103]. Moreover, cardiomyocytes from ZSF1 obese rats demonstrated slower contractile properties than lean controls[114] further supporting that skeletal muscle alterations may be a contributing factor in exertional intolerance. Lastly, ZSF1 obese rat aortas exhibit lower compliance, impaired vasomotor response, and greater collagen deposition compared to hypertensive and normotensive controls[115] implying that systemic impairments may be complementary to the central dysfunction in HFpEF. While the

ZSF1 obese rat model recapitulates common comorbidities of HFpEF, discoveries from this model may potentially only be generalizable to a particular population of HFpEF.

Transverse aortic constriction (TAC) surgery is a well-established surgical technique for inducing chronic ventricular pressure overload and hypertrophy in rodents[110], and simulates hypertension, which carries the highest risk for the development of HFpEF in humans. Imposing this constriction leads to an increase in afterload pressure that results in the development of concentric left ventricular hypertrophy and diastolic dysfunction[110]. Additionally, these animals develop myocardial fibrosis, and some may develop pulmonary congestion[116], both of which are symptoms of HFpEF. However, to our knowledge, the exertional tolerance of this model has yet to be ascertained. Rats with aortic banding have exhibited skeletal muscle alterations that suggest these animals could experience exertional intolerance. More specifically, extracted skeletal muscle from aortic-banded rats exhibited lower muscle mass, slow twitch fiber proportion, and capillary density compared to sham controls[101]. Although exertional intolerance has not been confirmed in aortic-banded rats, these adverse changes to cardiac and skeletal muscle tissue suggest that this could be a possibility.

1.6 Mitochondrial Function in Heart Failure

1.6.1 Regulation of Mitochondrial Function

The activity of the mitochondrial energy system is modulated by alterations in the relative differences in component forces. More specifically, mitochondrial respiration is primarily dictated by the differences between redox potential, membrane

potential, and the free energy of ATP (ΔG_{ATP}). The mitochondrial system operates through the accumulation of electron donors that transfer their electrons into the ETC to generate a proton gradient. Depletion of this proton gradient via the ATP synthase is used to generate ATP. The accumulation of electron donors represents redox potential and results from the activity of dehydrogenase (DH) enzymes of the tricarboxylic acid (TCA) cycle. This redox potential is used by the ETC to pump protons into the intermembrane space of the mitochondria thereby creating a strong negative membrane potential. Under ideal conditions, protons are allowed to flow back into the mitochondrial matrix through the activity of the ATP synthase, which increases the ΔG_{ATP} (more negative) by binding phosphate to ADP to produce ATP. In skeletal muscle, the ΔG_{ATP} is reduced (less negative) through ATP breakdown that occurs during muscular contraction. This reduction of ΔG_{ATP} acts as a "pulling" force, which provides one way to stimulate oxidative phosphorylation during periods of elevated contractile activity.

However, in cardiac mitochondria from healthy hearts, it has been reported that ΔG_{ATP} fluctuates minimally if at all[117,118] and is generally maintained at a high level[117]. This is likely a result of physiological necessity as the heart is working continuously. The specific mechanism by which oxidative phosphorylation is regulated in the heart in response to changing demands is still unknown. However, because the heart is critically reliant on aerobic metabolism, a tight matching (perhaps beat to beat) of energetic production with energetic demand at the mitochondrial level is likely important for the normal function and survival of the cardiac tissue. In isolated mitochondria, ADP availability strongly promotes respiration, but ADP levels in

cardiac tissue remain relatively stable[117,119]. While ADP may still play an important role in regulation of energetic flux, other signaling factors may also a role in the energetic regulation.

Ca^{2+} has an important role in the contractile function of cardiomyocytes, and the sarcoplasmic reticulum (SR) helps regulate a large pool of Ca^{2+} [120]. Ca^{2+} release from the SR appears to coincide with each beat in healthy hearts[121]. Moreover, Ca^{2+} is also known to be a prominent activator of oxidative phosphorylation in the mitochondria[122,123]. Specifically, it is known to promote the activity and conductance of DHs[124,125], ETC[126], and ATP synthase[127]. The collective increase in these areas of oxidative phosphorylation suggests that cardiac mitochondrial machinery may be extremely efficient at coordinating ATP turnover with the help of Ca^{2+}. This supports the notion that cardiac mitochondria are capable of tightly matching the energetic demands of the heart; however, more work is needed to ascertain the role of Ca^{2+} in energetic flux regulation in failing hearts.

1.6.1.1 Regulation of Intracellular Na^+

Influx of Na^+ into cardiomyocytes can happen through Na^+ channels, sarcolemmal Na^+/H^+ exchanger (NHE), and sarcolemmal Na^+/Ca^{2+} exchangers (NCE). Voltage-gated Na^+ channels are activated during the upstroke of an action potential. During inactivation, Na^+ channels exhibit a persistent inward current. Na^+ entry through these channels is dictated by the frequency of stimulation and the amount of persistent Na^+ current[128]. It has been suggested that the rise in extramitochondrial Na^+ in HF is primarily due to Na^+ influx via persistent Na^+ channels[129].

NHE uses the Na^+ gradient to extrude protons from the cardiac cell and is stimulated when there is a buildup of H^+ ions within the cell[130]. Different agonists can activate NHE through phosphorylation to uptake Na^+ at different pH levels. Prolonged activation of the NHE has been implicated in pathological cellular growth, proliferation, and hypertrophy[128,131] but the specific mechanism is poorly understood. It has been suggested that the NHE may assist in Na^+ influx in HF[132].

The NCE extrudes 1 Ca^{2+} ion for every 3 Na^+ ions by using the Na^+ concentration gradient, which is lesser inside the cell, to extrude Ca^{2+} out of the cardiac cell. Activity of the NCE is dictated by the intracellular concentrations of Na^+ and Ca^{2+} as well as the membrane potential. Na^+ influx is positively and linearly correlated with intracellular Ca^{2+} concentration[133], which is largely dictated by SR Ca^{2+} current. It has been reported that NCE expression and activity are increased in HF[134–136], potentially extruding more Ca^{2+} from the cardiac cell.

Efflux of Na^+ out of the cardiac cell is dictated by the Na^+/K^+ (NK) ATPase. The Na^+/K^+ ATPase uses the breakdown of ATP to exchange 3 intracellular Na^+ for 2 extracellular K^+[137]. It is currently inconclusive as to how the NK ATPase is affected in HF. A graphical overview of the Na^+ and Ca^{2+} transporters can be found in Illustration 1.

1.6.1.2 Regulation of Mitochondrial Na^+ and Ca^{2+}

The main Na^+ efflux pathway is through the mitochondrial Na^+/H^+ exchanger (NHX). During mitochondrial electron transport, protons are extruded out of the matrix, creating a matrix that is more alkaline than the cytosol[138]. In isolated mitochondria, the matrix pH has been reported to be around 7.1 to 7.8 when the

extramitochondrial pH is set to 7.1[139]. Furthermore, the NHX appears to operate close to equilibrium in isolated mitochondria[128,139].

The mitochondrial Na^+/Ca^{2+} exchanger (NCX_m) is the primary mitochondrial influx and efflux pathway for Na^+[128] and Ca^{2+} [140], respectively. The NCX_m is electrogenic and exchanges 3 Na^+ into and 1 Ca^{2+} out of the matrix[141–144]. It has been reported that matrix Na^+ is lower than intracellular Na^+ [128]. Energized mitochondria have a membrane potential ranging from -150 to 180 mV[128], which, when coupled with an inwardly directed Na^+ gradient, provides a large driving force for ejecting Ca^{2+} out and allowing Na^+ into the mitochondrial matrix[128]. Elevating extramitochondrial Na^+, which has been reported to be 3 fold greater in HF[128], results in decreased matrix Ca^{2+} [145], which reduces NADH generation[146]. The NCX_m does not appear to be at equilibrium in energized mitochondria because of the competing actions of the mitochondrial calcium uniporter (MCU). Furthermore, the NCX_m operates relatively slowly in comparison to the MCU[128]. Inhibition of the MCU leads to reduced matrix Ca^{2+} that are like those calculated when NCX_m is at equilibrium[147,148], and inhibition of the NCX_m leads to increased NADH production in response to preserved matrix Ca^{2+} [149]. These findings suggest a regulatory role of the NCX_m with mitochondrial Ca^{2+} and, in turn, its function.

The MCU is the primary Ca^{2+} influx pathway for the mitochondria. The uniporter has been reported to have a low affinity for Ca^{2+}, around 5 to 10 µM[150]. It has also been reported that intracellular Ca^{2+} exists between 100 nM to 1 µM[151] so it was believed that intracellular Ca^{2+} could not rise high enough to activate the MCU. However, it has been discovered that there are microdomains of high Ca^{2+} that exist

near the junction of mitochondria and the SR and these microdomains have concentrations high enough to allow Ca^{2+} influx through the MCU[152]. During an increase in work, there is greater Ca^{2+} entry via the MCU into the mitochondrial matrix to activate dehydrogenases[153], ETC[126], and ATP synthase[127] to increase ATP production. However, it is unclear how and if Ca^{2+} uptake via the MCU is altered and what the specific interplay between the NCX_m and MCU are in HF.

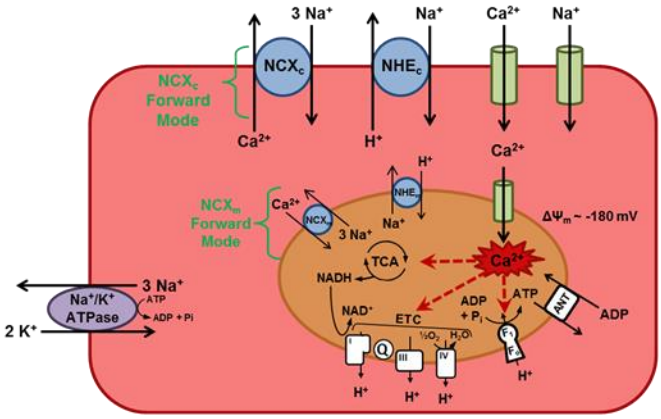

Illustration 1. Overview of sarcolemmal and mitochondrial transporters and the effects of mitochondrial Ca^{2+} uptake. NCX_c and NHE_m is equivalent to NCE and NHX in this dissertation. The mitochondrial Na^+/Ca^{2+} exchanger (NCX_m) and Ca^{2+} uniporter (MCU) are the primary controllers of the matrix Na^+ and Ca^{2+} concentrations. Matrix Ca^{2+} activates TCA cycle enzymes (NADH production) as well as ETC conductance and ATP synthase (NADH utilization). Adapted from Murphy & Eisner (2009).

1.6.2 ROS Production in Hearts

Oxidative stress has been implicated in the development of heart disease, and cardiac mitochondria are thought to contribute to this oxidative stress through the production of reactive oxygen species (ROS)[154]. More specifically, electron leak from the ETC is the largest contributor of ROS production in the heart[155]. The greatest amount of leak occurs when there is a large pool of electron donors and a large

membrane potential resulting in low flux for electrons passing through the ETC[156]. In this situation, the ETC is maximally reduced and endogenous mitochondrial antioxidants exhausted[156,157], and electrons become long-lived thereby increasing the probability that they leave spontaneously with an O_2 molecule from the ETC as ROS[158,159]. This situation occurs when the energetic environment surrounding the mitochondria is high and reduces flux through the oxidative phosphorylation pathway[123]. Sedentary behavior expends less energy and demands less mitochondrial activity resulting in lower flux through the oxidative phosphorylation pathway. As a result of this sedentary behavior and lower flux, electrons are more likely to escape the ETC as ROS and react non-specifically to promote atherosclerotic progression, activate remodeling factors, and reduce antioxidant capacity[160], all of which could potentially contribute to the development of HFpEF .

Conversely, ROS production may be low during periods of elevated physical activity. In this situation, Ca^{2+} signaling and ATP turnover are greater, stimulating the mitochondria to increase energetic flux through the oxidative phosphorylation pathway[123]. Electrons are donated and quickly pass through the ETC in an attempt to maintain the proton gradient, which is used to sustain the ATP pool. Because the electrons are quickly shuttled through the ETC, there is less probability for them to spontaneously leave the ETC as ROS[123,156,161]. Therefore, physical activity leads to greater mitochondrial activity but lower ROS production.

1.6.3 Cardiac Mitochondria in Animal Models of Heart Failure

The ZSF obese rat model of HFpEF exhibits molecular handling alterations that may contribute to cardiac mitochondrial dysfunction. Mitochondrial Ca^{2+}

concentrations in ZSF1 obese cardiomyocytes at baseline, end-diastole, and end-systole were all greater than ZSF1 lean controls[114]. Furthermore, the rise time in mitochondrial Ca^{2+} concentration is longer in the ZSF1 obese cardiomyocyte[114] suggesting slower Ca^{2+} influx possibly due to reduced MCU sensitivity or activity. Lastly, ZSF1 obese cardiomyocyte mitochondria were more prone to Ca^{2+} swelling[114], an indication of mitochondrial stress, than lean controls. Together, these findings suggest there may be impaired Ca^{2+} handling in mitochondria of HFpEF that might contribute to mitochondrial dysfunction.

Elevated Na^+ in HF has been thought to adversely alter mitochondrial bioenergetics by reducing the accumulation of matrix Ca^{2+} through the activity of the mitochondrial Na^+/Ca^{2+} exchanger (NCX_m). Cardiomyocytes taken from aortic constricted guinea pigs demonstrated elevated levels of Na^+ and NADH oxidation[149]. Treatment with mitochondrial NCX_m inhibitor CGP-37157 or lowering intracellular Na^+ concentration prevented NADH oxidation[149]. HF cardiomyocytes from guinea pigs appear to increase ROS production, which may play a role in the pathological development of HF, when Na^+ levels are elevated[162]. Moreover, blocking NCX_m activity appears to prevent ROS production in HF cardiomyocytes from guinea pigs[162]. Taken altogether, the opposing relationship between Na^+ and Ca^{2+} have a great impact on mitochondrial bioenergetics and requires further investigation into their specific role in HFpEF.

1.6.3.1 Potential Role of Na^+ and Ca^{2+} in Heart Failure Mitochondria

Elevated intracellular concentrations of Ca^{2+} and Na^+ have been reported in cardiomyocytes from animal models and patients with HF[128,132], and are thought to

contribute to altered mitochondrial function[132,163,164], ultimately resulting in diminished ATP production. During an increase in contractile activity, intracellular Ca^{2+} concentration rises and results in greater crossbridge cycling. This increase in intracellular Ca^{2+} subsequently stimulates the mitochondrial Ca^{2+} uniporter (MCU) to allow the influx of Ca^{2+} into the mitochondrial matrix. Ca^{2+} is a critical signaling molecule for the matching of ATP demand with production. Increasing mitochondrial matrix Ca^{2+} activates DH enzymes that increase NADH production[165,166], elevate ETC conductance[167], and increase ATP synthase activity[127]. Given that elevated intracellular Na^{+} has been observed in HF, it has been thought to decrease matrix Ca^{2+} by extruding Ca^{2+} from the mitochondrial matrix through the Na^{+}/Ca^{2+} exchanger (NCX_m)[128,168], thereby diminishing activation of ATP production. Indeed, in the absence of extramitochondrial Ca^{2+}, increasing extramitochondrial Na^{+} is capable of decreasing matrix Ca^{2+} and maximal respiration in isolated ventricular mitochondria[134]. Moreover, in the presence of elevated intracellular Na^{+}, mitochondrial Ca^{2+} uptake has been reported to be diminished in isolated cardiomyocytes resulting in a reduction of available NADH with workload demand[169] and ROS formation been reported to be increased in both healthy and failing cardiomyocytes[162]. However, intracellular Ca^{2+} is also reportedly elevated in HF[128] and would, in theory, stimulate Ca^{2+} influx into the mitochondrial matrix and activate the ATP production pathway. Therefore, the interplay of elevated Na^{+} and Ca^{2+} in HF is not well understood and warrants further investigation.

1.6.4 Skeletal Muscle Mitochondria in HFpEF

Aortic-banded rats may have adverse mitochondrial changes in the skeletal muscle. Myofibers from aortic-banded rats demonstrated lower mitochondrial respiration[101] and Complex IV activity[170] suggesting impairments in oxidative activity. Citrate synthase (CS) activity, mitochondrial creatine kinase (mi-CK) content, and mi-CK activity were lower than in control, suggesting less mitochondrial content in HF[101,170]. Moreover, expression of factors for mitochondrial transcription and biogenesis were less in aortic-banded rats than sham[170], further suggesting impaired mitochondrial potential in skeletal muscle of HF.

Reduced reliance on aerobic metabolism may be related to mitochondrial alterations. Patients with HFpEF undergoing exercise tests demonstrated lower VO_2 peak and walking distance compared to healthy controls[171]. Muscle biopsies from the quadriceps of these same patients demonstrated that expression of porins, outer mitochondrial membrane proteins, and mitofusin-2, regulatory protein for mitochondrial fusion, were lower in patients with HFpEF than healthy individuals. Furthermore, CS activity was lower in HFpEF samples than controls[171]. Together, skeletal muscle mitochondria in patients with HFpEF may be lower in quality and quantity, which may be contributing to the deficits in exercise capability. An investigation into the quadriceps of patients with HFpEF performing static exercise using magnetic resonance spectroscopy revealed that the muscle of these patients reached a similar metabolic state earlier and at a lower workload than controls[95] suggesting a reduced ability to cope with metabolic demand. Additionally, phosphocreatine recovery time was longer in patients with HFpEF than controls[95]

suggesting diminished oxidative capabilities. Altogether, oxidative capacity may be compromised in skeletal muscle and may mediate, in part, the faster onset of muscular fatigue in patients with HFpEF.

Chapter 2: Calcium Activation of Isolated Mitochondria from Rat Hearts is Preserved Despite Heart Failure Levels of Extramitochondrial Sodium

2.1 Introduction

Heart failure (HF) is characterized by the inability of the heart to provide adequate cardiac output to meet their body's demand for fuel and oxygen. The myocardium of the heart is reliant upon cardiac mitochondria to generate sufficient ATP to fuel this highly metabolically active tissue[172]. Hence, it is thought that insufficient mitochondrial ATP production may play a role in myocardial dysfunction and contribute to reduced cardiac output in HF. A variety of mitochondrial defects have been described in both human[128,173–175] and experimental models[132,170,176,177] of HF, suggesting mitochondrial function may be adversely altered and contribute to the cardiac dysfunction in HF[178].

A hallmark characteristic of HF is exertional intolerance where performing activities brings about, or exacerbates, symptoms of dyspnea and/or fatigue. Exertional intolerance is associated with lower quality of life and increased mortality[179]. Compromised cardiac output during physical exertion, manifesting as reduced cardiac reserve, has been considered a key limitation in individuals with HF[180] and implicated in exertional intolerance. If cardiac mitochondria are unable to increase their rate of ATP production to match the demand, this may, at least in part, explain reduced cardiac

reserve in individuals with HF. Therefore, an examination of how mitochondrial function is altered across a range of demands in HF is critical.

Mitochondria reside inside ventricular myocytes and utilize oxygen in the process of synthesizing ATP. Mitochondria respond to intracellular signals, and therefore, mitochondrial function is a product of both the mitochondria itself and the environment in which it resides. Indeed, molecular alterations occurring within the ventricular myocytes in HF may shed light on the cause of functional deficits occurring in this disease. Ca^{2+} and Na^{+} are of particular interest as they play a role in activating mitochondrial respiration and are altered in HF[128,162,181].

Ca^{2+} is a critical signaling molecule for the matching of energetic production with demand within cardiac tissue. During an increase in cardiac work, Ca^{2+} influx into the cardiomyocyte facilitates the sarcoplasmic reticulum (SR) to release Ca^{2+}, collectively raising cytosolic Ca^{2+} concentration. Elevated cytosolic Ca^{2+} not only allows for crossbridge cycling and myocardial contraction, but it leads to mitochondrial Ca^{2+} influx through the mitochondrial uniporter (MCU), which increases mitochondrial matrix Ca^{2+} and activates dehydrogenase enzymes[153] to increase NADH production[165,166]. Furthermore, increasing mitochondrial matrix Ca^{2+} promotes electron transport chain (ETC) conductance[167] and ATP synthase activity[127,165]. Therefore, the Ca^{2+} influx into the mitochondrial matrix during elevated cardiac activity helps match ATP production in the mitochondria with ATP utilization in the ventricular myocytes[127,157,182].

Mitochondrial Ca^{2+} efflux primarily occurs via the Na^{+}/Ca^{2+} exchanger (NCX_m)[128,149,168,169], which exchanges intracellular Na^{+} with matrix Ca^{2+} to lower the

mitochondrial Ca^{2+} concentration. Intriguingly, it has been reported that the rate of Ca^{2+} efflux via the NCX_m occurs much more slowly than Ca^{2+} influx via the MCU[183–185]. Further complicating the interplay between these two transporters is the fact that the activities of both transporters are linked to the mitochondrial membrane potential: Ca^{2+} influx via MCU is driven by the mitochondrial membrane potential[186,187] and Ca^{2+} efflux via the NCX_m is inhibited by mitochondrial depolarization[188,189].

Elevated intracellular Na^+ in ventricular myocytes has been reported in HF[128] and has been implicated in altered myocardial function[132,190–192] and disrupted energetics. It has been suggested elevated intracellular Na^+ could decrease mitochondrial matrix Ca^{2+} concentration and blunt the Ca^{2+}-mediated stimulation of oxidative phosphorylation and ATP production. Many investigation have demonstrated that elevating extramitochondrial Na^+ concentration reduces matrix Ca^{2+} and maximal respiration in isolated mitochondria, particularly in the absence of extramitochondrial Ca^{2+}[134,193–195]. However, as mentioned above, experimental data suggest the NCX_m operates approximately ten times slower than the Ca^{2+} influx pathway of the MCU[184,185]. Moreover, elevated extramitochondrial Ca^{2+} drives Ca^{2+} influx via the MCU. An increase in matrix Ca^{2+} promotes a large negative membrane potential, thereby further increasing Ca^{2+} influx[186]. Lastly, diastolic Ca^{2+} has also been reported to be elevated in HF[128], perhaps compensating for the fact elevated Na^+ is promoting Ca^{2+} extrusion from the matrix via the NCX_m.

A primary goal of this investigation was to compare the effects of normal and elevated extramitochondrial Na^+ concentration on the function of mitochondria isolated from ventricular tissue across a large range of extramitochondrial Ca^{2+} concentrations,

examining the combined effects of elevated Na^+ and Ca^{2+} together. Therefore, the purpose of this study was to determine if applying the ionic conditions of HF alone are sufficient to adversely impact mitochondrial function. In the present study, we assessed mitochondrial function in the presence of elevated Na^+ and Ca^{2+} to mimic the cellular environment of HF. The results demonstrated that the mitochondrial activating effects of Ca^{2+} still occur despite elevated Na^+ in healthy ventricular mitochondria suggesting that the ionic conditions of HF alone are not sufficient to disrupt mitochondrial function.

2.2 Methods

2.2.1 Mitochondrial Isolation from Cardiac Tissue

All protocols for animal handling were approved by the University of Maryland's Institutional Animal Care and Use Committee (IACUC). The University of Maryland at College Park is an AAALAC-accredited institution. A total of 32 male Sprague-Dawley (SD) rats (Hilltop Labs, Inc.) aged 4-8 months were used for the experiments. 9 animals were used in the Ca^{2+} dose response experiments and 23 were used for submaximal mitochondrial respiration experiments. On the day of experimentation, a rat was anaesthetized with 2-4% isoflurane and placed supinated on the surgical area. After the cessation of pain reflexes, the thoracic cavity was opened, and the heart located and quickly excised. The heart was rinsed, cannulated, and perfused with an isolation buffer containing (in mM) 280 sucrose, 21 EGTA, 10 HEPES, and 1 K_2EDTA at 4°C and pH = 7.1 to flush out blood.

The heart was trimmed down to ventricular tissue, minced, and transferred to a separate beaker containing 8.5 mL of ice-cold isolation buffer and 2.5 mg protease (Subtilisin A, Sigma-Aldrich). 1.26±0.07g (mean±SE, n=32) of ventricular tissue was used for mitochondrial isolation. The tissue was further minced manually with scissors for 7 minutes, and the protease digestion was terminated with the addition of 10 mL isolation buffer. The tissue was subjected to homogenization (6,000 rpm) for 30 sec, and the resulting homogenate was centrifuged at 700g for 10 min at 4°C. The supernatant was transferred to a separate centrifuge tube. To improve mitochondrial yield, the pellet was resuspended in 20 mL of isolation buffer and was spun again at 700g for 10 min at 4°C, and the resulting supernatant was combined with the supernatant from the first spin. The combined supernatants were then centrifuged at 10,000g for 10 min at 4°C to pellet the mitochondrial fraction. The resulting pellet was resuspended in 15 mL of isolation buffer using a Dounce homogenizer. The suspension was centrifuged again at 7,500 g for 10 min at 4°C. The resulting final pellet was resuspended with 400 µL of suspension solution containing (in mM) 137 KCl, 10 HEPES, 2.5 MgCl2, 0.5 EDTA at pH = 7.1. Protein concentration of this suspension was assessed using a Thermo Scientific Pierce BCA Protein Assay kit.

2.2.2 Bioenergetic Assessment of Cardiac Mitochondria

The mitochondria isolated from cardiac tissue allowed for the investigation of the effects of altered extramitochondrial ionic conditions on mitochondrial function. Mitochondrial oxygen consumption (J_O) was measured continuously using a Clark electrode in a custom-instrumented water jacketed chamber (World Precision Instruments) maintained at 37°C. Isolated mitochondrial suspension (~20 µg) was

added to the chamber containing 1.2 mL of a respiration media (RM) comprised of (in mM) 100 KCl, 50 MOPS, 20 glucose, 10 $MgCl_2$, 1 EDTA, and 0.2% (w/v) BSA, 37°C, pH=7.0 [126,196,197]. J_O was recorded on ADInstruments LabChart 8 software.

First, the effect of elevated extramitochondrial Na^+ on Ca^{2+} activation of respiration was assessed. Mitochondria were incubated in RM containing 5 mM or 15 mM Na^+ for 5 min to mimic the extramitochondrial environments of either healthy (5 mM) or elevated (15 mM) Na^+ and to deplete mitochondrial matrix Ca^{2+}. After depletion, 10 mM Pi was added to the chamber, followed by 10 mM glutamate and 1 mM malate. Following the addition of fuels (glutamate+malate), Ca^{2+} was added in separate trials to the chamber to generate total Ca^{2+} concentrations of 0, 0.17, 0.31, 0.62, 0.92, 1.25 mM. A bolus of 1.6 mM ADP was then added to the chamber to initiate max J_O (State 3) and the chamber oxygen content was depleted to anoxia. In a subset of experiments, mitochondria were incubated for 5 min in 5 mM Na^+ (mimicking the low Ca^{2+} condition), and then an addition of 10 mM Na^+ was added just prior to adding Pi.

For submaximal mitochondrial respiration experiments, in addition to J_O, mitochondrial reduction-oxidation (redox) status and mitochondrial membrane potential ($\Delta\Psi$) were continually monitored. NADH fluorescence within the chamber was assessed using a bifurcated cable connected to a UV light source for excitation while emitted light was collected with an QE Pro spectrometer and recorded using OceanView software (Ocean Optics). NADH reduction level was calculated in relation to the fully oxidized state (Ca^{2+}-depleted mitochondria with ADP and Pi but without substrates) and fully reduced state (mitochondria with substrates and Ca^{2+} during

anoxia) [126], and percent NADH reduction was analyzed through custom code on MATLAB software (MathWorks).

Mitochondrial membrane potential ($\Delta\Psi$) was assessed using a TPP^+ sensitive electrode (World Precision Instruments), which monitors the distribution of the lipophilic cation TPP^+ across the inner mitochondrial membrane [126,127]. Prior to the addition of mitochondria to the RM, a TPP^+ standard curve was created (1, 2, 3, and 4 µM). The addition of mitochondria decreased the TPP^+ signal as TPP+ distributed across the inner mitochondrial membrane in proportion to $\Delta\Psi$. A schematic overview of the setup for mitochondrial assessments can be found in Illustration 2.

Intermediate steady-state J_O was established by stepwise alteration of the ATP:ADP ratio, and thus the Gibbs free energy of ATP (ΔG_{ATP}), to determine the sensitivity of the mitochondria to respond to the extramitochondrial energetic environment. This was accomplished using the creatine kinase (CK) energetic clamp[126,196,197]. As with Ca^{2+} dose-response experiments, mitochondria were incubated with 5 mM or 15 mM Na^+ for 5 minutes, as described above, then 10 mM Pi and 125 µM ADP were added to achieve maximal mitochondrial oxidation. Next, 10 mM glutamate and 1 mM malate were added to the chamber. The CK reaction was used to respire the mitochondria at various ratios of ATP:ADP by manipulating the phosphocreatine (PCr):creatine (Cr) ratio. To do so, the chamber was loaded with 5 mM Cr, 5 mM ATP, 2.5 mM PCr, and excess CK. Subsequently, stepwise titrations of PCr, resulted in PCr:Cr ratios of 0.5, 1.0, 1.5, 2.0, 3.0, and 4.0. From this, the free energy of ATP hydrolysis can be calculated as follows:

$$\Delta G_{ATP} = \Delta G_{ATP}^{\circ} - 2.3RT \log[[PCr]K_{CK}/([Cr][P_i])]$$

where $\Delta G_{ATP}°$ is the standard ΔG_{ATP} (-7.592 kcal/mol), R is the gas constant (1.987 cal/K/mol), and T is the temperature (310 K)[126]. J_O, NADH, and $\Delta\Psi$ were recorded for each resulting ΔG_{ATP} from PCr additions, allowing for a determination of the responsiveness of respiration to mitochondrial driving forces in the presence of healthy (5 mM) or elevated (15 mM) Na^+, both in the absence and presence of Ca^{2+}.

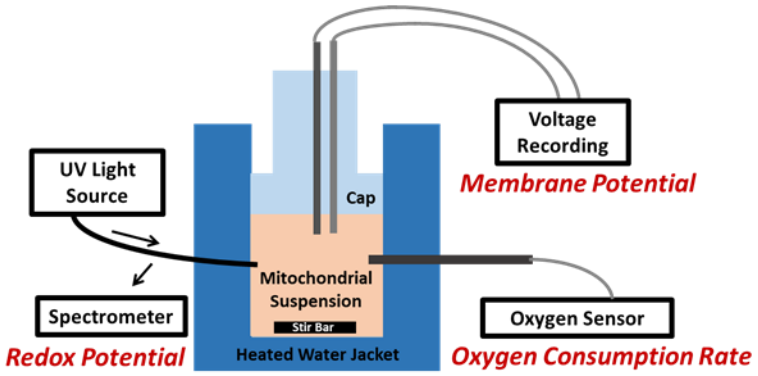

Illustration 2. Schematic of mitochondrial respiration chamber instrumentation. Isolated mitochondria are placed in a chamber of respiration media and are assessed for mitochondrial forces (i.e. redox and membrane potential) and flux (oxygen consumption rate).

2.2.3 Driving Forces and Pathway Conductance

An estimate of the effective conductance of each region of active oxidative phosphorylation was derived from the force-flow interaction of each component of the oxidative phosphorylation pathway as described previously[126,198,199]. The driving forces are determined from the $\Delta\Psi$ and reduction (redox) potential derived from NADH oxidation, while J_O provided the flux through the pathway.

The redox potential of the redox pair in the mitochondrial complex (E_h) can be determine with

$$E_h = E_m + 2.3(RT)/nF) \times \log([\text{oxidized}]/[\text{reduced}])$$

where E_m is the redox midpoint potential (-320 mV for NAD/NADH and 820 mV for O_2/H_2O), n is the number of electrons transferred, and F is the Faraday constant (23.062 cal/mV/mol). The free energies for redox, $\Delta\Psi$, and ATP were calculated as

$$\Delta G_{redox} = -nF(\Delta E_h + \Delta\Psi)$$

$$\Delta G_{\Delta\Psi} = -mF\Delta\Psi$$

$$\Delta G_{ATP} = p\Delta G_{ATPe}$$

assuming that a molecule of NADH donates two electrons (n) to the ETC leading to ten protons pumped into the intermembrane space (m) that will eventually be shuttled back to the matrix to produce 2.7 ATP molecules (p).

It was assumed that flux through oxidative phosphorylation varied in accordance with the thermodynamic driving forces and is represented as

$$J = L(\Delta G_1 - \Delta G_2)$$

where J is the flux down the pathway, L is the conductance of the component pathway, and ΔG_1 and ΔG_2 represent the respective front- and back-end driving forces of the component pathway. Concurrent measurement of the thermodynamic driving forces (ΔG_{redox}, $\Delta G_{\Delta\Psi}$, and ΔG_{ATP}) and oxygen flux (J_O) allows for the calculation of conductance for the full oxidative phosphorylation pathway ($\Delta G_{redox} - \Delta G_{ATP}$) and its two major components, ETC ($\Delta G_{redox} - \Delta G_{\Delta\Psi}$) and ATP synthesis/transport ($\Delta G_{\Delta\Psi} - \Delta G_{ATP}$).

2.2.4 ROS Assay

To assess the production of reactive oxygen species (ROS) released from healthy ventricular mitochondria in the presence of healthy (5 mM) and elevated (15 mM) Na^+, mitochondria were respired at three intermediate rates and the resulting H_2O_2

release was assessed using Invitrogen Amplex Red [196]. An assay buffer (200 µL) comprised of RM, 10 mM G, 1 mM M, 50 µM Amplex Red, and 0.1 U/mL Horseradish Peroxidase was added into each standard curve and experimental wells in a 96-well plate. Experimental wells were prepared with 5 mM Cr, 5 mM ATP, excess CK, and either 2.5, 5, 15 mM PCr, mimicking 3 respiration rate conditions from above. A subset of wells contained the ATP synthase inhibitor oligomycin (2 µg Oligomycin) to stimulate maximal ROS production. Isolated mitochondrial suspension was then added to both standard curve wells (run daily) and experimental wells. The plate was shaken for 30 sec and transferred to a fluorescence plate reader, incubated at 37°C, and fluorescence (excitation 550 nm, emission 590 nm) was recorded every 5 minutes at for 35 min.

2.2.5 Statistical Analysis

Statistical analyses were performed using GraphPad Prism 7 and IBM SPSS Statistics Version 28.0.0.0. Differences in maximal respiration, intermediate respiration, conductance, and ROS production were assessed using a using a two-way (healthy vs. failing $[Na^+]$ × present vs. absent Ca^{2+}) repeated measures ANOVA. A p value of 0.05 was used to determine statistical significance. A broad overview of the study design can be found in Illustration 3.

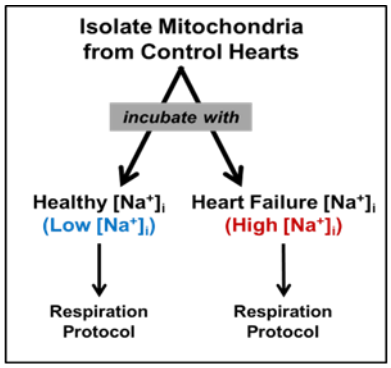

Illustration 3. Schematic overview of Study #1. Isolated cardiac mitochondria from wild type rats were incubated with healthy or failing [Na^+] to see the effect of Na^+ on mitochondrial function.

2.3 Results

2.3.1 Mitochondrial Isolation

Mitochondria were isolated from 1.26±0.07g ventricular tissue, and mitochondrial yield was 23.42±1.18 mg mitochondrial protein per g ventricular tissue (n=32).

2.3.2 Effect of Elevated Extramitochondrial Na^+ on Ca^{2+} Activation of Respiration

Mitochondria were incubated in RM containing healthy (5 mM) or elevated (15 mM) Na^+, and then stimulated with a bolus of ADP to initiate maximal respiration in the presence of a range of extramitochondrial Ca^{2+} concentrations. Incubation in the absence of extramitochondrial Ca^{2+} resulted in low respiration rates, as expected, and increasing the total Ca^{2+} concentration up to 1.25 mM resulted in maximal stimulation of mitochondrial respiration. Extramitochondrial Na^+ concentration did not alter the

Ca^{2+} concentration that achieved maximal mitochondrial respiration nor did it alter respiration rates across any of the Ca^{2+} concentrations (Figure 1).

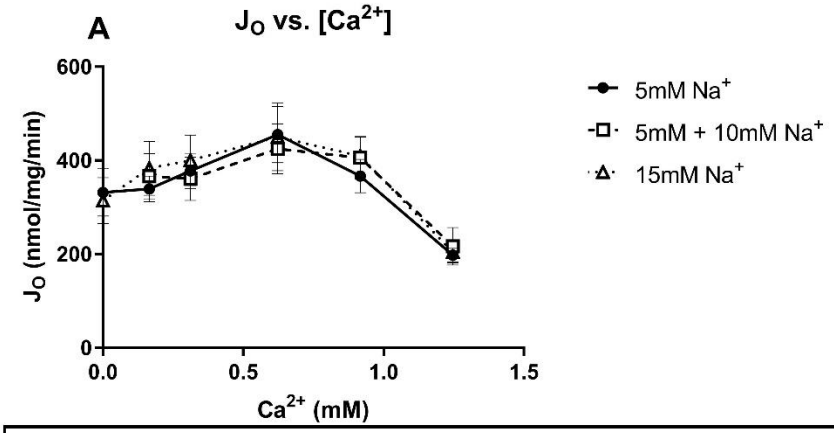

Figure 1. Response of mitochondrial respiration to increasing [Ca^{2+}] when incubated in healthy or failing [Na^+]. Maximal J_O was not different between 5 and 15mM [Na^+] incubations across [Ca^{2+}] of 0.17, 0.31, 0.62, 0.92, & 1.25mM . Split additions of Na^+ (5mM + 10mM Na^+) resulted in no difference in J_O compared to 5 and 15 mM [Na^+] incubations. Maximal J_O was greatest with 0.62mM of Ca^{2+} activation under all conditions.

2.3.3 Submaximal Mitochondrial Function in Response to Ca^{2+} and Elevated Na^+

Isolated cardiac mitochondria underwent submaximal respiration assay using a CK energetic clamp that resulted in extramitochondrial ADP concentrations of 8.33, 11.11, 16.67, 22.22, 33.33, and 66.67 mM, which resulted in extramitochondrial Gibbs free energy of ATP hydrolysis (ΔG_{ATPe}) values of -13.1, -13.5, -13.8, -14.0, -14.2, and -14.4 kcal/mol. Mitochondrial respiration increased with increasing concentrations of ADP ($p<0.001$); however, this increase was blunted in the absence of Ca^{2+} ($p<0.001$; Figure 2A). Respiration rates did not differ between healthy (5 mM) and elevated (15 mM) Na^+, in the absence or presence of Ca^{2+} ($p=0.410$; Figure 2A).

The Eadie-Hofstee plot of these data allowed for the determination of the predicted maximal respiration by calculating the y-intercept of the Jo/ADP:J_O relationship (Figure 2B). The calculated V_{max} values were not significantly different (p=0.7699) between 5 mM (mean±SE, 204.4±5.7 nmol/mg/min) and 15 mM (228.2±5.8 nmol/mg/min) Na^+ incubations without Ca^{2+}. Moreover, the addition of maximal Ca^{2+} activation demonstrated no significant difference (p=0.1657) in predicted maximal respiration of 5 mM Na^+ incubation (409.0±14.8 nmol/mg/min) compared to 15 mM Na^+ incubation (454.3±10.02 nmol/mg/min). These data corroborate the findings of maximal respiration stimulated with ADP reported in Figure 1. Using the same data, the results were reorganized into an Eadie-Hofstee plot (Figure 2B). Without Ca^{2+}, V_{max} did not differ significantly (p=0.7699) between 5 mM Na^+ (198.9 ± 6.9 nmol/mg/min) and 15 mM Na^+ (218.5 ± 12.71 nmol/mg/min). Similarly, V_{max} did not differ significantly (p=0.1657) between 5 mM Na^+ (390.3 ± 22.44 nmol/mg/min) and 15 mM Na^+ (462.6 ± 12.21 nmol/mg/min) in the presence of Ca^{2+}. Predicted maximal mitochondrial respiration was determined to be significantly greater ($p<0.001$) in all incubations involving the final chamber [Ca^{2+}] of 0.62 mM compared to Ca^{2+} absent conditions.

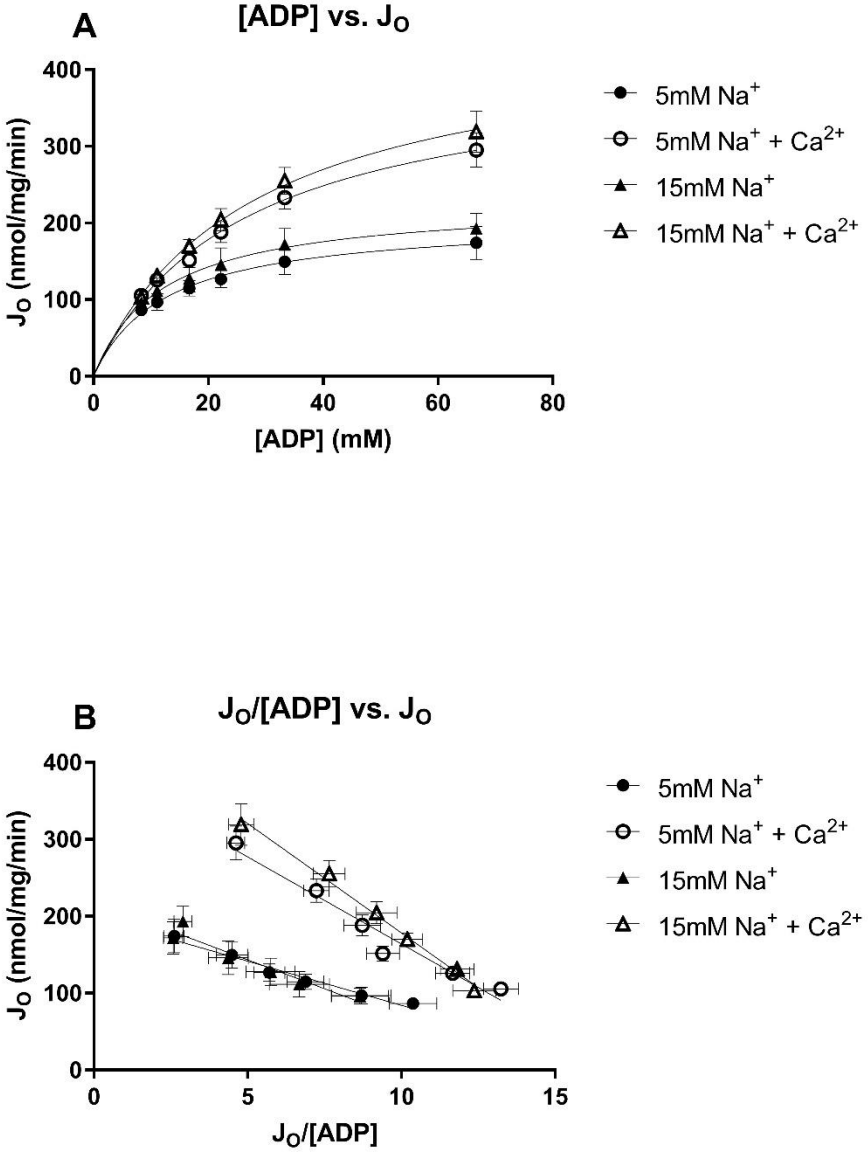

Figure 2. Mitochondria demonstrate similar kinetics when incubated with healthy or failing [Na^+]. A) Michaelis-Menten plot demonstrating Ca^{2+} activation increases K_m similarly between 5mM and 15mM Na^+. B) Eadie-Hofstee plot demonstrating a greater V_{max} with Ca^{2+} activation with 5mM and 15mM Na^+ incubations.

Submaximal respiration from the CK clamps demonstrated that 0.62 mM Ca^{2+} was sufficient to significantly increase submaximal respiration from ΔG_{ATP} of -13.1 kcal/mol to -14.2 kcal/mol in 5 mM Na^+ incubation conditions ($p<0.05$) and from ΔG_{ATP} of -13.1 kcal/mol to -13.9 kcal/mol in 15 mM Na^+ incubation conditions ($p<0.05$) (Figure 3A). No significant differences were found between 5 and 15 mM Na^+

incubation, regardless of Ca^{2+} condition, across all ΔG_{ATP} perturbations. The addition of Ca^{2+} increased the relative pool of reduced NADH (Figure 3B) and hyperpolarized the mitochondrial membrane potential (Figure 3C) at a given submaximal respiration rate.

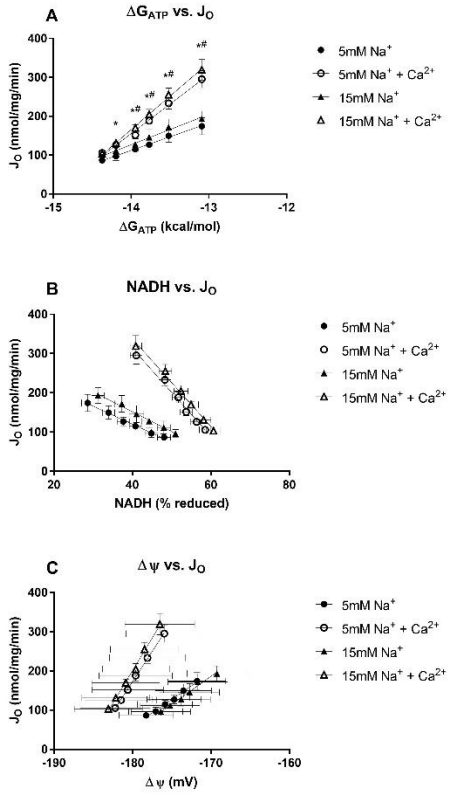

Figure 3. Ca^{2+} activates mitochondrial respiration and augments the driving forces similarly in the presence of healthy and failing [Na^+]. A) Calcium activation elevates J_O across ΔG_{ATP} from -13.1 to -14.2 kcal/mol with 5mM Na^+ incubation (*p<0.05) and from -13.1 to -13.9 kcal/mol with 15mM Na^+ incubation (#p<0.05). B) Calcium activation increases the relative pool of reduced NADH for a given J_O similarly between 5mM and 15mM Na^+ incubations C) Calcium activation hyperpolarizes membrane potential ($\Delta\psi$) for a given J_O similarly between 5mM and 15mM Na^+ incubations.

2.3.4 Mitochondrial Conductance

Mitochondrial respiration is the product of conductance and energetic potential; therefore, conductance represents the slope of mitochondrial respiration against a specified energetic difference (Figure 4). There was a main effect of Ca^{2+} on improving the conductance (in nmol/mg/min/kcal/mol) of the full oxidative phosphorylation

pathway ($\Delta G_{redox} - \Delta G_{ATP}$; $p<0.0001$; Figure 4A) in both 5 mM Na^+ incubations (-35.2 ± 8.5 vs. -81.5 ± 8.6) and 15 mM incubations (-39.7 ± 5.3 vs. -102.2 ± 9.0). Conversely, there was no main effect of Na^+ ($p=0.1274$) nor interaction effect of Na^+ and Ca^{2+} ($p=0.3196$) on conductance of the oxidative phosphorylation pathway. When examining the conductance of the electron transport chain (ETC) specifically ($\Delta G_{redox} - \Delta G_{\Delta\Psi}$; Figure 4B) Ca^{2+} had a main effect of increasing the conductance ($p=0.0003$) in both the 5 mM Na^+ (-122.6 ± 28.6 vs. -325.3 ± 72.8) and 15 mM Na^+ incubations (-132.1 ± 36.9 vs. -392.1 ± 69.5). There was no effect of Na^+ ($p=0.4981$) nor interaction effect of Na^+ and Ca^{2+} ($p=0.6096$) on ETC conductance. Lastly, there was a main effect of Ca^{2+} on ATP synthase/adenine nucleotide translocase (ANT) conductance ($\Delta G_{\Delta\Psi} - \Delta G_{ATP}$; $p<0.0001$) for both 5 mM Na^+ (-53.4 ± 13.1 vs. -121.2 ± 17.4) and 15 mM Na^+ conditions (-56.7 ± 6.5 vs. -144.4 ± 12.2). There was no main effect of Na^+ ($p=0.3155$) nor interaction effect of Na^+ and Ca^{2+} ($p=0.4495$) on ATP synthase/ANT conductance.

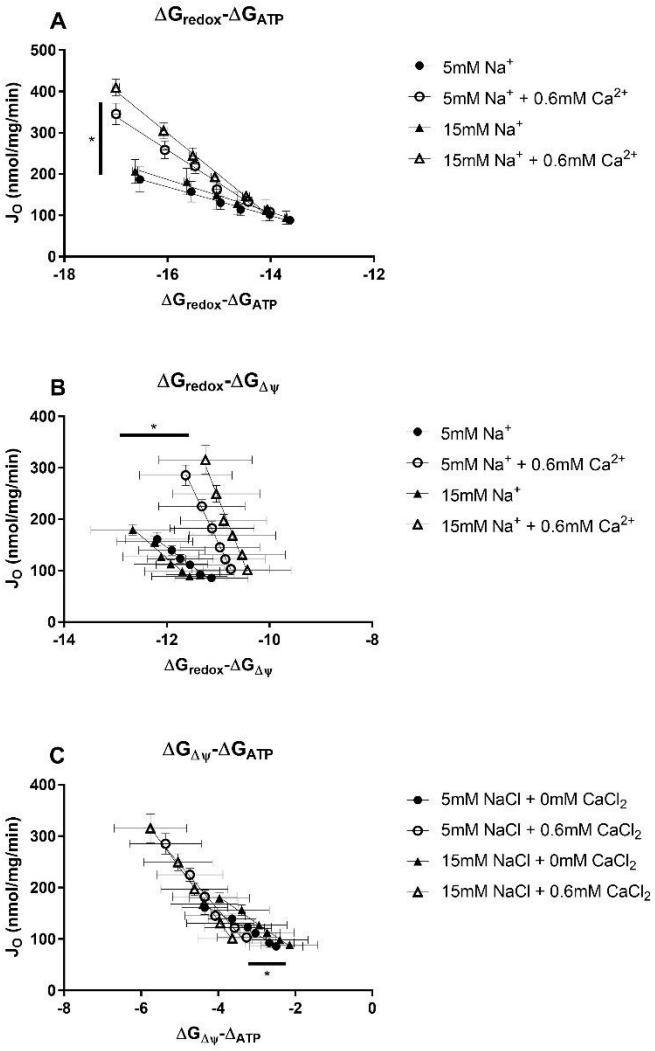

Figure 4. Effect of healthy and failing [Na^+] and Ca^{2+} on the activation state of each component of the mitochondrial energy transduction pathway. Slopes of the regressions represent conductances of each condition. A) Conductance of the oxidative phosphorylation pathway is significantly improved with Ca^{2+} activation similarly between 5mM and 15mM Na^+ incubation. B) Conductance of the electron transport chain is significantly improved with Ca^{2+} activation similarly between 5mM and 15mM Na^+ incubation. C) Conductance of the ATP synthase and ANT is significantly improved with Ca^{2+} activation similarly between 5mM and 15mM Na^+ incubation. (*p<0.01). No significant differences were observed in conductances between 5mM and 15mM Na^+ conditions.

2.3.5 ROS Production in Response to Ca^{2+} and Elevated Na^+

ROS production was measured by Amplex Red assay for H_2O_2 production in isolated rat cardiac mitochondria (n=7). The results demonstrated no main effect of Na^+ and nor interaction effect of Na^+ with Ca^{2+} at ΔG_{ATP} of -13.1, -13.6, and -14.1 kcal/mol. However, there was a main effect of Ca^{2+} on H_2O_2 production at ΔG_{ATP} of -13.1 kcal/mol (p=0.048; Figure 5A), which significantly increased production of H_2O_2 from 168.17±38.08 to 426.57±133.54 pmol/mg/min in the 5 mM Na^+ conditions and from

188.66±114.12 to 514.79±164.52 in the 15 mM Na^+ conditions. H_2O_2 production tended to increase (p=0.066) from 166.16±38.73 to 485.61±164.78 pmol/mg/min at -13.6 kcal/mol and 224.13±44.23 to 626.30±207.57 pmol/mg/min at -14.1 kcal/mol (p=0.065) in the 5 mM Na^+ conditions with Ca^{2+}. Similarly, in the 15 mM Na^+ conditions with Ca^{2+}, H_2O_2 production tended to increase from 215.02±45.56 to 503.56±157.08 pmol/mg/min at -13.6 kcal/mol (p=0.066). and 272.46±78.64 to 610.72±206.31 pmol/mg/min at -14.1 kcal/mol (p=0.065). The percent free radical leak was no different between 5 mM Na^+ and 15 mM Na^+ at ΔG_{ATP} of -13.1 (p=0.260), -13.6 (p=0.700), and -14.1 kcal/mol (p=0.512). No main effect of Ca^{2+} nor interaction effect of elevated Na^+ and Ca^{2+} was observed on percent free radical leak. The conductance (in pmol/mg/min/kcal/mol) through the H_2O_2 leak pathway was not significantly different (p=0.260) between 5 mM Na^+ (174.8±57.7) and 15 mM Na^+ (151.0±60.4) conditions (Figure 5C). There was no main effect of Ca^{2+} on conductance through the H_2O_2 leak pathway between Ca^{2+} present (232.8± 87.0) and Ca^{2+} absent conditions (93.0±34.5); however, this trended towards significance (p=0.067). No interaction effect of Na^+ and Ca^{2+} was observed in the conductance of the H_2O_2 leak pathway.

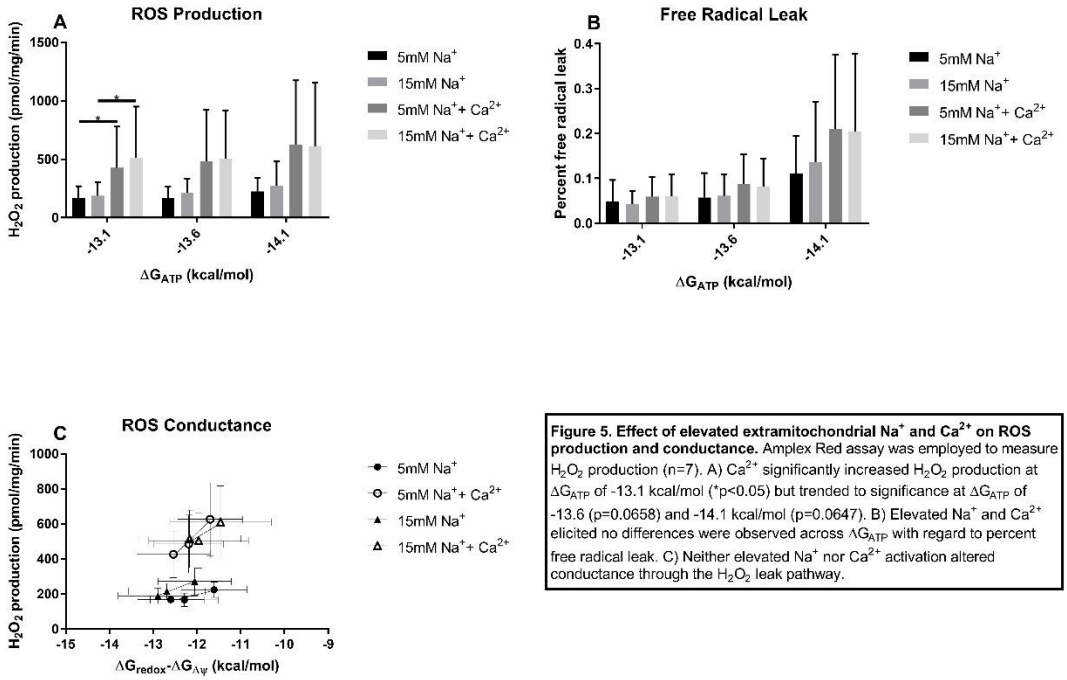

Figure 5. Effect of elevated extramitochondrial Na^+ and Ca^{2+} on ROS production and conductance. Amplex Red assay was employed to measure H_2O_2 production (n=7). A) Ca^{2+} significantly increased H_2O_2 production at ΔG_{ATP} of -13.1 kcal/mol (*p<0.05) but trended to significance at ΔG_{ATP} of -13.6 (p=0.0658) and -14.1 kcal/mol (p=0.0647). B) Elevated Na^+ and Ca^{2+} elicited no differences were observed across ΔG_{ATP} with regard to percent free radical leak. C) Neither elevated Na^+ nor Ca^{2+} activation altered conductance through the H_2O_2 leak pathway.

2.4 Discussion

It has been reported that cardiac tissue from animal models and patients with HF have elevated levels of intracellular Na^+ and Ca^{2+} [128,132], which has been theorized to adversely alter mitochondrial function[132]. The present study addresses whether failing levels of Na^+ in combination with Ca^{2+} is sufficient to adversely impact mitochondrial function in isolated cardiac mitochondria from healthy male rats. To our knowledge, this is the first study of its kind to investigate the combined effects of Na^+ and Ca^{2+} on mitochondrial function isolated from healthy rat hearts.

By isolating cardiac mitochondria, we were able to introduce and control the specific extramitochondrial conditions and observe the effects. More specifically, we incubated isolated mitochondria from healthy rat hearts in either control (5 mM) or HF levels (15 mM) of Na^+ and observed whether Ca^{2+}-activated mitochondrial function

was adversely affected under maximal and submaximal conditions. Our findings demonstrate that Ca^{2+} activation of cardiac mitochondria is preserved regardless of the extramitochondrial levels of Na^{+}, therefore, suggesting that an elevated extramitochondrial Na^{+} alone or in combination with Ca^{2+} is insufficient to diminish ATP production thought to occur in HF. Contradictory to our findings, maximal mitochondrial respiration was reduced in isolated mitochondria from healthy rat hearts when exposed to low and high levels of Na^{+}[193]. More importantly, addition of extramitochondrial Ca^{2+} was able to reverse the Na^{+} depressant effects[193], which supports our finding that elevated Na^{+} alone cannot alter mitochondrial function in the presence of physiological levels Ca^{2+}. However, this does not preclude the possibility that prolonged elevated intracellular Na^{+} may elicit changes in ion transporter expression, such as NCX or NHX, that may lend toward decompensated mitochondria.

Not only is this the first study to explore the combined effects of Na^{+} and Ca^{2+} on cardiac mitochondria, but these findings also demonstrate that mitochondrial function extends beyond just maximal respiration and is an aggregate of many components that respond differently during varying levels of submaximal activity. By employing a CK energetic clamp and observing submaximal respiration, we are better able to delineate when differences may begin to occur, and it allows us to analyze the force, flow, and conductance of the full oxidative phosphorylation pathway and its components. The findings from this study reveal that isolated healthy mitochondria respire similarly at all submaximal levels in the presence of extramitochondrial Ca^{2+} regardless of Na^{+} levels. Furthermore, Ca^{2+} improves both redox and membrane

potential as well as the conductance of the ETC, the ATP synthase/ANT, and the full oxidative phosphorylation pathway.

These findings are in agreement with Ca^{2+} activation of mitochondrial respiration in porcine skeletal[167] and cardiac muscle[127]. It has been previously demonstrated that Ca^{2+} uptake through the MCU increases mitochondrial matrix Ca^{2+} to increase NADH production[165,166], ETC conductance[167], and ATP synthase activity[127], which has been reproduced in our study. This Ca^{2+} activation of the oxidative phosphorylation pathway appears to be maintained in the presence of elevated Na^{+}. In contrast, findings from one study reported that elevated Na^{+} reduced mitochondrial matrix Ca^{2+} and redox potential in isolated cardiomyocytes[149]. Moreover, in that study, when the isolated cardiomyocytes were subjected to CGP-37157, a NCX_m inhibitor, a reduction in redox potential was prevented. However, the inhibitor CGP-37157 is not only a NCX_m inhibitor, but it is also a SERCA ATPase antagonist and RyR agonist. Given that cellular (SERCA ATPase) and mitochondrial Ca^{2+} efflux (NCX_m) pathways have been inhibited and cellular Ca^{2+} influx (RyR) has been enhanced or unchanged (MCU), it is unsurprising that this inhibitor prevented a decrease in mitochondrial matrix Ca^{2+}. In combination with the present findings, it is possible that elevated Na^{+} may alter mitochondrial function, but through upstream extramitochondrial pathways rather than on the mitochondria itself.

Elevated extramitochondrial Na^{+} alone may not be sufficient to elicit an increase in mitochondrial ROS production. From our findings in isolated cardiac mitochondria, no significant differences were observed in percent free radical leak. Furthermore, elevated extramitochondrial Na^{+} and Ca^{2+} did not alter the conductance

through the H_2O_2 leak pathway in our isolated mitochondria. Contradictory to our findings, H_2O_2 formation has been reported to increase in patch-clamped guinea pig cardiomyocytes subjected to 15mM Na^{+}[162]. It was suggested that elevating cytosolic Na^+ concentration promoted mitochondrial Ca^{2+} efflux via the NCX_m[149,168,181] thereby reducing electron flux and the NADPH/$NADP^+$ pool leading to greater H_2O_2 formation[200]. Additionally, when MCU was blocked, there was a greater formation of H_2O_2[162]. When comparing these findings with those from our isolated mitochondria, it is possible that there are other mechanisms at play that are susceptible to extramitochondrial fluctuations of Na^+ and Ca^{2+} that could contribute to these differing results.

Although in the present study no effect of Na^+ was found in young healthy Sprague-Dawley male rats, this does not rule out the potential for an interaction effect of Na^+ with aging, sex, or HF. To ascertain whether Na^+ or a combination of Na^+ and Ca^{2+} disrupts mitochondrial function in the HF disease, it will be necessary to perform a similar investigation comparing the potential difference in mitochondrial function in isolated mitochondria from healthy and failing heart tissue. Doing so would help explain whether cardiac mitochondria from failing hearts are intrinsically altered or if they are only disrupted in the presence of an altered extramitochondrial environment.

The present findings are the first to study the effects of elevated Na^+ and Ca^{2+} on mitochondrial function in isolated cardiac mitochondria. Ca^{2+} activation promoted redox potential, membrane potential, and conductance of all components of the oxidative phosphorylation pathway, regardless of Na^+ levels. Na^+ did not change the optimal Ca^{2+} required for maximal respiration. Moreover, Na^+ concentrations observed

in HF cardiomyocytes were unable to elicit a greater mitochondrial production of ROS in isolated mitochondria. Importantly, this suggests that an acute exposure to intracellular Na^+ levels observed in HF does not adversely impact cardiac mitochondrial function nor does it alter the amount of ROS generated by the mitochondria. These findings support our hypothesis that Ca^{2+} activation of mitochondrial function is preserved in the presence of HF levels of Na^+. Although no adverse effects were found with elevated Na^+, this does not exclude the potential for cardiac mitochondria from HF to be intrinsically altered nor does this suggest that mitochondria from failing hearts dos not respond adversely to elevated Na^+. Therefore, isolated cardiac mitochondria from failing heart tissue and their response to elevated Na^+ and Ca^{2+} is required.

Chapter 3: Cardiac Mitochondrial Membrane Potential is Diminished in a Rat Model of Pressure-Overload Induced Heart Failure

3.1 Introduction

In individuals with HF, the heart is unable to supply enough blood to provide adequate fuel and oxygen to meet the demands of the body, leading to lower quality of life and greater all-cause mortality. The heart is a highly metabolically active tissue, with the cardiac mitochondria providing over 90% of the ATP to fuel cardiac work[201]. As such, proper mitochondrial function is essential to maintain adequate ATP production and normal contractile function. Therefore, it is not surprising that mitochondrial dysfunction has been implicated in HF, with mitochondrial defects described in both human[128,173–175] and experimental models[132,170,176,177]. However, depending on the conditions of the study, whether mitochondrial function is altered in HF is debated[173,176,202].

Not only must cardiac mitochondria continually provide ATP to fuel constant myocardial contractions, they must also be able to increase the rate at which they produce ATP when there is an increase in heart rate[203,204]. Some individuals with HF experience dyspnea and/or fatigue at rest[23–26]; however, all individuals with HF experience these symptoms upon the initiation of activity[31–35]. Indeed, a key characteristic of HF is exertional intolerance. If mitochondria are unable to increase

their ATP production to meet this demand, this may, in part, explain exertional intolerance in individuals with HF.

While intrinsic changes within the mitochondria could alter function, changes in the cellular environment in which the mitochondria reside could also play a role. Elevated intracellular concentrations of Ca^{2+} and Na^{+} in ventricular myocytes have been reported in HF[128,132], and are thought to contribute to altered mitochondrial function[132,163,164], ultimately resulting in reduced ATP production. When there is an increase in contractile activity, intracellular Ca^{2+} concentration increases and results in increased crossbridge cycling. This increase in intracellular Ca^{2+} concentration stimulates the influx of Ca^{2+} into the mitochondrial matrix, primarily via the mitochondrial Ca^{2+} uniporter (MCU). Ca^{2+} is a critical signaling molecule for the matching of ATP demand with production. Increasing mitochondrial matrix Ca^{2+} activates dehydrogenase enzymes that increase NADH production[165,166], elevate ETC conductance[167], and increase ATP synthase activity[127]. It has been suggested that elevated intracellular Na^{+}, as observed in HF, decreases matrix Ca^{2+} by extruding Ca^{2+} from the mitochondrial matrix through the Na^{+}/Ca^{2+} exchanger (NCX_m)[128,168]. In the absence of extramitochondrial Ca^{2+}, increasing Na^{+} is capable of decreasing matrix Ca^{2+} and maximal respiration in mitochondria isolated from healthy hearts[134]. Further, in the presence of elevated intracellular Na^{+}, mitochondrial Ca^{2+} uptake has been demonstrated to be impaired in isolated cardiomyocytes resulting in a reduction of available NADH with workload demand[169], and elevated intracellular Na^{+} has been reported to increase ROS formation in both healthy and failing cardiomyocytes[162]. However, intracellular Ca^{2+} is also reportedly elevated in HF, which would promote

Ca^{2+} influx into the mitochondrial matrix. Previously, we have demonstrated that, in mitochondrial isolated from healthy ventricular tissue, Ca^{2+} activation of mitochondrial function is maintained whether the extramitochondrial environment contains healthy (5 mM) or elevated (15 mM) Na^{+} concentrations.

While these data suggest that an altered ionic environment *alone* is not sufficient to negatively impact mitochondrial function, this does not preclude the possibility that mitochondria from failing hearts might be impacted by an altered ionic environment. For example, altered expression or activity of the NCX_m and MCU could, *in combination* with an altered ionic environment, result in diminished mitochondrial function in HF. A greater expression of NCX_m has been reported in a rabbit model of HF[205], while a metabolic rat model of HF has demonstrated no differences in the expression of mitochondrial Ca^{2+} uniporter (MCU)[114]. Further, Ca^{2+} influx via MCU is influenced by the mitochondrial membrane potential, in addition to the intracellular Ca^{2+} concentration, which may be altered in failing ventricular mitochondria.

In the present study, mitochondria were isolated from either healthy or failing rat hearts, and the effects of healthy (5 mM) and elevated (15 mM) extramitochondrial Na^{+} on the Ca^{2+} activation of the mitochondrial oxidative phosphorylation pathway was explored utilizing force-flow analysis. Mitochondria were stimulated to respire across a range of respiration rates and the resultant mitochondrial driving forces (redox potential and membrane potential ($\Delta\Psi$)) were measured. Additionally, the effective activity of the dehydrogenase enzymes, the electron transport chain, and the combined activities of the ATP synthase and adenine nucleotide translocase (ANT) were determined[126,199,206]. We found no differences between 5 and 15 mM

extramitochondrial Na^+ in the activation of mitochondrial oxidative phosphorylation. Regardless of extramitochondrial Na^+ concentration, mitochondria isolated from failing hearts demonstrated similar mitochondrial respiration rates compared to healthy hearts, however, failing mitochondria exhibited depolarized $\Delta\Psi$ values across these respiration rates.

3.2 Methods

3.2.1 Animals and Transverse Aortic Constriction Surgery

All protocols for animal handling were approved by the University of Maryland's Institutional Animal Care and Use Committee (IACUC). The University of Maryland at College Park is an AAALAC-accredited institution. A total of 40 male Hilltop Sprague-Dawley rats were used in this study with 13 rats dedicated to Ca^{2+} dose response assays, 19 to creatine kinase (CK) energetic clamp assays, and 8 to ROS and proton leak assays.

Male Sprague-Dawley rats aged 4 weeks underwent transverse aortic constriction (TAC) or sham surgery. Each animal was weighed and then anesthetized via inhalation of isoflurane (2% isoflurane supplemented with 100% oxygen (400-500 mL/min)). After the anesthesia had taken effect and the animal was unresponsive to tail and toe pinches, a single dose of buprenorphine (0.05-0.1 mg/kg) was injected via subcutaneous injection. A surgical area was clipped clean of fur, sterilized with sequential swabs of alcohol-betadine-alcohol, and, after another reflex check via tail and toe pinches, a longitudinal skin incision was made from the ventral mid-neck area to the suprasternal notch region. Submandibular salivary glands and the sternohyoid

muscle were gently separated to reveal the trachea and the left and right common carotid arteries. The sternum was cut as low as the 4th rib and the thymus was retracted to reveal the aortic arch. A 4-0 silk suture was passed around the aortic arch between the origin of the innominate artery and the left common carotid artery. Correct placement was confirmed by pulling up on the suture and observing increased flow through the right common carotid artery and ceased flow through the left common carotid artery. A blunted, 20-guage needle was placed adjacent to the aorta and a 4-0 suture was tied tightly around the aorta and the needle. The needle was then removed, resulting in a chronic partial aortic constriction. Sham-operated controls underwent the same procedure; however, the suture was not tied. The sternum was closed with a single suture, the salivary glands were replaced, and the skin was sutured shut with 5-0 monofilament suture and treated with betadine. Illustration 4 provides a graphical representation of the transverse aortic constriction in rats.

After skin closure the rat was removed from anesthesia and placed into a clean cage with a heating pad on its side for recovery until spontaneous movement occurred. Once the rat was awake and self-propping, the heating pad was removed. Continual post-operation observation occurred for one hour after the animal recovered from anesthesia and every 12 hours for the subsequent three days.

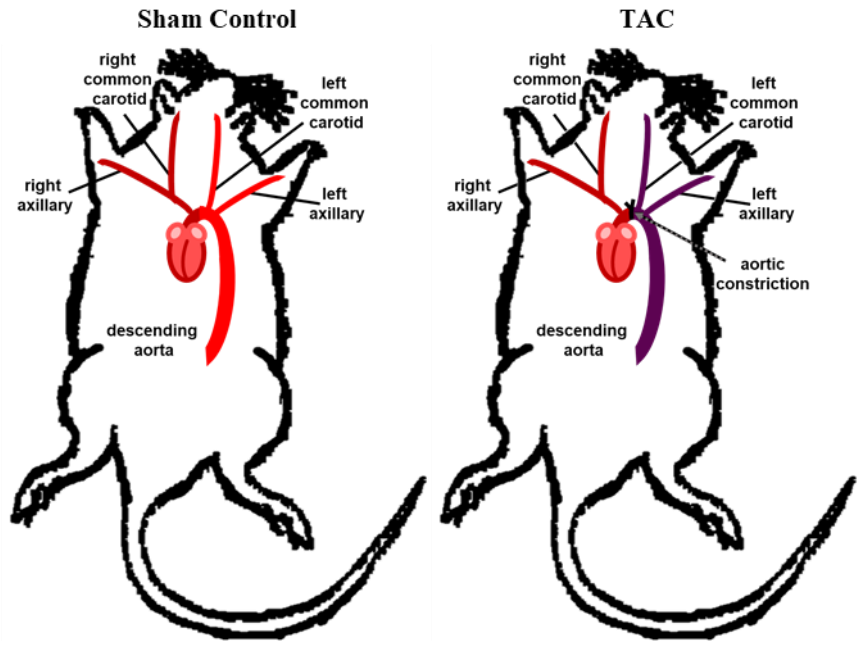

Illustration 4. Overview of the transverse aortic constriction surgical intervention. Left: Sham control rat without aortic constriction. Right: Rat with transverse aortic constriction (TAC) between the innominate (not labeled) and left carotid artery. Successful placement of the constriction will induce chronic pressure overload on the heart.

3.2.2 Mitochondrial Isolation from Cardiac Tissue

Cardiac mitochondria were isolated from ventricular tissue of male sham control and TAC rats that were aged 48.8±18.4 weeks post-surgery. The animals were anaesthetized with 2-4% isoflurane and placed supinated on the surgical area. The thoracic cavity was opened, and the heart located and quickly excised. The heart was rinsed and perfused with an isolation buffer containing (in mM) 280 sucrose, 21 EGTA, 10 HEPES, and 1 K_2EDTA at 4°C and pH = 7.1 to flush out blood. The heart was cut twice cross-sectionally such that chambers of both ventricles are clearly revealed in the middle of the three sections. The left ventricular (LV) and septal widths were measured at the thickest portions of the middle heart section with calipers. The heart sections were dabbed dry, weighed together, and recorded as heart mass.

The heart was trimmed down to ventricular tissue, minced, and transferred to a separate beaker containing 8.5 mL of ice-cold isolation buffer and 2.5 mg protease (Subtilisin A, Sigma-Aldrich). The tissue was further minced manually with scissors for 7 minutes, and the protease digestion was terminated with the addition of 10 mL isolation buffer. The supernatant was transferred to a separate centrifuge tube. To improve mitochondrial yield, the pellet was resuspended in 20 mL of isolation buffer and was spun again at 700g for 10 min at 4°C, and the resulting supernatant was combined with the supernatant from the first spin. The combined supernatants were then centrifuged at 10,000g for 10 min at 4°C to pellet the mitochondrial fraction. The resulting pellet was resuspended in 15 mL of isolation buffer using a dounce homogenizer. The suspension was centrifuged again at 7,500 g for 10 min at 4°C. The resulting final pellet was resuspended with 400 µL of suspension solution containing (in mM) 137 KCl, 10 HEPES, 2.5 MgCl2, 0.5 EDTA at pH = 7.1. Protein concentration of this suspension was assessed using a Thermo Scientific Pierce BCA Protein Assay kit.

3.2.3 Ca^{2+} Dose Response

Ca^{2+} activated mitochondrial respiration was assessed in mitochondria isolated from ventricular tissue from TAC and sham hearts. A subset of mitochondria (n=13) was incubated in healthy (5 mM) or elevated (15 mM) Na^{+} across increasing Ca^{2+} concentrations to determine if the concentration of Ca^{2+} required for maximal respiration was altered by TAC. Mitochondrial oxygen consumption (J_O) was measured continuously using a Clark electrode in a water jacket chamber maintained at 37°C. Mitochondria (~20 µg) was added to the chamber containing 1.2 mL of a respiration

media comprised of (in mM) 100 KCl, 50 MOPS, 20 glucose, 10 $MgCl_2$, 1 EDTA, and 0.2% (w/v) BSA, 37°C, pH=7.0. J_O was recorded on ADInstruments LabChart 8 software. Isolated mitochondria were incubated in 5 or 15mM Na^+ for 5 min to deplete mitochondrial matrix Ca^{2+}. After depletion, 10 mM Pi was added to the chamber, followed by 10 mM glutamate (G) and 1 mM malate (M) with total Ca^{2+} concentrations of to 0.17, 0.31, 0.62, 0.92 or 1.25 mM. A bolus of 1.6 mM ADP was then added to the chamber to initiate max J_O (state 3) and was driven to anoxia that resulted in the fully reduced state.

3.2.4 Creatine Kinase Energetic Clamp Assay

Intermediate steady-state J_O was assessed through the manipulation of the creatine kinase (CK) energetic clamp. Briefly, the ratio of ATP:ADP was fixed by manipulating the phosphocreatine (PCR):creatine (CR) ratio. Mitochondria were incubated with (in mM) 5 Cr, 5 ATP, 10 Pi, 0.83 PCr, and excess CK. Afterwards, ΔG_{ATP} was manipulated through stepwise titrations of PCr, resulting in PCr:Cr ratios of 0.5, 2.0, and 4.0. From this, the free energy of ATP hydrolysis can be calculated as follows:

$$\Delta G_{ATP} = \Delta G_{ATP}^{\circ} - 2.3RT \log[[PCr]K_{CK}/([Cr][P_i])]$$

where ΔG_{ATP}° is the standard ΔG_{ATP} (-7.592 kcal/mol), R is the gas constant (1.987 cal/K/mol), and T is the temperature (310 K). J_O, NADH, and membrane potential ($\Delta\Psi$) were recorded for each resulting ΔG_{ATP} from PCr additions.

NADH was measured continuously and simultaneously with J_O using a bifurcated cable connecting a UV light source and Ocean Optics QE Pro spectrometer to measure NADH fluorescence, which was recorded on Ocean Optics OceanView

software. NADH reduction level was calculated in relation to the fully oxidized state (Ca^{2+}-depleted mitochondria with ADP and Pi but without substrates) and fully reduced state (mitochondria with substrates and Ca^{2+} after the onset of anoxia)[126], and percent NADH reduction was analyzed through custom code on MathWorks MATLAB software.

Similarly, $\Delta\Psi$ was measured continuously and concurrently with J_O using a TPP^+ sensitive electrode that senses the distribution of the lipophilic cation TPP^+ across the inner mitochondrial membrane[126,127] and the results were recorded on ADInstruments LabChart 8. Briefly, a TPP^+ standard curve was created with steady-state TPP^+ concentration of 1, 2, 3, and 4 µM. TPP^+ disappearance was observed when mitochondrial suspension was added to the chamber and TPP^+ binding was mediated by the proton gradient generated across the inner mitochondrial membrane in response to substrate additions.

3.2.5 Force Flow Relationship and Conductance

An estimate of the effective conductance of each region of active oxidative phosphorylation was derived from the force-flow interaction of each component of the oxidative phosphorylation pathway. The driving forces are determined from the $\Delta\Psi$ and reduction (redox) potential derived from NADH oxidation, while J_O provided the flux through the pathway.

The electrical potential of the redox pair in the mitochondrial complex (E_h) can be determined with

$$E_h = E_m + 2.3(RT)/nF) \times \log([\text{oxidized}]/[\text{reduced}])$$

where E_m is the redox midpoint potential (-320 mV for NAD/NADH and 820 mV for O_2/H_2O), n is the number of electrons transferred, and F is the Faraday constant (23.062 cal/mV/mol). The free energies for redox, $\Delta\Psi$, and ATP were calculated as

$$\Delta G_{redox} = -nF(\Delta E_h + \Delta\Psi)$$

$$\Delta G_{\Delta\Psi} = -mF\Delta\Psi$$

$$\Delta G_{ATP} = p\Delta G_{ATPe}$$

assuming that a molecule of NADH donates two electrons (n) to the ETC leading to ten protons pumped into the intermembrane space (m) that will eventually be shuttled back to the matrix to produce 2.7 ATP molecules (p).

It was assumed that flux through oxidative phosphorylation varied in accordance with the thermodynamic driving forces and is represented as

$$J = L(\Delta G_1 - \Delta G_2)$$

where J is the flux down the pathway, L is the conductance of the component pathway, and ΔG_1 and ΔG_2 represent the respective front and back end driving forces of the component pathway. Concurrent measurement of the thermodynamic driving forces (ΔG_{redox}, $\Delta G_{\Delta\Psi}$, and ΔG_{ATP}) and oxygen flux (J_O) allows for the calculation of conductance for the full oxidative phosphorylation pathway ($\Delta G_{redox} - \Delta G_{ATP}$) and its two major components, ETC ($\Delta G_{redox} - \Delta G_{\Delta\Psi}$) and ATP synthesis/transport ($\Delta G_{\Delta\Psi} - \Delta G_{ATP}$).

3.2.6 ROS Assay

To assess the production of reactive oxygen species (ROS) released from TAC mitochondria in the presence of healthy (5 mM) and elevated (15 mM) Na^+ with or without Ca^{2+}, mitochondria were respired at three intermediate rates using Invitrogen

Amplex Red[196]. An assay buffer (125 µL) comprised of DMSO, Amplex Red, Horseradish Peroxidase, RM, KCl, Pi, and Bovine Serum Albumin (BSA) was added to the standard curve and experimental wells. Substrates comprised of 2 µL Glutamate (2 M) and 2 µL Malate (100 mM) were added to experimental wells containing the ATP synthase inhibitor (1 µL Oligomycin) or PCr (1,4, or 8 µL; 500 mM), 2 µL ATP (500 mM), 10 µL Cr (100 mM), and 1 µL CK (15 U/mL). Isolated mitochondrial suspension was then added to both standard curve and experimental wells and H_2O_2 (0.6, 1.2, 2.4, & 4.9 µL) was added to the standard curve wells. The 96-well plate was shaken for 30 sec and transferred to a fluorescence plate reader and measured at F585 at 37°C for 35 min.

3.2.7 Proton Leak Assay

The kinetics of proton leak were assessed in TAC mitochondria incubated in healthy or elevated Na^+ with or without Ca^{2+} by titrating mitochondrial respiration in the absence of ATP synthesis (state 4) using malonate, a competitive succinate inhibitor. In a custom-built mitochondrial respiration chamber filled with 1.2 mL RM, the chamber was capped with the TPP electrode. A TPP standard curve was created by titrating in 400 µM TPP four times in 3 µL boluses, pausing for a plateau after each addition.

Mitochondrial suspension (10-40 µL) was added to the chamber, which reduced the TPP signal by mitochondrial TPP uptake. Mitochondria were previously demonstrated to maximally activate in 0.62 mM $CaCl_2$. Subsequently, 1.2 µL of ATP synthase inhibitor oligomycin (1 mg/mL) and 2 µL of Complex I inhibitor rotenone (2.66 mM) were added to the chamber, uncoupling oxygen consumption from ATP

synthesis and preventing Complex I electron contribution, respectively. Complex II fuel succinate (6 µL) was added to initiate respiration. Malonate, a Complex II inhibitor, was generally titrated in at 10 µL (100 mM), 20 µL (100 mM), 20 µL (100 mM), 2.5 µL (1 M), 2.5 µL (1 M), 2.5 µL (1 M), 2.5 µL (1 M), pausing briefly for steady state. Because ATP synthesis is uncoupled from oxygen consumption, the resulting respiration was a product of electrons shuttling through the ETC to combat the depolarization of $\Delta\Psi$ resulting from proton leak back into the mitochondrial matrix.

3.2.8 Statistical Analysis

Statistical analyses were performed with IBM SPSS Statistics Version 28.0.0.0. A one-tailed Student's t-test was performed between TAC and sham control rats for body mass, heart mass, LV width, septal width, and age. For Ca^{2+} dose response assay, t-tests were performed for each free Ca^{2+} concentration to find differences between Na^{+} conditions (5mM vs. 15mM) and animal type (sham control vs. TAC). For CK clamp assays, three-way mixed (5mM vs. 15mM Na^{+} × without vs. with Ca^{2+} × sham control vs. TAC) ANOVA was performed on all force-flow relationships (J_O vs. ΔG_{ATP}, NADH, or $\Delta\Psi$) and conductance (L_{oxphos}, L_{ETC}, L_{ATPase}). Statistical significance was accepted at $p \leq 0.05$.

In the absence of Na^{+} main effect or interaction, healthy and failing Na^{+} conditions were collapsed together and a separate 3-way (TAC vs. Sham × without vs. with Ca^{2+} × 3 levels of ΔG_{ATP}) mixed ANOVA was performed on $\Delta\Psi$. Statistical significance was accepted at $p \leq 0.05$. A broad overview of the study design can be found in Illustration 5.

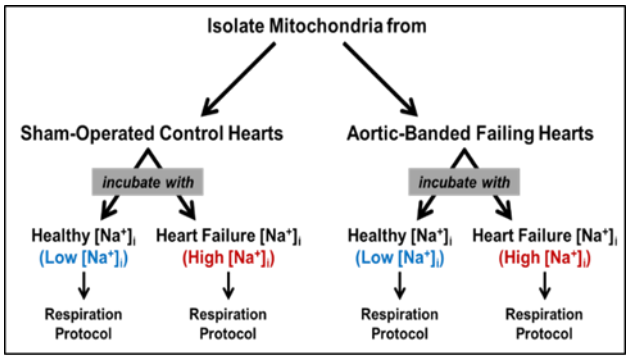

Illustration 5. Schematic overview of Study #2. Isolated cardiac mitochondria from TAC and Sham rats were incubated with healthy or failing [Na^+] to ascertain if mitochondria from failing hearts are inherently altered or influenced by Na^+.

3.3 Results

3.3.1 Animal Characteristics

In the Ca^{2+} dose response assays, sham control (n=5) and TAC rats (n=8) had a combined average surgical age of 35.6±3.3 weeks (mean ± SE), body mass of 623.6±19.2 g, and heart mass of 1.754±0.056 g. Average septal width was 3.22±0.19 mm for sham controls and 3.55±0.26 mm for TAC rats. Average left ventricular (LV) width was 3.98±0.23 mm for sham controls and 4.46±0.15 mm for TAC rats and tended to be different (p=0.051). No significant differences were observed for surgical age, body mass, heart mass, or septal width between sham control and TAC rats. Specific group means and p-values can be found in Table 1.

During the CK clamp assays to assess intermediate mitochondrial respiration, a separate subset of sham control (n=9) and TAC rats (n=10) were used. These animals had an average surgical age of 48.1±3.4 weeks and body mass of 676.7±19.4 g. Average heart mass was 1.743±0.067 g for sham controls and 1.869±0.056 g for TAC

rats and tended to be different (p=0.085). Mean LV width was significantly greater (p<0.01) in TAC (4.47±0.15 mm) than sham control rats (3.57±0.32 mm). Similarly, average septal width was significantly larger (p<0.01) in TAC (3.47±0.19 mm) than sham control rats (2.81±0.17 mm). No significant differences were found for surgical age or body mass. Specific group averages can be found in Table 1.

Another separate subset of sham control (n=4) and TAC rats (n=4) were used in both the ROS and proton leak assays. The average post-surgical age of both sham and TAC rats was 70.4±0.8 weeks, body mass was 762.8±18.5 g, and heart mass was 1.784±0.050 g. Both LV width and septal width of TAC rats (4.56±0.24 and 3.77±0.15 mm, respectively) were significantly greater (p = 0.009, p = 0.004) than sham control (3.61±0.17 and 2.78±0.20). Detailed group means can be found in Table 1.

Table 1. Animal Characteristics

	Ca^{2+} Dose Response		
	Sham Control (n = 5)	TAC (n = 8)	*p* value
Age after surgery (weeks)	34.1 ± 5.3	36.5 ± 4.5	0.370
Body mass (g)	642.3 ± 41.7	611.8 ± 18.9	0.230
Heart mass (g)	1.751 ± 0.116	1.756 ± 0.064	0.483
LV width	3.98 ± 0.23	4.46 ± 0.15	0.051
Septal width	3.22 ± 0.19	3.55 ± 0.26	0.184
	CK Energetic Clamp		
	Sham Control (n = 9)	TAC (n = 10)	*p* value
Age after surgery (weeks)	49.0 ± 4.1	47.3 ± 4.0	0.387
Body mass (g)	691.8 ± 22.5	663.2 ± 23.0	0.195
Heart mass (g)	1.743 ± 0.067	1.869 ± 0.056	0.085
LV width	3.57 ± 0.32	4.47 ± 0.15	0.008*
Septal width	2.81 ± 0.17	3.47 ± 0.19	0.009*
	ROS & Proton Leak		

	Sham Control (n = 4)	TAC (n = 4)	*p* value
Age after surgery (weeks)	70.8 ± 1.9	70.0 ± 1.3	0.379
Body mass (g)	750.5 ± 41.8	775.0 ± 27.2	0.320
Heart mass (g)	1.742 ± 0.112	1.827 ± 0.072	0.272
LV width	3.61 ± 0.17	4.56 ± 0.24	0.009*
Septal width	2.78 ± 0.20	3.77 ± 0.15	0.004*

*Denotes significantly different from sham control

3.3.2 Ca^{2+} Dose Response

Cardiac mitochondria from sham control and TAC rats were incubated with either healthy (5 mM) or elevated (15 mM) Na^+ and underwent a Ca^{2+} dose response to determine if there were any differences in the Ca^{2+} required to elicit maximal mitochondrial respiration. With sham control mitochondria, Ca^{2+} activated respiration ranged from 160.0±15.9 to 426.9±40.1 nmol/mg/min when incubated in 5mM Na^+ and from 193.3±26.9 to 448.5±46.0 nmol/mg/min when incubated in 15mM Na^+ and were not significantly different (p=0.787) (Figure 6A). TAC mitochondria demonstrated Ca^{2+} activated respiration ranging from 198.5±23.3 to 490.7±31.9 nmol/mg/min when incubated in 5mM Na^+ and from 204.6±26.9 to 510.6±44.9 nmol/mg/min when incubated in 15mM Na^+ and were not significantly different (p=0.842) (Figure 6B). The greatest Ca^{2+} activation of mitochondrial respiration occurred at a total Ca^{2+} concentration of 6.2 μM in both sham control and TAC mitochondria. No significant differences were observed for Ca^{2+} activated mitochondrial respiration between sham control and TAC mitochondria (p=0.535).

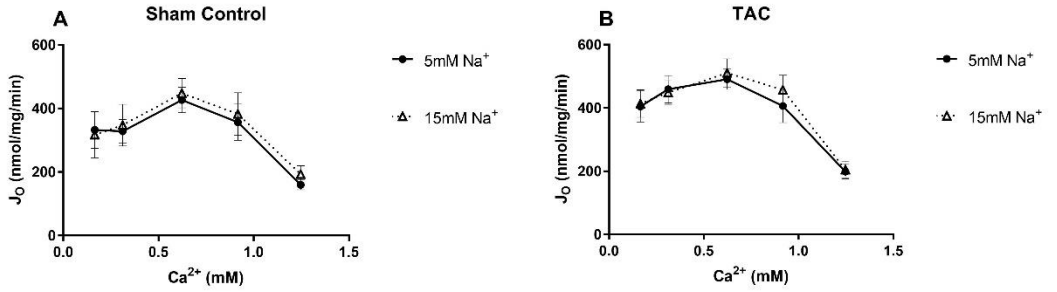

Figure 6. Response of mitochondrial respiration to increasing [Ca^{2+}] when incubated in healthy or failing [Na^{+}] in TAC and sham mitochondria. Maximal J_O was not different between 5 and 15mM [Na^{+}] incubations across [Ca^{2+}] of 0.17, 0.31, 0.62, 0.92, & 1.25mM in either A) sham control mitochondria or B) TAC mitochondria. Maximal J_O was greatest with 0.62mM of Ca^{2+} activation in both A) sham control mitochondria or B) TAC mitochondria.

3.3.3 Intermediate Mitochondrial Function and Energetic Driving Forces

Intermediate mitochondrial function and the energetic driving forces involved were assessed using CK clamp assays. No significant main effect of Na^{+} was found in the Ca^{2+} dose response assays; therefore, comparisons henceforth will be between with and without Ca^{2+} conditions and between sham control and TAC mitochondria. Intermediate respiration was significantly increased ($p<0.001$) by ~1.96 fold in sham control mitochondria and by ~1.56 in TAC mitochondria with a main effect of Ca^{2+} (Figure 7A). The conversion of the free energy in NADH into $\Delta\Psi$ is the primary potential energy for oxidative phosphorylation. These specific force-flow relationships are presented in Figure 7B and 7C where the forces of $\Delta\Psi$ and NADH, respectively, are plotted on the x-axis and the flow of J_O is plotted on the y-axis. Ca^{2+} significantly increased the force-flow relationship ($p=0.010$) by ~1.54 fold in sham control and by ~1.30 in TAC mitochondria for NADH. There was a significant main effect of Ca^{2+} ($p=0.017$) that increased the force-flow relationship by ~1.94 fold in sham control and by ~1.43 fold in TAC mitochondria for $\Delta\Psi$. No significant main effect of Na^{+} or

interaction effects of Na^+ and TAC were found for intermediate mitochondrial respiration or driving forces.

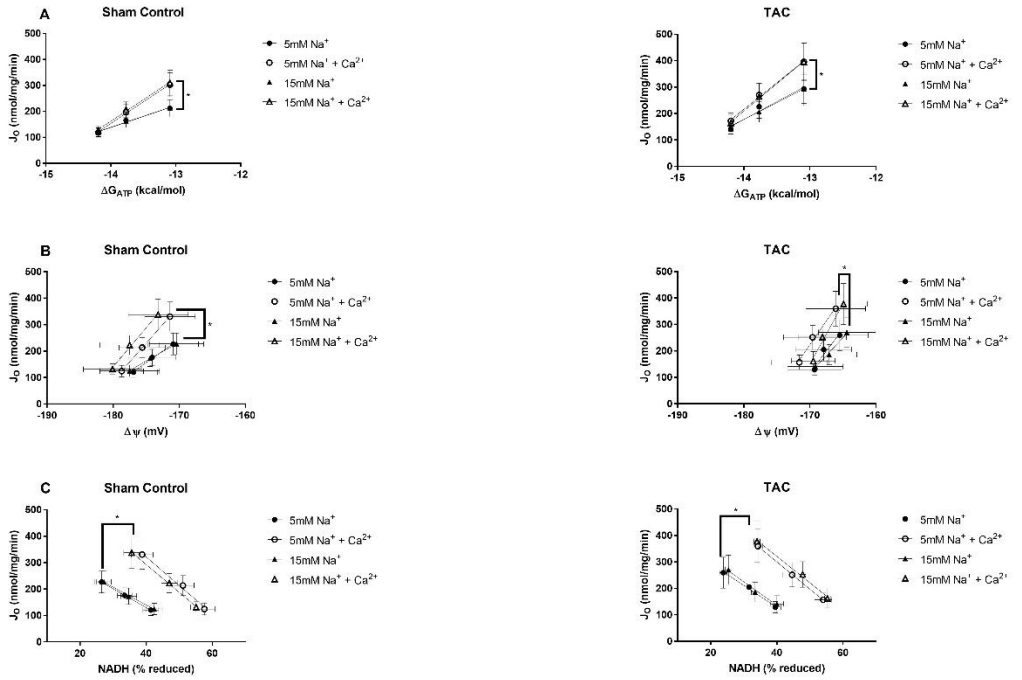

Figure 7. Effect of elevated Na^+ and Ca^{2+} on oxidative phosphorylation energetic driving forces and J_O during intermediate respiration in TAC and sham mitochondria. (A) Relationship between ΔG_{ATP} and J_O in sham control and TAC mitochondria. (B) Relationship between membrane potential ($\Delta\psi$) and J_O in sham control and TAC mitochondria. (C) Relationship between NADH and J_O in sham control and TAC mitochondria. Error bars indicate standard error. Sham control: n = 7; TAC: n = 9. Main effect of Ca^{2+} on respective slopes, *p<0.05.

A separate three-way ANOVA (animal × Ca^{2+} × ΔG_{ATP}) was performed to evaluate the differences in $\Delta\Psi$. There was a significant main effect of ΔG_{ATP} ($p<0.001$) in which $\Delta\Psi$ decreased from -168.3±2.9 to -171.8±2.8 to -174.1±2.7 at -13.1, -13.8, and -14.2 kcal/mol, respectively. Interestingly, there was a significant interaction effect of ΔG_{ATP} and TAC ($p=0.005$) such that TAC mitochondria had lower $\Delta\Psi$ and range of $\Delta\Psi$ (-165.2±3.8 to -169.9±3.6 mV) compared to sham mitochondria (-171.5±4.3 to -178.3±4.1 mV) across ΔG_{ATP} of -13.1 to -14.2 kcal/mol. The interaction effect of ΔG_{ATP} and Ca^{2+} tended to be different ($p=0.058$) such that the average difference was 1.1±0.8, 1.8±0.9, and 1.7±1.0 mV at ΔG_{ATP} of -13.1, -13.8, and -14.2 kcal/mol

respectively. These findings demonstrate that Ca^{2+} activated improvements to mitochondrial conductances are maintained in failing mitochondria.

3.3.4 Mitochondrial Conductance

The conductance of the entire oxidative phosphorylation pathway, ETC, and Complex V and ANT can be determined by plotting J_O against $\Delta G_{NADH} - \Delta G_{ATP}$, $\Delta G_{NADH} - \Delta G_{\Delta\Psi}$, and $\Delta G_{\Delta\Psi} - \Delta G_{ATP}$, respectively. The overall L_{oxphos} demonstrated a significant increase due to Ca^{2+} activation ($p=0.003$) by ~1.55 fold in sham control and ~1.69 fold in TAC mitochondria (Figure 8A). Ca^{2+} appeared to increase L_{ETC} by ~2.01 fold in sham control and ~1.05 fold in TAC mitochondria (Figure 8B); however, no main or interaction effect was found involving Ca^{2+}, Na^{+}, or animal type for L_{ETC}. Similarly, L_{ATPase} showed a significant increase due to Ca^{2+} activation ($p<0.001$) by ~2.11 fold in sham control and ~1.77 fold in TAC mitochondria (Figure 8C). Although not significant, the interaction effect of Ca^{2+} with TAC condition tended to be different ($p=0.060$) for L_{ATPase}.

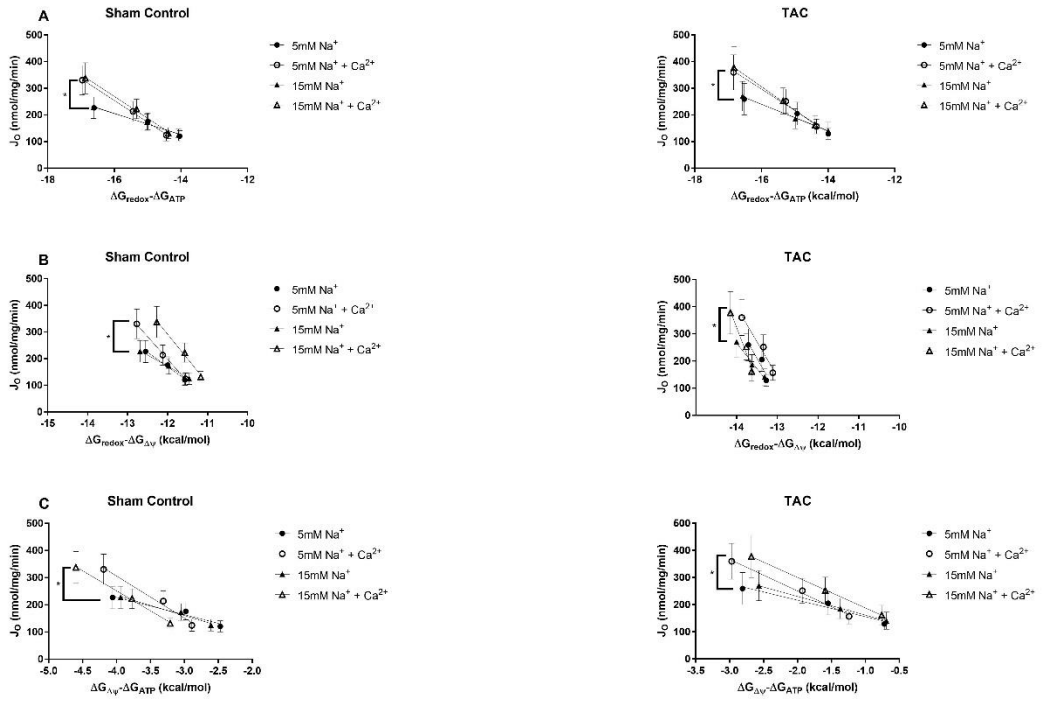

Figure 8. Effect of elevated Na^+ and Ca^{2+} on mitochondrial conductance in TAC and sham mitochondria. (A) Relationship of J_O and the free energy difference between redox potential and ΔG_{ATP} representing the conductance of the oxidative phosphorylation pathway (L_{oxphos}) in sham control and TAC mitochondria (B) Relationship of J_O and the free energy difference between redox potential and $\Delta\psi$ representing the conductance of the electron transport chain (L_{ETC}) in sham control and TAC mitochondria. (C) Relationship of J_O and the free energy difference between $\Delta\psi$ and ΔG_{ATP} representing the conductance of Complex V and ANT translocase (L_{ATPase}) in sham control and TAC mitochondria. Error bars indicate standard error. Sham control: n = 7; TAC: n = 9. Main effect of Ca^{2+} on respective slopes, * $p<0.05$.

3.3.5 ROS production

ROS production was measured by Amplex Red assay for H_2O_2 production with or without Ca^{2+} in isolated cardiac mitochondria from sham (n=4) and TAC (n=4) rats. No main effect of Ca^{2+} nor of TAC and no interaction effect of Ca^{2+} and TAC were observed at ΔG_{ATP} of -13.1, -13.8, and -14.2 kcal/mol on H_2O_2 production (Figure 9A). These results demonstrate that neither Ca^{2+} nor TAC increase H_2O_2 production in isolated cardiac mitochondria.

Percent free radical leak was calculated by half of the quotient between H_2O_2 production and J_O. No main effect of Ca^{2+} nor of TAC and no interaction effect of Ca^{2+}

and TAC were observed at ΔG_{ATP} of -13.1, -13.8, and -14.2 kcal/mol on percent free radical leak (Figure 9B). These results demonstrate that Ca^{2+} nor TAC impact the percentage of J_O that is leaked as free radicals in isolated cardiac mitochondria.

Conductance through the ROS leak was determined from the slope of H_2O_2 production against the free energy difference across the ETC (ΔG_{redox}-$\Delta G_{\Delta\Psi}$). No main effect of Ca^{2+} nor of TAC and no interaction effect of Ca^{2+} and TAC were observed on the conductance of the ROS leak pathway (Figure 9C). These results suggest that conductance through the ROS leak pathway is independent of Ca^{2+} activation and TAC.

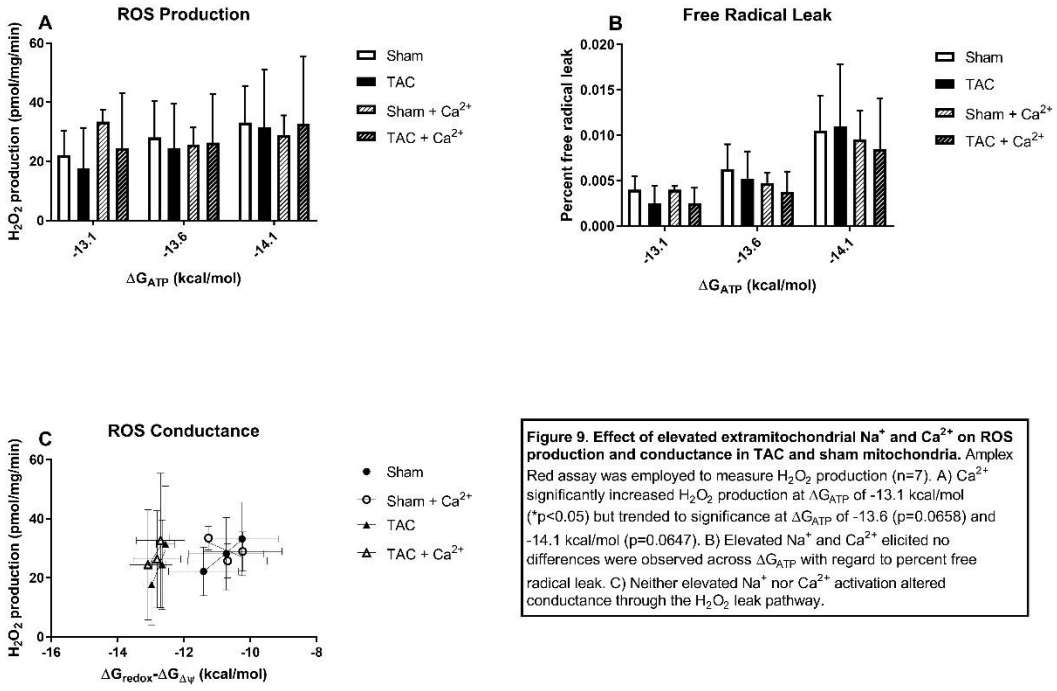

Figure 9. Effect of elevated extramitochondrial Na^+ and Ca^{2+} on ROS production and conductance in TAC and sham mitochondria. Amplex Red assay was employed to measure H_2O_2 production (n=7). A) Ca^{2+} significantly increased H_2O_2 production at ΔG_{ATP} of -13.1 kcal/mol (*p<0.05) but trended to significance at ΔG_{ATP} of -13.6 (p=0.0658) and -14.1 kcal/mol (p=0.0647). B) Elevated Na^+ and Ca^{2+} elicited no differences were observed across ΔG_{ATP} with regard to percent free radical leak. C) Neither elevated Na^+ nor Ca^{2+} activation altered conductance through the H_2O_2 leak pathway.

3.3.6 Proton Leak

To determine if Ca^{2+} and/or TAC altered mitochondrial proton leak, state 4 oxygen consumption was assessed against membrane potential in isolated cardiac mitochondria from sham (n=4) and TAC (n=4) rats. Comparisons were performed on

calculated J_O from exponential regressions of proton leak assays at ΔΨ of -180 and -150 mV. No main or interaction effect of Ca^{2+} and TAC were observed in mitochondrial proton leak at -180 mV (Figure 10B) or -150 mV (Figure 10C). These results suggest that neither Ca^{2+} nor TAC alter the proton leak pathway in isolated cardiac mitochondria.

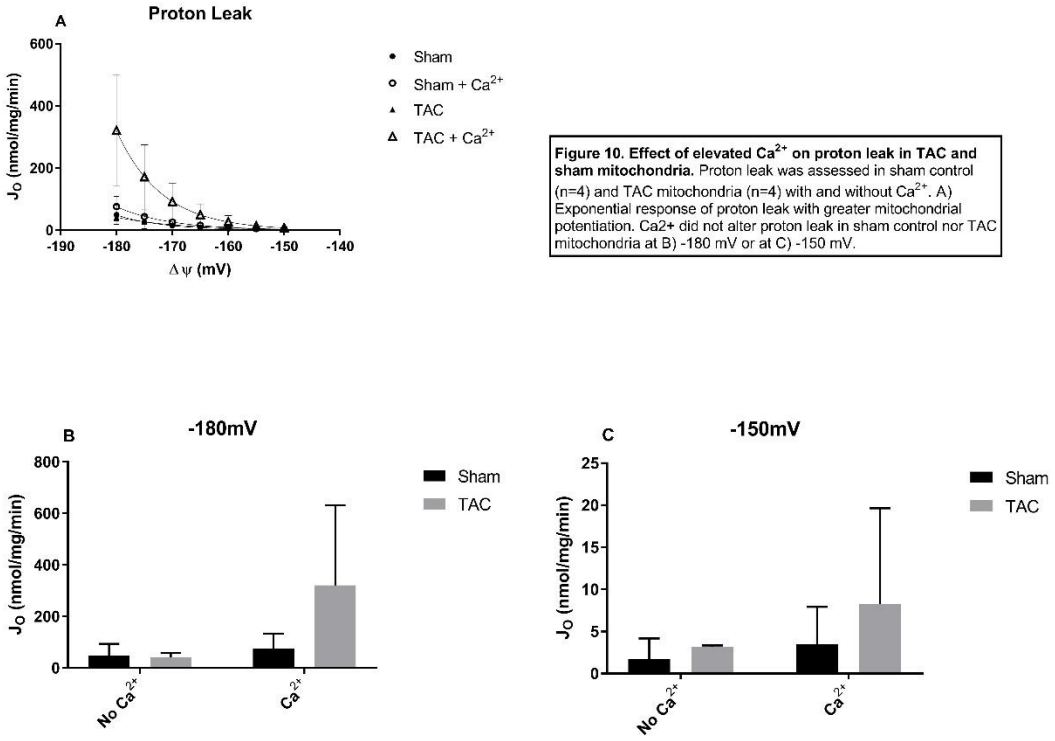

Figure 10. Effect of elevated Ca^{2+} on proton leak in TAC and sham mitochondria. Proton leak was assessed in sham control (n=4) and TAC mitochondria (n=4) with and without Ca^{2+}. A) Exponential response of proton leak with greater mitochondrial potentiation. Ca2+ did not alter proton leak in sham control nor TAC mitochondria at B) -180 mV or at C) -150 mV.

3.4 Discussion

It has been reported that cardiac tissue from animal models and patients with HF have elevated levels of Na^+ and Ca^{2+}[128,132], which has been theorized to adversely alter mitochondrial function[132]; further, previous results from healthy rat ventricular tissue demonstrated that altering Na^+, or Na^+ and Ca^{2+} together, were insufficient to adversely affect mitochondrial function. The present study addresses whether altering

extramitochondrial Na^+ around isolated failing mitochondria is not enough to adversely impact mitochondrial function.

This study investigated the combined effects of Na^+ and Ca^{2+} on mitochondria isolated from Sprague-Dawley rat hearts with pressure-overload induced hypertrophy. By isolating cardiac mitochondria from sham control and TAC hearts, we were able to introduce and control the specific extramitochondrial conditions and observe whether the effects only manifest themselves in the HF model. More specifically, we incubated isolated mitochondria from failing and healthy rat hearts in either control (5 mM) or HF levels (15 mM) of Na^+ and observed whether Ca^{2+}-activated mitochondrial function was adversely affected under maximal and submaximal conditions. Our findings demonstrate that Ca^{2+} activation of mitochondrial function is similar between sham control and TAC mitochondria. Furthermore, Ca^{2+} activation of mitochondrial function is preserved regardless of the extramitochondrial levels of Na^+ in both sham control and TAC mitochondria. These results suggest that HF levels of Na^+ do not appear to negatively impact Ca^{2+} activated maximal respiration capacity in failing mitochondria. Similar findings have been reported in isolated left ventricular mitochondria from human failing hearts[202,207] in which mitochondrial function was preserved. However, other animal models, using coronary microembolization[208], rapid ventricular pacing[209], or drug-induced hypertension[210] to cause HF have demonstrated impaired mitochondrial oxidative phosphorylation. Reduced respiratory capacity has been reported in aortic-banded rats, but only when these animals have developed impaired ejection fraction[211]. Although the two dominant forms of HF, HFpEF and HFrEF,

manifest an inadequate cardiac output, the specific changes affecting mitochondrial function lending to insufficient hemodynamics may be different.

This the first study to explore the combined effects of Na^+ and Ca^{2+} on cardiac mitochondria from failing hearts, and we also assessed mitochondrial function measures beyond simply maximal respiration. By employing a CK energetic clamp and observing submaximal respiration, the forces, flux, and conductance of the full oxidative phosphorylation pathway and its components were observed and analyzed. Our findings reveal that isolated failing mitochondria respire similarly to healthy mitochondria in the presence of extramitochondrial Ca^{2+} regardless of Na^+ levels at all submaximal levels. It appears Ca^{2+} improved both redox and membrane potential as well as the conductance of the ETC, the ATP synthase/ANT, and the full oxidative phosphorylation pathway. These findings are in agreement with Ca^{2+} activation of mitochondrial respiration in porcine skeletal[167], cardiac muscle[127], and our previous findings in isolated mitochondria from healthy rat hearts. It has been previously demonstrated that Ca^{2+} uptake through the MCU increases mitochondrial matrix Ca^{2+} to increase NADH production[165,166], ETC conductance[167], and ATP synthase activity[127], which has been recapitulated in our study.

Interestingly, there was a significant interaction effect of ΔG_{ATP} and TAC such that TAC mitochondria demonstrated lower membrane potential and a blunted ability to potentiate the membrane. These findings would suggest that the driving force that is the proton gradient necessary for ATP production during oxidative phosphorylation is lower in TAC mitochondria. Although the maximal respiration in TAC mitochondria does not appear to be different than sham control mitochondria, these results suggest

that ATP production may be hampered in this model of HF and may help explain the reduced hemodynamic response in the HF condition. Although only one other group has reported lower mitochondrial membrane potentials in cardiomyocytes isolated from canines with chronic HF[212,213], to our knowledge, we are the first to demonstrate that isolated mitochondria from rats with HF have an impaired ability to polarize their membrane.

The findings for intermediate mitochondrial function, proton leak and ROS production were interpreted with Na^+ conditions collapsed together. This was performed primarily because no significant differences between Na^+ conditions were observed for intermediate mitochondrial function, proton leak, and ROS production. The primary goal was to determine if failing mitochondria demonstrated impaired intermediate mitochondrial function, larger proton leak, and more electron leak than healthy mitochondria, so collapsing the Na^+ conditions together allowed for greater statistical power to examine these differences, or lack thereof.

Proton leak and ROS production were investigated to ascertain whether these were possible sources contributing to the lower membrane potential and diminished membrane potentiation in TAC mitochondria. No statistical differences were found between TAC and sham control mitochondria regarding proton leak or ROS production suggesting that another factor may be involved in the aberrant nature of the TAC mitochondrial membrane potential. Proton leak has been reported to be increased in hearts of a fly model of HF; however, in the same study, isolated cardiomyocytes from catecholamine-injected mice exhibited no differences in proton leak compared to the vehicle control[214] suggesting that differing models of HF may not have the same

metabolic alterations. Aging models of HF in mice and rats have demonstrated greater proton leak than younger counterparts[215]. The lack of an age difference between our TAC and sham controls may explain why no differences in proton leak were found in this study. ROS production has been found to be greater in failing cardiomyocytes from guinea pigs[216], failing myocardial tissue from mice[217], and failing ventricular tissue from dogs[218,219]. The post-intervention age of these animals was relatively young (~4-8 weeks post-intervention) compared to the animals within this study (~35-70 weeks post-intervention), suggesting that the greater ROS production observed could be of an acute nature. Although oxidative stress has been reported to increase with age in humans[220,221], antioxidant capacity also appears to increase with age[222,223]. Thus, it is possible that our animals have developed a greater antioxidant capacity with age resulting in no observable differences in ROS production. Together, the results suggest that the deficits observed in TAC membrane potential are not due to changes in cardiac mitochondrial proton leak or ROS production.

The present findings are the first to demonstrate the combined effects of elevated Na^+ and Ca^{2+} on mitochondrial function in isolated cardiac mitochondria from rats with pressure-overload induced HF. Elevated Na^+ did not alter the optimal Ca^{2+} required for maximal respiration in TAC compared to sham control mitochondria. Ca^{2+} activation was preserved and promoted redox potential, membrane potential, and conductance of all components of the oxidative phosphorylation pathway, regardless of Na^+ levels. However, isolated mitochondria from TAC rats had lower membrane potentials and were unable to potentiate their membranes to the same degree as their sham counterparts suggesting that the electrochemical driving force required to

produce ATP is diminished, which may contribute to the systolic and diastolic dysfunction in HF. Moreover, the two major leak pathways, as protons or ROS, do not appear to be any greater in TAC suggesting there may be another source that is contributing to this membrane potential deficit. Although the current study has found this deficit in mitochondrial function in male rats of pressure-overload induced HF, it is unknown whether this alteration is recapitulated or exacerbated in female rats. HFpEF, which the pressure-overload model generally manifests, has a greater prevalence in older females suggesting that manifestation of mitochondrial alterations may be different according to sex. While HFpEF has a greater prevalence in females than males, males with HFpEF have worse survivability[224] suggesting that mitochondrial dysfunction may have a differential impact according to sex. Therefore, it will be important to ascertain the link between membrane potential deficit and ATP production in HF, the mechanisms behind this diminished membrane potential, and whether these deficits are also exhibited in females with HF for future investigations.

Chapter 4: In Vivo and Ex Vivo Assessments of Exertional Tolerance in Rats with Pressure Overload Induced Heart Failure

4.1 Introduction

The results of the two previous studies suggest that an elevation in extramitochondrial Na^+ environment alone is not sufficient to adversely alter mitochondrial function in cardiac mitochondria from healthy or failing hearts. Perhaps more importantly, cardiac mitochondria from failing hearts demonstrated a lower membrane potential and a reduced capacity to potentiate their membrane compared to isolated mitochondria from healthy hearts. This deficiency in mitochondrial membrane potential suggests a reduction in electrochemical driving force required for ATP production by ATP synthase. In other words, there is an intrinsic alteration in cardiac mitochondria resulting in a more costly production of ATP.

During graded exercise, when the demand and turnover of ATP rises, this more costly production of ATP may be a limiting factor in cardiac force production resulting in a lower cardiac output and VO_2 max in patients with HF. This less efficient production of ATP may potentially explain, at least in part, the inability of failing hearts to match the demands of the body, particularly during activities of heightened physical exertion, manifesting as exercise intolerance.

Impaired exercise tolerance is a cornerstone characteristic of HF. It is indicated by fatigue, palpitations, and dyspnea that worsen with exertion, and is the basis of the

New York Heart Association Functional Classification[225]. Even though exercise intolerance is a critical functional marker of HF, there are few small animal models of HF that demonstrate this important phenotypic characteristic[110,226,227]. Although mice with TAC exhibit exercise intolerance as reduced VO_2 peak on a graded exercise test[227], there has been no study, to our knowledge, that has investigated a functional measure of exercise intolerance in rats with TAC. Therefore, we expected to observe deficits in exertional and functional capacity of this rodent model of HF to demonstrate its translational value in future studies of this disease.

4.2 Methods

4.2.1 Animals and Transverse Aortic Constriction Surgery

All protocols for animal handling and exercise testing were approved by the University of Maryland's Institutional Animal Care and Use Committee (IACUC). The University of Maryland at College Park is an AAALAC-accredited institution. A total of 27 male (n=16) and female (n=11) Hilltop Sprague-Dawley rats were used in this study.

Male and female Sprague-Dawley rats 4 weeks of age underwent TAC or sham surgery. Each animal was weighed then anesthetized via inhalation of isoflurane (2% isoflurane supplemented with 100% oxygen (400-500 mL/min)). After the anesthesia had taken effect and the animal was unresponsive to tail and toe pinches, a single dose of buprenorphine (0.05-0.1 mg/kg) was injected via subcutaneous injection. A surgical area was clipped clean of fur, sterilized with sequential swabs of alcohol-betadine-alcohol, and, after another reflex check via tail and toe pinches, a longitudinal skin

incision was made from the ventral mid-neck area to the suprasternal notch region. Submandibular salivary glands and the sternohyoid muscle were gently separated to reveal the trachea and the left and right common carotid arteries. The sternum was cut as low as the 4th rib and the thymus was retracted to reveal the aortic arch. A 4-0 silk suture was passed around the aortic arch between the origin of the innominate artery and the left common carotid artery. Correct placement was confirmed by pulling up on the suture and observing increased flow through the right common carotid artery and ceased flow through the left common carotid artery. A blunted, 20-guage needle was placed adjacent to the aorta and a 4-0 suture was tied tightly around the aorta and the needle. The needle was then removed, resulting in a chronic partial aortic constriction. Sham-operated controls underwent the same procedure; however, the suture was not tied. The sternum was closed with a single suture, the salivary glands were replaced, and the skin was sutured shut with 5-0 monofilament suture and treated with betadine. Illustration 4 provides a graphical representation of the transverse aortic constriction in rats.

After skin closure, the rat was removed from anesthesia and placed on its side into a clean cage with a heating pad for recovery until spontaneous movement occurred. Once the rat was awake and self-propping, the heating pad was removed. Continual post-operation observation occurred for one hour after the animal recovered from anesthesia and every 12 hours for the subsequent three days.

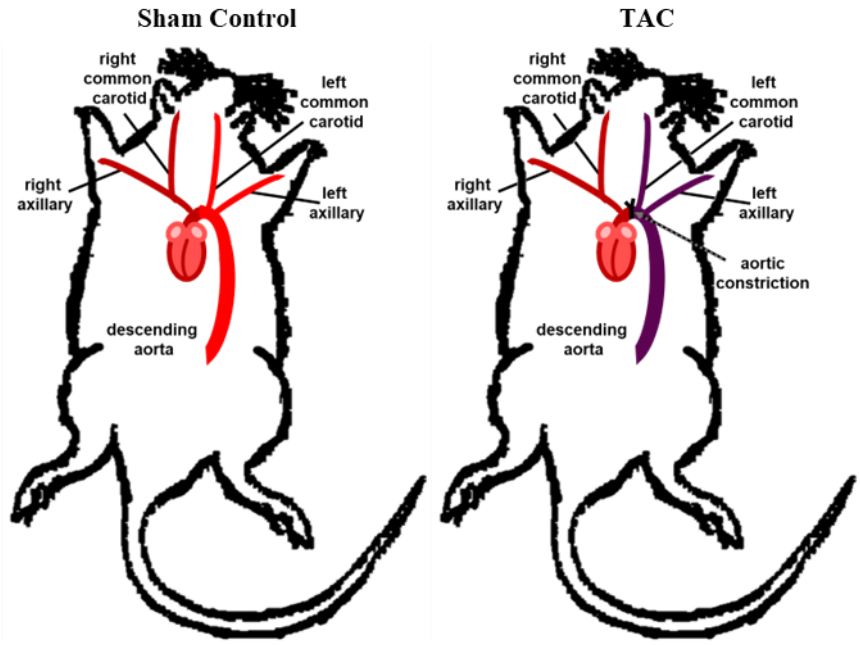

Illustration 4. Overview of the transverse aortic constriction surgical intervention. Left: Sham control rat without aortic constriction. Right: Rat with transverse aortic constriction (TAC) between the innominate (not labeled) and left carotid artery. Successful placement of the constriction will induce chronic pressure overload on the heart.

4.2.2 Treadmill Acclimatization

A Columbus Instruments Exer 3/6 Treadmill with an electrically charged grid on the downhill end was used to assess the maximal exercise capacity of rats. Starting from 20 weeks post-surgery, rats (TAC or sham control) underwent an acclimatization period on the treadmill every 10 weeks. Rats were placed on the treadmill with 5% grade for 5-10 min of quiet rest on the first day as an introduction to the machine. The rats then ran on the treadmill for 10 min/day for 4-5 days at progressively increasing speeds over the course of each day. Rats initially began acclimatization at 5 m/min for 2 min, then an additional 2.5-5 m/min increase in treadmill speed every 2 min until 10 min of running was completed. Each subsequent day, the initial speed began 2.5 or 5 m/min faster than the previous session depending on performance. If the rat was unable

to keep up with the treadmill, the initial speed was returned to the speed of the previous session to an attempt to encourage participation and discourage attrition. The treadmill and electrical grid were shut off when the rat touched the electrical grid 6 times during a 30 sec period. After each bout of treadmill running, the rats were allowed 5 min of quiet rest on the treadmill before they were returned to their cages. The following week, the rats underwent a maximal exercise test, a slow speed (15 m/min) endurance test, and a fast speed (25 m/min) endurance test, with each test occurring on separate days at least 48 hours apart.

4.2.3 Treadmill Running

Maximal exercise testing was performed to assess the peak running speed of TAC and sham control rats. Exercise tests were evaluated by one experimenter who was not blinded to the rats' surgical condition. Rats were placed onto the treadmill with 5% grade, which was left unchanged for all exercise tests, and allowed 5 min of quiet rest with the electrical grid off to minimize anxiety. Subsequently, the electrical grid was turned on and the shock was titrated down to the lowest level that was sufficient to stimulate the animal to run without harming the animal (1 Hz, ~10-30V, 0.5A). Rats began the maximal exercise test with brief warmup period of 15 m/min for 3 min before increasing the treadmill speed by 5 m/min every minute until exhaustion or was unable to keep up with the treadmill, More specifically, if the rat was unable or unwilling to maintain the treadmill pace despite stimulation from the electrical grid for approximately 6 shocks during a 30 sec time period on the electrically charged grid[228], then the electrical grid and the treadmill are stopped. If a rat previously demonstrated poor running performance, as indicated by an inability to adapt quickly to changes in

treadmill speed and/or dragging of paws against the treadmill belt, during the acclimatization period, then the maximal exercise test began with a warmup of 10 m/min for 3 min and subsequent speed increase of 2.5 m/min every minute. The treadmill speed at the time of test termination was recorded and used for analysis.

Two endurance tests, one at a slow (15 m/min) and one at a fast (25 m/min) pace, were employed to assess the endurance capacity of TAC rats. Each test was employed on separate days with at least 48 hours between each test. Prior to the endurance test, rats were placed onto the treadmill with the electrical grid off and allowed 5 min of quiet rest. The test then began with a 10-sec ramp up to the final speed (15 or 25 m/min). The test continued until the animal refused to run or contacted the electrical grid 6 times during a 30-sec period[228] in which case the treadmill was stopped and the electrical grid was shut off. The distance and running time were recorded, and endurance was determined by the work performed on the test. Work was calculated as

$$W = F \times D$$

$$W = mg \times (5\% \times d)$$

where work is W, force is F, distance is D, body mass is m, g is acceleration due to gravity, d is the treadmill distance, and vertical distance traveled is 5% of d. After each treadmill test, rats were allowed to rest quietly on the treadmill for 5 min then weighed and returned to their cages. These testing procedures were approved by UMD's IACUC.

4.2.4 Forelimb Grip Strength Testing

A grip strength meter (Ugo Basile) was used to assess the strength capacity of the forelimb muscle of rats with TAC. On the day of sacrifice, about 40 weeks post-surgery, a rat was held over the base plate, in front of a T-shaped grasping bar that connected to a force sensor. The rat was allowed to grasp the bar with both forelimb paws and pulled away by the tail until grip was released. Only measures with both forelimb paws with intentional grasping were accepted. Each rat underwent several trials until three successful grips were performed, and the data were recorded onto the grip strength meter. Rats were subsequently weighed just prior to sacrifice. This procedure was approved by UMD's IACUC.

4.2.5 Skeletal Muscle Excision and Isolated Muscle Testing

On the day of sacrifice, rats were anaesthetized as described above (please refer to 3.2.2 Mitochondrial Isolation from Cardiac Tissue). After the animal was sacrificed via rapid cardiac exsanguination, the skin on the forelimbs was removed to expose the musculature underneath. The left and right biceps were excised by first cutting the origin tendon, cutting away the connective tissue, and severing the insertion tendon. The left and right biceps were weighed, washed with 1X PBS, and stored away at -20ºC for future studies. Lungs were also excised, dabbed free of blood, weighed, and placed in an incubator to dry for a week, and then weighed again. The wet-to-dry lung weight ratio was calculated and recorded for analysis.

Isolated skeletal muscle force production was assessed to ascertain the intrinsic maximal functional capacity of slow (soleus) and fast twitch (extensor digitorum

longus) hindlimb skeletal muscle in TAC rats. To excise the soleus and extensor digitorum longus muscle (EDL), the skin on the hindlimb of the rat was removed to expose the musculature underneath, and the tibialis anterior was removed. Two separate sutures were thread underneath the proximal and distal tendons of the EDL muscle and tied off with loops. The muscle was then excised off the hindlimb with the suture loops intact on the tendons. To access the soleus muscle, the Achilles tendon was severed, and the gastrocnemius muscle was reflected away. Like the EDL, two suture loops were created on the proximal and distal end, then the muscle was excised. Both excised muscles were transferred to ice cold Ringer's solution. Just prior to testing, each muscle was transferred to the Aurora Scientific 3-in-1 Whole Animal System horizontal muscle bath that was filled with Ringer's solution bubbled with 100% O_2 at 37ºC.

On the Aurora muscle system, one loop is attached to an anchor point and the other was attached to an adjustable force transducer. The force transducer was gently pulled away to apply <5 mN of tension on the muscle. To ensure adequate electrical stimulation is applied to the entire muscle, current was increased until resting tension plateaued then current was further increased by 10%. In order to obtain optimal length for maximal force production, the muscle underwent single twitch contractions at 1 Hz followed by stretching the passive tension by about 10 mN and continued until maximum twitch force was recorded.

Following the optimization of muscle length and maximal twitch force measurement, the muscles underwent a force-frequency protocol to assess alterations in tension production across different frequencies. During the force-frequency

protocol, the muscle was stimulated across 9 frequencies (i.e., 10, 20, 40, 50, 60, 80, 100, 120, and 140 Hz) with 1-min rest periods between each stimulation. The maximum tension production was recorded for each frequency.

Each muscle was allowed to rest for a period of 2 min before undergoing the fatigue protocol to assess the ability of the muscle to resist a decline in force production. In this protocol, the muscle was stimulated at 100 Hz each second for 5 min. Fatigue was assessed as the time taken to reach 50% of maximum force production.

4.2.6 Statistical Analysis

Statistical analyses were performed with IBM SPSS Statistics Version 28.0.0.0. Differences in body mass, heart mass, LV width, septal width, and wet-to-dry lung weight ratios were analyzed using a two-way (TAC vs. sham × sex) ANOVA. A one-tailed Student's t-test was used to analyze the difference in left and right biceps size for TAC female, TAC males, sham females, and sham males. For treadmill running, the same two-way ANOVA was performed for maximal speed, work performed at 15 m/min, and work performed at 25 m/min. Two Chi-square tests were performed to determine if sex or TAC had any association with running compliance, which was measured by recording when the animals refused to run at the start of an exercise test. A two-way (TAC vs. sham × sex) ANOVA was performed on grip strength, grip strength relative to body mass, and grip strength relative to tibial length. For isolated skeletal muscle tests, soleus and EDL muscle were each analyzed using a two-way (TAC vs. sham × sex) ANOVA on peak force for each frequency, peak force relative to muscle mass, and time to fatigue.

4.3 Results

4.3.1 Animal Characteristics

Some physical characteristics of TAC and sham rats of both sexes were measured to determine if this model recapitulated characteristic manifestations experienced by patients with HFpEF, such as cardiac hypertrophy and pulmonary edema. There was significant main effect of sex such that males had a greater body mass (603±9 g vs. 326.2±11.4 g; $p<0.001$; Figure 11A) and tibial length (52.45±1.47mm vs. 42.77±1.80 mm; $p=0.001$; Figure 11B) than females. There were no statistical difference between TAC (4.53±0.04) and sham rats (4.43±0.04) in their wet-to-dry lung weight ratio ($p=0.095$; Figure 11C).

Left and right biceps muscle masses were compared with each other to evaluate if TAC could affect muscle size given that the constriction could alter blood flow to the left and right forelimbs (Figure 11D). TAC females exhibited significantly smaller left biceps mass (0.236±0.006 g) than right biceps mass (0.288±0.018 g; 1-tailed $p=0.012$). Neither sham females (left vs. right; 0.250±0.019 g vs. 0.236±0.011 g; $p=0.274$), TAC males (0.405±0.013 g vs. 0.401±0.0s13 g; $p=0.410$), nor sham males (0.396±0.018 g vs. 0.393±0.015 g; $p=0.435$) shared these same left and right biceps mass differences.

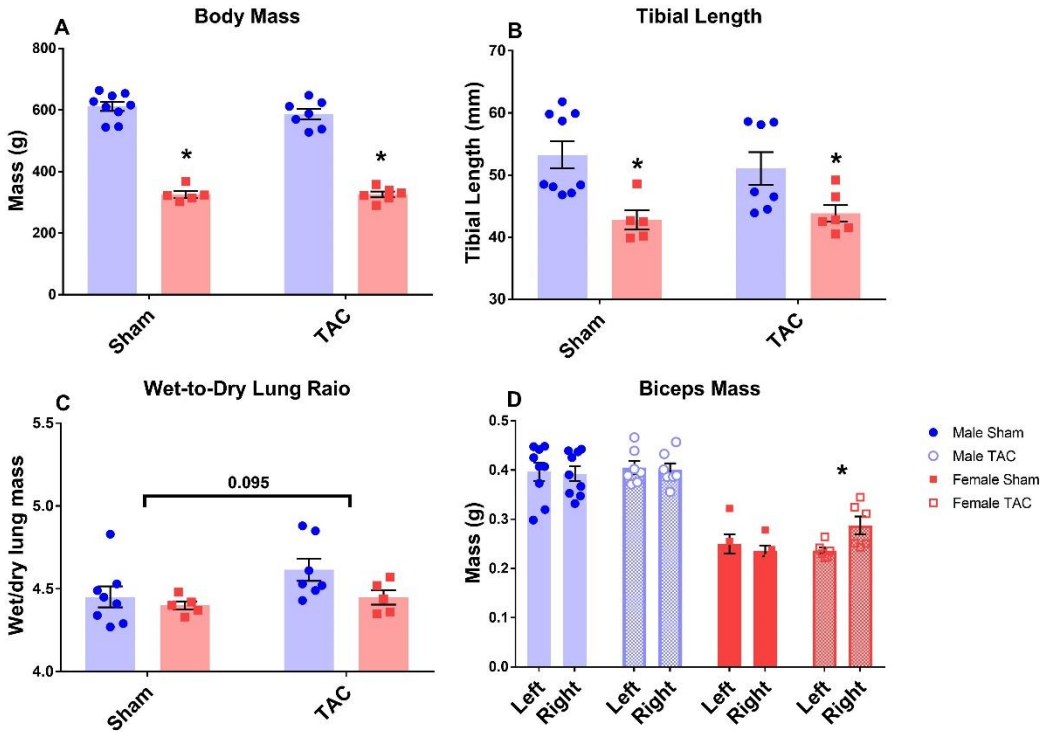

Figure 11. Body phenotype of TAC and sham rats. Males are colored blue and females are colored red. General sizes were measured by A) body mass and B) tibial length..Pulmonary congestion was estimated using C) wet-to-dry lung ratio. Forelimb size difference was measured by D) left and right biceps mass. Main effect of TAC, ^p<0.05. Main effect of sex *p<0.05

There was a main effect of sex such that males had greater heart mass (1.81±0.04 g vs. 1.09±0.05 g; p<0.001; Figure 12A) and LV width (4.39±0.08 mm vs. 3.64±0.10 mm; p<0.001; Figure 12B) than females. There was a significant main effect of TAC in that TAC had greater LV width (4.22±0.09 mm vs. 3.81±0.09 mm; p=0.004) (Figure 12B) and LV width relative to body mass (9.90±0.27 mm/g vs. 8.63±0.26 mm/g; p=0.003) (Figure 12E) than sham controls, respectively. Females had a significantly greater heart-to-body mass ratio (3.34±0.12 vs. 3.02±0.10; p=0.042; Figure 12D), LV width relative to body mass (11.21±0.29 mm/g vs. 7.32±0.24 mm/g; p<0.001; Figure 12E), and septal width relative to body mass (9.14±0.34 mm/g vs. 5.60±0.28; p<0.001; Figure 12F) compared with males.

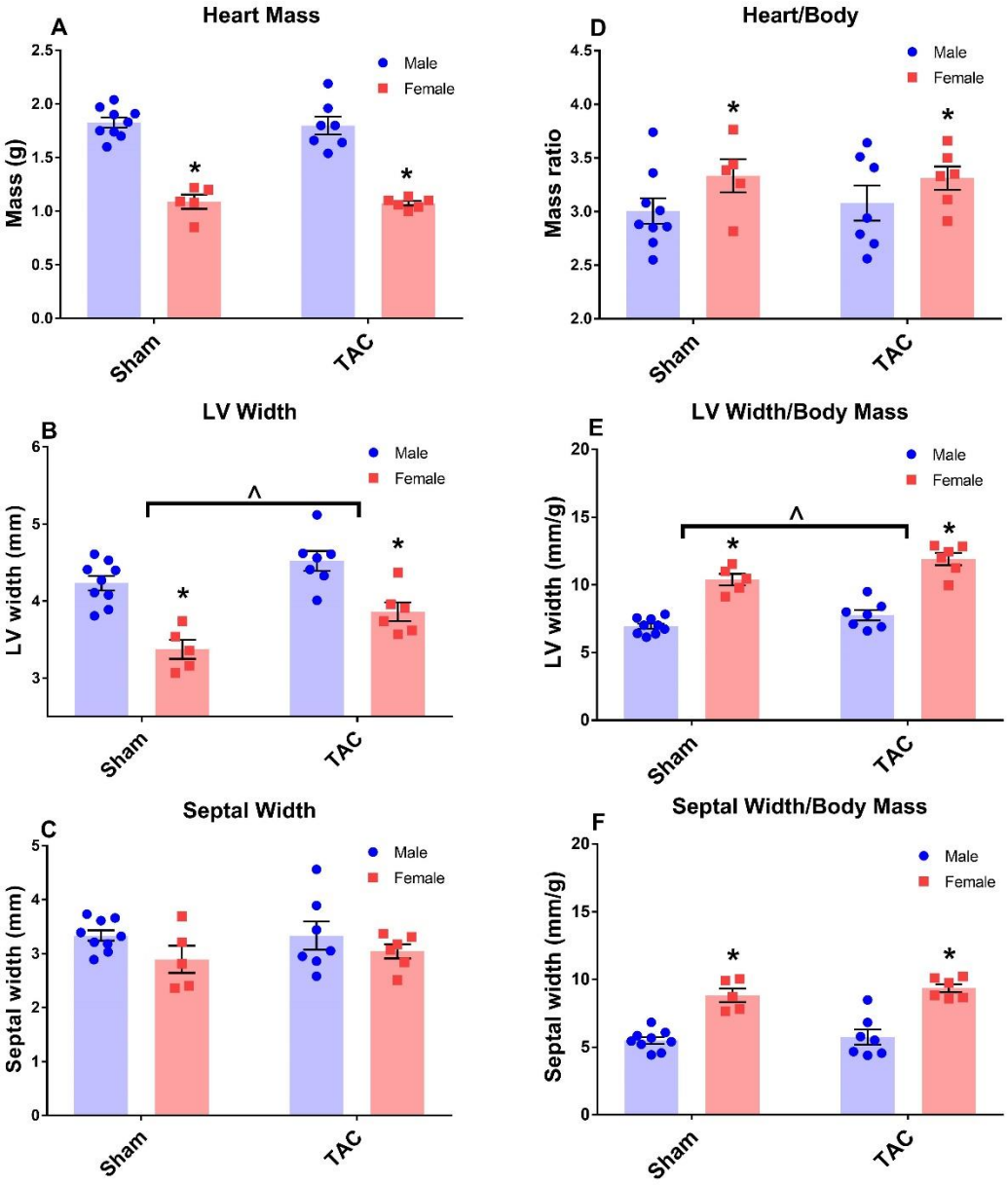

Figure 12. Heart phenotype of TAC and sham rats. Absolute A) heart mass, B) LV width, and C) septal width measured on the day of sacrifice. Normalization to body mass (D-F). Main effect of TAC, ^p<0.05. Main effect of sex, *p<0.05

4.3.2 Maximal and Endurance Capacity with Treadmill Running

Of the 27 rats that were included in this study, 13 rats completed all treadmill running tests. Of the 13 TAC rats, 6 completed all treadmill running tests while 7 of the 14 sham control rats completed all treadmill running tests. Noncompliance was

defined as refusal to begin running during the start of an exercise test. Surgical condition was not significantly associated with treadmill running noncompliance (p=0.842). Females (8 of 11 female rats) were significantly more likely to complete all treadmill running tests than males (5 of 16 male rats; p=0.034).

No significant differences were found between TAC and sham control rats regarding maximum running speed (Figure 13A), work performed during slow speed (Figure 13B), or work performed during fast speed (Figure 13C). Female rats ran significantly faster (28.4±1.6 m/min vs. 21.3±2.1 m/min; p<0.023) and had greater maximal work capacity at 15 m/min (309.5±18.6 J vs. 26.9±24.7; p<0.001) and 25 m/min (29.6±4.4 J vs. 10.6±5.7 J; p=0.027) than male rats, respectively.

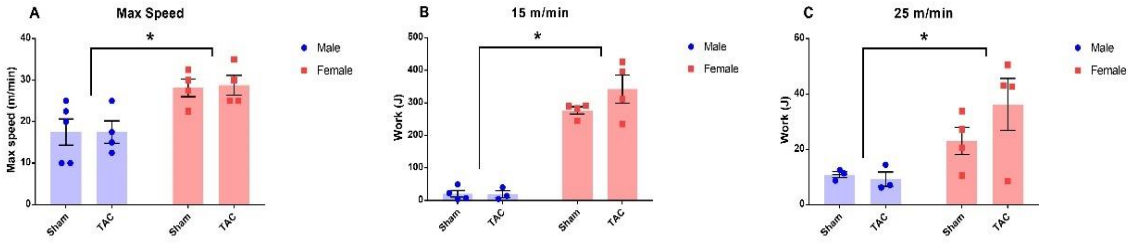

Figure 13. Treadmill running performance of TAC and sham rats. A maximal exercise test was used to assess A) max speed. Endurance was assessed as the work performed to exhaustion during B) slow (15 m/min) and C) fast (25 m/min) speeds. Main effect of sex *p<0.05.

4.3.3 Forelimb Grip Strength

Forelimb grip strength was assessed in 44-week-old TAC and sham rats. No significant difference in forelimb grip strength (p=0.327) was observed between TAC (1108.6±65.4 g) and sham control rats (1015.8±65.5 g). There was significant main effect of sex such that females had lower absolute grip strength (929.0±71.1 g vs. 1195.4±59.2 g; p=0.008) (Figure 14A) but greater grip strength relative to body mass (2.87±0.14 vs. 2.00±0.12; p<0.001) than males (Figure 14B).

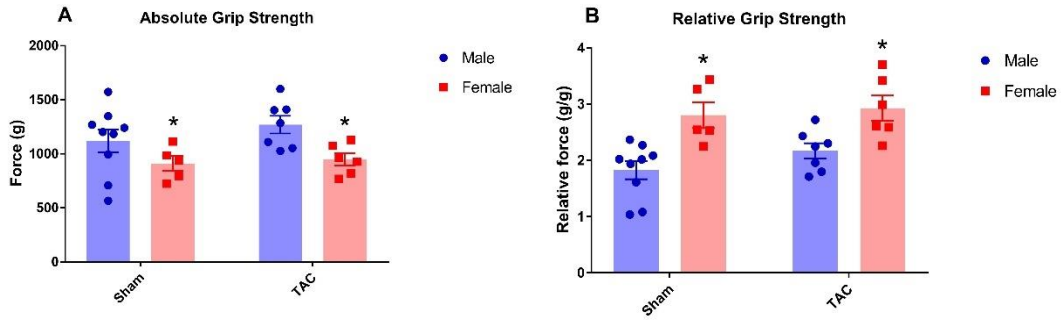

Figure 14. Forelimb grip strength performance of TAC and sham rats. A) Absolute grip strength and B) grip strength relative to body mass were assessed via the tension applied onto the grip strength meter using both forelimbs. Main effect of sex *p<0.05.

4.3.4 Isolated Skeletal Muscle Force Production and Fatiguability

Differences in soleus and EDL muscle mass were assessed to determine if TAC might induce skeletal muscle atrophy in male and female rats. A significant main effect of sex was observed in the average muscle mass of the soleus ($p<0.001$) and EDL ($p<0.001$) muscle. Female solei (0.153±0.011 g) were significantly smaller than the male solei (0.283±0.009 g). Similarly, female EDL (0.152±0.008 g) were significantly smaller than male EDL (0.253±0.006 g). No main effect of TAC was observed on the average muscle mass of soleus ($p=0.689$) or EDL ($p=0.544$) muscles. The average soleus mass in TAC rats was 0.221±0.010 g compared to 0.215±0.010 g in sham control rats. The average EDL mass in TAC rats was 0.205±0.007 g compared to 0.199±0.007 g in sham control rats. There was no TAC and sex interaction on average solei or EDL masses.

Force production from excised slow-twitch (soleus) and fast-twitch (EDL) skeletal muscle was assessed to determine if TAC surgery resulted in skeletal muscle weakness. Tension force was assessed during electrical stimulation from 1 Hz to 140 Hz. No significant main effect of TAC was observed for soleus absolute twitch force

(p=0.189) resulting from 1 Hz stimulation (Figure 15A), yet soleus twitch force relative to muscle mass tended to be lower (p=0.058) in TAC rats (834.7±86.3 mN/g) than sham control rats (1076.1±85.5 mN/g) (Figure 15C). There were main effects of sex on absolute and relative soleus twitch force. Absolute soleus twitch force from females (176.3±20.4 mN) were significantly lower (p=0.024) than males (240.5±17.0 mN) (Figure 15A). Relative soleus twitch force from females (1097.5±92.8 mN/g) were significantly greater (p=0.027) than males (813.3±77.3 mN/g) (Figure 15C).

In the EDL muscle, no main effect of TAC was observed for absolute (p=0.359; Figure 15B) or relative twitch force (p=0.975; Figure 15D). There was a main effect of sex in EDL such that males had a significantly (p=0.01) greater absolute EDL twitch force (318.5±23.0 mN) than females (217.4±27.7 mN; Figure 15B).

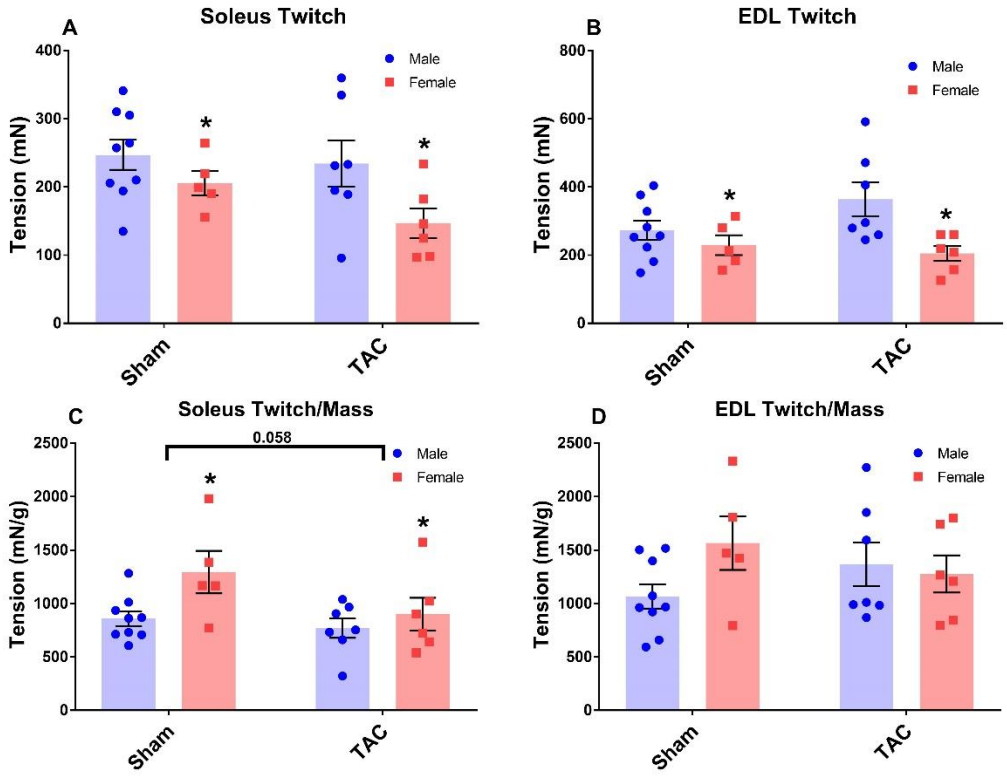

Figure 15. Ex vivo twitch force assessment in TAC and sham hindlimb muscles. Absolute A) soleus and B) EDL twitch force was measured on an electrically stimulated (1 Hz) muscle testing system. Relative C) soleus and D) EDL was calculated in relation to their respective muscle masses. Main effect of sex *p<0.05.

No main effect of TAC or interaction effect of TAC and sex on absolute soleus force was observed in frequencies from 10 to 140 Hz (Figure 16A). No main effect of TAC was observed on soleus force relative to muscle mass across all frequencies; however, there was a tendency toward a TAC and sex interaction effect ($0.05<p<0.06$) such that TAC females, but not males, appeared to have lower relative soleus force than sham control females from 20 Hz to 140 Hz (Figure 16C). Females had a significantly lower ($p<0.02$) absolute soleus force than males across frequencies of 40 Hz to 140Hz (Figure 16A). No interaction effect of sex and TAC was found for absolute ($p=0.395$) and relative soleus twitch force ($p=0.220$). Female relative soleus force was significantly greater than males during 20 Hz ($p=0.045$) and 120 Hz ($p=0.049$);

however, all other frequencies from 40 Hz to 140 Hz had relative soleus force that tended to be greater ($0.05<p<0.06$) in females than males (Figure 16C).

No main effect of TAC was observed for absolute (Figure 16B) or relative EDL force (Figure 16D) across all frequencies from 10 Hz to 140 Hz. No interaction effect of TAC and sex was observed on absolute or relative force across frequencies of 1 Hz through 140 Hz. There was a main effect of sex on the absolute forces of the EDL at the lower frequencies ranging from 10 Hz to 60 Hz ($p<0.05$; Figure 16B). Similarly, EDL from male rats exhibited significantly greater absolute force than female rats across frequencies of 20 Hz through 60 Hz (Figure 16B). When EDL force production was normalized to muscle mass, no significant differences were observed between male and female rats (Figure 16D).

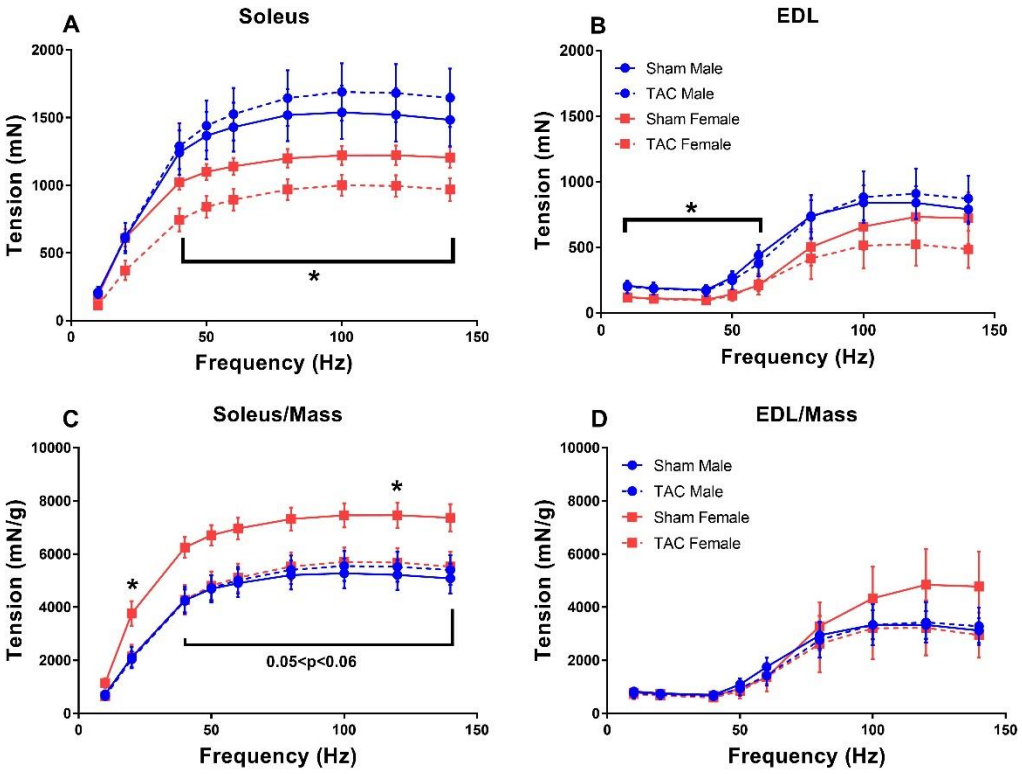

Figure 16. Ex vivo force-frequency assessments in TAC and sham hindlimb muscles. Male sham (blue solid), male TAC (blue dashed), female sham (red solid), female TAC (red dashed). Absolute A) soleus and B) EDL peak force was measured during electrical stimulation at frequencies of 10, 20, 40, 50, 60, 80, 100, 120, and 140 Hz. Relative C) soleus and D) EDL was calculated in relation to their respective muscle masses. Main effect of sex *p<0.05.

Fatiguability of the soleus and EDL muscle from TAC rats were determined from the time required to reach 50% of peak force production during continuous electrical stimulation at 100 Hz. No main effect of TAC or sex on time to fatigue was observed in the soleus or EDL muscle. Soleus from TAC rats took 24.4±2.7 s to reach fatigue compared to 23.6±2.7 s in sham control rats (p=0.851). EDL from TAC rats took 13.7±1.0 s to reach fatigue compared to 12.6±1.0 in sham control rats (p=0.472). Time to fatigue in female soleus muscle was 26.4±3.0 s compared to 21.6±2.5 s in males (p=0.224). Time to fatigue in female EDL muscle was 12.2±1.1 s compared to 14.2±0.9 s in males (p=0.179). No interaction effect of TAC and sex was seen on time to fatigue in either soleus (p=0.905) or EDL (p=0.116) muscle.

4.4 Discussion

This study provided phenotypic characteristics of the TAC rat for the heart, lungs, and forelimb and hindlimb skeletal muscles. The results demonstrate that TAC rats recapitulate an important physical characteristic of HFpEF, a thickening of the LV wall. Although not significant, the greater wet-to-dry lung ratio in TAC rats suggest that these animals may experience another HF symptom of pulmonary congestion. These findings suggest some evidence of cardiac remodeling is occurring in these aged TAC rats and that they may be experiencing a mild form of HF.

To our knowledge, this is the first study to investigate the exercise capacity and exertional tolerance in rats with TAC. Although a metabolic chamber was not available, exercise capacity and performance were evaluated via the maximal speed attained during a graded treadmill test and work performed during separate high and low speed treadmill endurance tests. TAC rats did not appear to run slower or exhibit lower endurance than their sham counterparts. Moreover, TAC rats were similar rates of noncompliance towards treadmill running than sham control rats. These results are somewhat surprising given that other rat models of HF, such as coronary ligation[229], ZSF1 obese[113], and Fischer 344[230] rats were reported to have reduced exercise capacity and exertional tolerance. Similarly, it has been reported that several mouse models of HFpEF, such as angiotensin II-infused[231], seipin knockout[232], and nephrectomized[233] mice, also exhibit exercise intolerance. However, abdominal aortic constricted rats have reported no deficits in VO_2 peak or exercise duration and time[234] suggesting that constriction of this conduit artery may not be sufficient to manifest deficits in running capacity. During the treadmill running tests in this study, only electrical shocks were

used to motivate the rats to run, which may have led to lower effort and attrition in this study. Future testing could potentially benefit from using treats as a positive reinforcement to encourage maximal effort and greater compliance[235].

Grip strength was evaluated to ascertain whether TAC was sufficient to impair forelimb motor function and performance. The placement of TAC causes a potential alteration in blood flow to the right and left forelimb. In partial support of this theory, it has been reported that TAC mice have increased peak blood velocity through the right carotid and decreased peak velocity through the left carotid artery[236]. However, it was also shown that the mean blood flow velocity through the two carotid arteries were similar, suggesting that adaptations could be occurring to maintain adequate peripheral and cerebral perfusion[236]. It is currently unknown if these same alterations in carotid blood flow occur in the TAC rat. In the present study, the right biceps mass of the female TAC rat was found to be greater than the left biceps mass. This could be evidence of muscular atrophy due to potential blood flow deficits through the left forelimb in female TAC rats. Future work should investigate whether alterations in forelimb blood flow are present in the TAC rat and, if so, lead to skeletal muscle atrophy. Regardless, the differences in left and right biceps mass in female TAC rats did not manifest in grip strength differences, although it should be noted that limb-specific grip strength was not measured. Grip strength does not appear to be a common measure of motor performance in murine models of HF. However, there are some reports that the severity of the disease is correlated with lower grip strength outcomes in patients with HFpEF[237,238]. It has also been separately reported that grip strength in patients with HFpEF were no different compared to healthy age-matched controls[239].

The findings from this study and ours suggest that grip strength testing may not be a reliable method to evaluate exertional intolerance in this model of HF.

Isolated skeletal muscle testing suggested that the intrinsic contractile function of the soleus, but not the EDL, was adversely affected by TAC, but only in females. The relative force production of the soleus muscle appeared to be lower in TAC females than sham females across most stimulation frequencies. In support of the findings of this study, soleus specific force of female salt-sensitive Dahl rats, a hypertension-based HF model, tended to be diminished[102] while ZSF1 obese rat, an obesity-based HF model, exhibited lower absolute and relative soleus force production than controls[240]. Moreover, HFpEF occurs more frequently in females[241–243], although HFpEF appears to be more severe in male patients[224]. Thus, TAC and HFpEF may lead to skeletal muscle weakening in a potentially sex specific manner, although it remains to be seen in future work if this skeletal muscle weakening correlates well with HFpEF survival outcomes in men and women.

This study is the first to evaluate treadmill running and grip strength performance in TAC rats as a means to determine if this animal model recapitulates the exertional intolerance seen in patients with HFpEF. Although TAC rats appear to show no functional deficits in treadmill running or grip strength, female TAC rats seem to exhibit diminished force production in their soleus muscle. The findings of this study suggest that HFpEF may preferentially weaken slow-twitch skeletal muscle force capacity in the female sex.

Chapter 5: Summary, Limitations, and Future Directions

5.1 Summary of Findings

In the first study, we were the first to investigate the combined effects of Na^+ and Ca^{2+} on mitochondrial function isolated from healthy male Sprague-Dawley rat hearts. Our findings indicated that Ca^{2+} activation of mitochondrial function was maintained despite failing levels of extramitochondrial Na^+. Indeed, mitochondrial respiration, forces (i.e., redox and membrane potential), and conductances (i.e., oxidative phosphorylation, ETC, and ATP synthase/ANT) were all improved with Ca^{2+} activation regardless of extramitochondrial Na^+ levels. This suggests that elevating Na^+ alone was insufficient to adversely impact cardiac mitochondrial function in the presence of Ca^{2+}, which occur normally during periods of increased work. Moreover, failing levels of extramitochondrial Na^+ alone or in combination with Ca^{2+} does not appear to elicit a greater increase in ROS production, which has been implicated in the development and progression of HF[162,244,245]. Therefore, from an isolated mitochondrial system perspective, elevated extramitochondrial Na^+ alone or in combination with Ca^{2+} is not sufficient to adversely impact cardiac mitochondrial function in healthy male rats.

Although Ca^{2+} activation of mitochondrial function was preserved regardless of extramitochondrial Na^+ levels, it was unknown if failing mitochondria were intrinsically impaired and would respond differently to Ca^{2+} in the presence of failing

levels of extramitochondrial Na^+. In the second study, we investigated the combined effects of Na^+ and Ca^{2+} on mitochondrial function from failing hearts in male rats. Our findings indicated that Ca^{2+} activation of maximal and submaximal mitochondrial respiration was preserved in failing mitochondria despite failing levels of extramitochondrial Na^+ levels and were comparable to healthy mitochondria. Furthermore, Ca^{2+} was able to activate failing mitochondria and bolster their redox potential, membrane potential, and conductance across all pathways of the oxidative phosphorylation pathway. However, and perhaps most importantly, failing mitochondria exhibited a more depolarized membrane potential than sham mitochondria, implicating a deficit in the proton gradient required for ATP production. We assessed proton leak and ROS production to explain the diminished membrane potential observed in failing mitochondria. A leak in the proton gradient could directly dissipate the membrane potential while a leak of electrons from the ETC as ROS could indirectly diminish the membrane potential by reducing the pumping of protons into the intermembrane space. Interestingly, failing mitochondria did not demonstrate a greater proton leak nor ROS production than healthy mitochondria; therefore, the cause of this diminished membrane potential in failing mitochondria remains a mystery.

The aforementioned findings suggest that mitochondria from failing hearts may produce ATP inefficiently, which in turn may hinder the heart's ability to respond to increasing workload demand during exertion. Indeed, exertional intolerance is a key characteristic of HFpEF, and it is unknown if rats with TAC recapitulate this exertional intolerance. Therefore, in the third study, we assessed exercise capacity to evaluate exertional tolerance in TAC rats. We also assessed *in vivo* and *ex vivo* force production

to evaluate if HF elicits exertional intolerance through skeletal muscle weakness. During a maximal exercise and two endurance treadmill tests, TAC rats exhibited similar maximal running speeds and work performed to sham control rats. Additionally, TAC rats demonstrated similar forelimb grip strength to sham control rats. Interestingly, during isolated skeletal muscle assessments, female, but not male, TAC solei appeared to exhibit lower relative force production than sham solei suggesting that HF may weaken slow-twitch muscle in a sex-specific manner. Although we were unable to observe exertional intolerance in our model of HF, we demonstrated that HF not only negatively affected cardiac mitochondria but also differentially weakens slow-twitch skeletal muscle according to sex. Collectively, these findings implicate a potential impairment to ATP production in HF, a greater need to assess mitochondrial function beyond simply mitochondrial respiration alone, and a need reevaluate our understanding of HF with sex as a biological variable.

5.2 Limitations & Future Directions

Although we demonstrated in the first and second studies that Ca^{2+} activation is preserved in healthy and failing mitochondria regardless of Na^{+} perturbations and that the Ca^{2+} required to elicit maximal mitochondrial respiration is no different in healthy or failing mitochondria, it is not known how much matrix Ca^{2+} was present within the healthy or failing mitochondria prior to Na^{+} incubation. The Na^{+} incubations were performed to extrude Ca^{2+} from the matrix to allow us to control for extramitochondrial Ca^{2+} levels. As seen in our Ca^{2+} dose response assays, differing amounts of extramitochondrial Ca^{2+} will elicit different responses of mitochondrial

respiration. Therefore, it is undetermined whether failing mitochondria demonstrate an inherent difference in mitochondrial matrix Ca^{2+} amount that might lead to differences in mitochondrial respiration compared to healthy mitochondria. However, one of the goals of this dissertation was to evaluate the capacity of mitochondrial function in healthy and failing mitochondria. Moreover, there is a potential alteration in mitochondrial matrix Ca^{2+} content during the transient rupture and resealing of mitochondrial membranes of the isolation process[246], which necessitated the need for Na^{+} incubation to control for possible mitochondrial matrix Ca^{2+} differences, inherent to the mitochondria or as a result of the isolation procedure.

Using isolated mitochondria allows for greater control of conditions and specific observation of responses; however, the procedure for isolation has been shown to alter mitochondrial morphology[246,247]. Mitochondrial structure appear in branching networks alongside sarcomeres in skeletal muscle[248–250] while mitochondria appear in aggregated columns of varying sizes in cardiomyocytes[251]. When compared to permeabilized skeletal myofibers, which are assumed to preserve the mitochondrial structure within the cell, isolated mitochondria exhibit more exaggerated mitochondrial responses such as greater mitochondrial respiration, mitochondrial permeability transition pore sensitivity, and ROS production[246,252]. Although isolation of mitochondria has been reported to exaggerate mitochondrial responses[246,252], isolated mitochondria still retain and provide an accurate depiction of the mitochondrial bioenergetics of its host. For example, aging rats exhibit diminished respiratory capacity compared to younger rats in both isolated mitochondria and permeabilized myofibers, albeit to a greater extent in isolated mitochondria[252]. Because isolated

mitochondria exhibit exaggerated mitochondrial responses, the lack of differences in mitochondrial respiration, redox potential, proton leak, and ROS production in our studies only further supports that failing levels of extramitochondrial Na^+ alone is not sufficient to adversely alter mitochondrial function in healthy or failing mitochondria.

Although the NCX_m and the MCU are the primary transporters that regulate mitochondrial response via the control of mitochondrial matrix Ca^{2+}, the NHX can also influence Na^+ movement and thereby complicates the mitochondrial Na^+ and Ca^{2+} interaction. Under extramitochondrial and physiological pH of 7.1, the NHX provides the primary Na^+ efflux pathway from the mitochondria and operates close to equilibrium in isolated mitochondria[128,139]. Because extramitochondrial Na^+ is elevated in HF, extrusion of Na^+ from the matrix via the NHX is unfavorable as the it must operate against the Na^+ gradient. Additionally, operation of the NHX returns protons back into the mitochondrial matrix and dissipates the membrane potential as a result. However, it was observed that proton leak was no greater in failing mitochondria than sham mitochondria suggesting that the activity of the NHX may not be different in HF. Future work assessing mitochondrial function and proton leak while using an NHX inhibitor, such a phloretin, cariporide, or benzamil[253–257], can help elucidate the impact of NHX on mitochondrial function in HF. Our findings indicate that failing mitochondria have diminished membrane potentials and inhibiting the activity of NHX would prevent the return of protons back into the mitochondrial matrix, and as such, prevent the dissipation of membrane potential. Interestingly, it has been suggested that SGLT2 inhibitors, one of the few pharmacological therapies that have demonstrated improvements in quality of life and reduced hospitalization in patients with HFpEF[48–

[50], may inhibit NHE to alleviate symptoms of HF, such as arrhythmias, ischemic and reperfusion injury, and myocardial edema[258,259]. SGLT2 inhibitors have also been suggested to inhibit NHX[260], an NHE isoform, which if true, may impart cardioprotective effects, in part, by preventing the depolarizing effects of proton influx via the NHX. A better understanding of the mechanistic interactions between the NCX, MCU, and the NHX may contribute toward the development of effective therapies to combat mitochondrial dysfunction in HF.

Although our HF model demonstrated deficits in mitochondrial membrane potential and exhibited evidence of concentric hypertrophy, we were unable to observe evidence of exertional intolerance. Importantly, our animal cohort exhibited extremely high rates of attrition that were no different between TAC and sham rats. This suggests that perhaps only employing a unpleasant stimulus may lead to avoidance behavior to either terminate the test early or fail to initiate any testing[261]. Moreover, the exercise tests require volitional participation and the use of electrical stimulation without a reward may not incentivize the animals to perform to their maximal capacity[235]. Therefore, future work reassessing the exertional intolerance in the TAC model of HF should employ positive and negative reinforcement training to incentivize maximal volitional performance to best observe these potential exercise deficits. Additionally, these exercise tests were performed without experimenter blinding and may introduce bias, despite having objective criteria for termination, to the results. However, any possible bias may not have had a great effect as the findings indicated that TAC rats did not exhibit lower performance, which would be expected out of a HF model, compared to sham controls.

Because the exercise and strength tests required volitional participation, *ex vivo* muscle assessments were performed to elucidate whether there were deficits in skeletal muscle force production that could limit exertional capacity. Interestingly, female, but not male, slow-twitch muscle exhibited lower force production with TAC than sham. This suggests that females may respond differently to pressure-overload induced HF than males. Importantly, the findings from the first and second study were only performed in male rats. Therefore, it begs the question if failing mitochondria from female rats also demonstrate the deficits in membrane potential as seen in male rats, and if so, to what degree. Specific female or male differences would lend support for the greater consideration of sex as an important biological variable for the development of HF therapies.

5.3 Conclusions

This dissertation research sought to examine the interaction of elevated extramitochondrial Na^+ and Ca^{2+} on mitochondrial function in both healthy and failing mitochondria as well as assess the exertional tolerance in a rat model of pressure overload induced HF. Our findings demonstrated that Ca^{2+} activation of mitochondrial function was preserved regardless of extramitochondrial Na^+ levels. Moreover, failing mitochondria exhibited diminished membrane potential despite having similar respiration rates to healthy mitochondria. Although exertional intolerance was not observed during the exercise tests employed, female, but not male, rats with TAC demonstrated lower slow-twitch muscle force production than their sham counterparts. The findings of this dissertation support the theory that mitochondrial dysfunction

could contribute to an energetic imbalance in the HF. Lastly, this research demonstrates a greater need to explore mitochondrial function beyond simply mitochondrial respiration as well as supports the need to investigate sex as an important biological variable in HF.

Bibliography

1. Benjamin EJ, Blaha MJ, Chiuve SE, et al. *Heart Disease and Stroke Statistics'2017 Update: A Report from the American Heart Association*. Vol 135.; 2017. doi:10.1161/CIR.0000000000000485
2. Benjamin EJ, Blaha MJ, Chiuve SE, et al. Heart Disease and Stroke Statistics—2017 Update: A Report From the American Heart Association. *Circulation*. 2017;135(10):e146-e603. doi:10.1161/CIR.0000000000000485
3. Heidenreich PA, Trogdon JG, Khavjou OA, et al. Forecasting the future of cardiovascular disease in the United States: A policy statement from the American Heart Association. *Circulation*. 2011;123(8):933-944. doi:10.1161/CIR.0b013e31820a55f5
4. Malik A, Brito D, Vaqar S, Lovely C. *Congestive Heart Failure*. StatPearls Publishing https://www.ncbi.nlm.nih.gov/books/NBK430873/.
5. Shah A, Gandhi D, Srivastava S, Shah KJ, Mansukhani R. Heart Failure: A Class Review of Pharmacotherapy. *Pharm Ther*. 2017;42(7):464. /pmc/articles/PMC5481297/. Accessed April 24, 2022.
6. Wintrich J, Kindermann I, Ukena C, et al. Therapeutic approaches in heart failure with preserved ejection fraction: past, present, and future. *Clin Res Cardiol*. 2020;109(9):1079-1098. doi:10.1007/S00392-020-01633-W/FIGURES/3
7. Owan TE, Hodge DO, Herges RM, Jacobsen SJ, Roger VL, Redfield MM. Trends in Prevalence and Outcome of Heart Failure with Preserved Ejection Fraction. *N Engl J Med*. 2006;355:251-260. file:///C:/Users/Sarah

Clancy/Desktop/PDFs/CURRENT PDFs/Owan (Redfield) 2006 Trends in Prevalence and Outcome of Heart failure with preserved ejection fraction.pdf.

8. Gerber Y, Weston SA, Redfield MM, et al. A contemporary appraisal of the heart failure epidemic in Olmsted County, Minnesota, 2000 to 2010. *JAMA Intern Med*. 2015;175(6):996-1004. doi:10.1001/JAMAINTERNMED.2015.0924

9. Tsao CW, Lyass A, Enserro D, et al. Temporal Trends in the Incidence of and Mortality Associated With Heart Failure With Preserved and Reduced Ejection Fraction. *JACC Hear Fail*. 2018;6(8):678-685. doi:10.1016/J.JCHF.2018.03.006

10. Shah AM, Claggett B, Loehr LR, et al. Heart Failure Stages Among Older Adults in the Community. *Circulation*. 2017;135:224-240. doi:10.1161/CIRCULATIONAHA.116.023361

11. Tromp J, MacDonald MR, Ting Tay W, et al. Heart failure with preserved ejection fraction in the young. *Circulation*. 2018;138(24):2763-2773. doi:10.1161/CIRCULATIONAHA.118.034720

12. Dunlay SM, Roger VL, Redfield MM. Epidemiology of heart failure with preserved ejection fraction. *Nat Rev Cardiol*. 2017;14(10):591-602. doi:10.1038/NRCARDIO.2017.65

13. Masoudi FA, Havranek EP, Smith G, et al. Gender, age, and heart failure with preserved left ventricular systolic function. *J Am Coll Cardiol*. 2003;41(2):217-223. doi:10.1016/S0735-1097(02)02696-7

14. Devereux RB, Roman MJ, Liu JE, et al. Congestive heart failure despite

normal left ventricular systolic function in a population-based sample: the Strong Heart Study. *Am J Cardiol*. 2000;86(10):1090-1096. doi:10.1016/S0002-9149(00)01165-6

15. Smith GL, Masoudi FA, Vaccarino V, Radford MJ, Krumholz HM. Outcomes in heart failure patients with preserved ejection fraction: mortality, readmission, and functional decline. *J Am Coll Cardiol*. 2003;41(9):1510-1518. doi:10.1016/S0735-1097(03)00185-2
16. Scantlebury DC, Borlaug BA. Why are women more likely than men to develop heart failure with preserved ejection fraction? *Curr Opin Cardiol*. 2011;26(6):562-568. doi:10.1097/HCO.0B013E32834B7FAF
17. Yancy CW, Lopatin M, Stevenson LW, De Marco T, Fonarow GC. Clinical presentation, management, and in-hospital outcomes of patients admitted with acute decompensated heart failure with preserved systolic function: a report from the Acute Decompensated Heart Failure National Registry (ADHERE) Database. *J Am Coll Cardiol*. 2006;47(1):76-84. doi:10.1016/J.JACC.2005.09.022
18. Kannel WB, Castelli WP, McNamara PM, McKee PA, Feinleib M. Role of blood pressure in the development of congestive heart failure. The Framingham study. *N Engl J Med*. 1972;287(16):781-787.
19. Ho KK, Pinsky JL, Kannel WB, Levy D. The epidemiology of heart failure: the Framingham Study. *J Am Coll Cardiol*. 1993;22(4 Suppl A):6A-13A. http://www.ncbi.nlm.nih.gov/pubmed/8376698.
20. Lee DS, Gona P, Vasan RS, et al. Relation of Disease Pathogenesis and Risk

Factors to Heart Failure With Preserved or Reduced Ejection Fraction Insights From the Framingham Heart Study of the National Heart , Lung , and Blood Institute. 2009:3070-3077. doi:10.1161/CIRCULATIONAHA.108.815944

21. Lam CSP, Donal E, Kraigher-krainer E, Vasan RS. Epidemiology and clinical course of heart failure with preserved ejection fraction. 2011:18-28. doi:10.1093/eurjhf/hfq121

22. Dewan P, Rørth R, Raparelli V, et al. Sex-Related Differences in Heart Failure With Preserved Ejection Fraction. *Circ Heart Fail*. 2019;12(12). doi:10.1161/CIRCHEARTFAILURE.119.006539

23. Yturralde RF, Gaasch WH. Diagnostic criteria for diastolic heart failure. *Prog Cardiovasc Dis*. 2005;47(5):314-319. doi:10.1016/J.PCAD.2005.02.007

24. Carlson KJ, Lee DCS, Goroll AH, Leahy M, Johnson RA. An analysis of physicians' reasons for prescribing long-term digitalis therapy in outpatients. *J Chronic Dis*. 1985;38(9):733-739. doi:10.1016/0021-9681(85)90115-8

25. Marantz PR, Tobin JN, Wassertheil-Smoller S, et al. The relationship between left ventricular systolic function and congestive heart failure diagnosed by clinical criteria. *Circulation*. 1988;77(3):607-612. doi:10.1161/01.CIR.77.3.607

26. Solomon SD, Rizkala AR, Lefkowitz MP, et al. Baseline Characteristics of Patients With Heart Failure and Preserved Ejection Fraction in the PARAGON-HF Trial. *Circ Heart Fail*. 2018;11(7). doi:10.1161/CIRCHEARTFAILURE.118.004962

27. Reddy YNV, Andersen MJ, Obokata M, et al. Arterial Stiffening With

Exercise in Patients With Heart Failure and Preserved Ejection Fraction. *J Am Coll Cardiol*. 2017;70(2):136-148. doi:10.1016/J.JACC.2017.05.029

28. Paulus WJ, Tschöpe C. A novel paradigm for heart failure with preserved ejection fraction: comorbidities drive myocardial dysfunction and remodeling through coronary microvascular endothelial inflammation. *J Am Coll Cardiol*. 2013;62(4):263-271. doi:10.1016/J.JACC.2013.02.092

29. Srivaratharajah K, Coutinho T, Dekemp R, et al. Reduced Myocardial Flow in Heart Failure Patients With Preserved Ejection Fraction. *Circ Heart Fail*. 2016;9(7). doi:10.1161/CIRCHEARTFAILURE.115.002562

30. Abudiab MM, Redfield MM, Melenovsky V, et al. Cardiac output response to exercise in relation to metabolic demand in heart failure with preserved ejection fraction. *Eur J Heart Fail*. 2013;15(7):776-785. doi:10.1093/eurjhf/hft026

31. Borlaug BA, Nishimura RA, Sorajja P, Lam CSP, Redfield MM. Exercise Hemodynamics Enhance Diagnosis of Early Heart Failure with Preserved Ejection Fraction. *Circ Hear Fail*. 2010;3(5):588-595. doi:10.1161/CIRCHEARTFAILURE.109.930701.Exercise

32. Borlaug BA, Kane GC, Melenovsky V, Olson TP. Abnormal right ventricular-pulmonary artery coupling with exercise in heart failure with preserved ejection fraction. *Eur Heart J*. 2016;37(43):3294-3302. doi:10.1093/EURHEARTJ/EHW241

33. Obokata M, Olson TP, Reddy YNV, Melenovsky V, Kane GC, Borlaug BA. Haemodynamics, dyspnoea, and pulmonary reserve in heart failure with

preserved ejection fraction. *Eur Heart J*. 2018;39(30):2810-2821. doi:10.1093/EURHEARTJ/EHY268

34. Reddy YNV, Olson TP, Obokata M, Melenovsky V, Borlaug BA. Hemodynamic Correlates and Diagnostic Role of Cardiopulmonary Exercise Testing in Heart Failure With Preserved Ejection Fraction. *JACC Heart Fail*. 2018;6(8):665-675. doi:10.1016/J.JCHF.2018.03.003

35. Dorfs S, Zeh W, Hochholzer W, et al. Pulmonary capillary wedge pressure during exercise and long-term mortality in patients with suspected heart failure with preserved ejection fraction. *Eur Heart J*. 2014;35(44):3103-3112. doi:10.1093/EURHEARTJ/EHU315

36. Reddy YNV, Carter RE, Obokata M, Redfield MM, Borlaug BA. A Simple, Evidence-Based Approach to Help Guide Diagnosis of Heart Failure With Preserved Ejection Fraction. *Circulation*. 2018;138(9):861-870. doi:10.1161/CIRCULATIONAHA.118.034646

37. Reddy YNV, Obokata M, Gersh BJ, Borlaug BA. High Prevalence of Occult Heart Failure With Preserved Ejection Fraction Among Patients With Atrial Fibrillation and Dyspnea. *Circulation*. 2018;137(5):534-535. doi:10.1161/CIRCULATIONAHA.117.030093

38. Nauta JF, Hummel YM, van der Meer P, Lam CSP, Voors AA, van Melle JP. Correlation with invasive left ventricular filling pressures and prognostic relevance of the echocardiographic diastolic parameters used in the 2016 ESC heart failure guidelines and in the 2016 ASE/EACVI recommendations: a systematic review in patients with heart failure with preserved ejection

fraction. *Eur J Heart Fail*. 2018;20(9):1303-1311. doi:10.1002/EJHF.1220

39. Obokata M, Borlaug BA. The strengths and limitations of E/e' in heart failure with preserved ejection fraction. *Eur J Heart Fail*. 2018;20(9):1312-1314. doi:10.1002/EJHF.1250

40. Tanase DM, Radu S, Al Shurbaji S, et al. Natriuretic Peptides in Heart Failure with Preserved Left Ventricular Ejection Fraction: From Molecular Evidences to Clinical Implications. *Int J Mol Sci*. 2019;20(11). doi:10.3390/IJMS20112629

41. Meijers WC, van der Velde AR, de Boer RA. Biomarkers in heart failure with preserved ejection fraction. *Netherlands Hear J*. 2016;24(4):252. doi:10.1007/S12471-016-0817-7

42. Grewal J, McKelvie RS, Persson H, et al. Usefulness of N-terminal pro-brain natriuretic Peptide and brain natriuretic peptide to predict cardiovascular outcomes in patients with heart failure and preserved left ventricular ejection fraction. *Am J Cardiol*. 2008;102(6):733-737. doi:10.1016/J.AMJCARD.2008.04.048

43. Dickstein K, Cohen-Solal A, Filippatos G, et al. ESC Guidelines for the diagnosis and treatment of acute and chronic heart failure 2008‡. *Eur J Heart Fail*. 2008;10(10):933-989. doi:10.1016/j.ejheart.2008.08.005

44. Faris RF, Flather M, Purcell H, Poole-Wilson PA, Coats AJS. Diuretics for heart failure. Faris RF, ed. *Cochrane database Syst Rev*. 2012;2(2):CD003838. doi:10.1002/14651858.CD003838.pub3

45. B P, MA P, SF A, et al. Spironolactone for heart failure with preserved ejection

fraction. *N Engl J Med*. 2014;370(15):10. doi:10.1056/NEJMOA1313731

46. de Denus S, O'Meara E, Desai AS, et al. Spironolactone Metabolites in TOPCAT - New Insights into Regional Variation. *N Engl J Med*. 2017;376(17):1690-1692. doi:10.1056/NEJMC1612601

47. Pfeffer MA, Claggett B, Assmann SF, et al. Regional variation in patients and outcomes in the Treatment of Preserved Cardiac Function Heart Failure With an Aldosterone Antagonist (TOPCAT) trial. *Circulation*. 2015;131(1):34-42. doi:10.1161/CIRCULATIONAHA.114.013255

48. Anker SD, Butler J, Filippatos G, et al. Empagliflozin in Heart Failure with a Preserved Ejection Fraction. *N Engl J Med*. 2021;385(16):1451-1461. doi:10.1056/NEJMOA2107038

49. Bhatt DL, Szarek M, Steg PG, et al. Sotagliflozin in Patients with Diabetes and Recent Worsening Heart Failure. *N Engl J Med*. 2021;384(2):117-128. doi:10.1056/NEJMOA2030183

50. Nassif ME, Windsor SL, Borlaug BA, et al. The SGLT2 inhibitor dapagliflozin in heart failure with preserved ejection fraction: a multicenter randomized trial. *Nat Med*. 2021;27(11):1954-1960. doi:10.1038/S41591-021-01536-X

51. Klingbeil AU, Schneider M, Martus P, Messerli FH, Schmieder RE. A meta-analysis of the effects of treatment on left ventricular mass in essential hypertension. *Am J Med*. 2003;115(1):41-46. doi:10.1016/S0002-9343(03)00158-X

52. Aronow WS, Kronzon I. Effect of enalapril on congestive heart failure treated with diuretics in elderly patients with prior myocardial infarction and normal

left ventricular ejection fraction. *Am J Cardiol*. 1993;71(7):602-604. doi:10.1016/0002-9149(93)90520-M

53. Massie BM, Carson PE, McMurray JJ, et al. Irbesartan in patients with heart failure and preserved ejection fraction. *N Engl J Med*. 2008;359(23):2456-2467. doi:10.1056/NEJMOA0805450

54. Cleland JGF, Bunting K V., Flather MD, et al. Beta-blockers for heart failure with reduced, mid-range, and preserved ejection fraction: an individual patient-level analysis of double-blind randomized trials. *Eur Heart J*. 2018;39(1):26-35. doi:10.1093/EURHEARTJ/EHX564

55. Ahmed A, Rich MW, Fleg JL, et al. Effects of digoxin on morbidity and mortality in diastolic heart failure: the ancillary digitalis investigation group trial. *Circulation*. 2006;114(5):397-403. doi:10.1161/CIRCULATIONAHA.106.628347

56. Redfield MM, Chen HH, Borlaug BA, et al. Effect of phosphodiesterase-5 inhibition on exercise capacity and clinical status in heart failure with preserved ejection fraction: a randomized clinical trial. *JAMA*. 2013;309(12):1268-1277. doi:10.1001/JAMA.2013.2024

57. Hoendermis ES, Liu LCY, Hummel YM, et al. Effects of sildenafil on invasive haemodynamics and exercise capacity in heart failure patients with preserved ejection fraction and pulmonary hypertension: a randomized controlled trial. *Eur Heart J*. 2015;36(38):2565-2573. doi:10.1093/EURHEARTJ/EHV336

58. Redfield MM, Anstrom KJ, Levine JA, et al. Isosorbide Mononitrate in Heart Failure with Preserved Ejection Fraction. *N Engl J Med*. 2015;373(24):2314-

2324. doi:10.1056/NEJMOA1510774

59. Abraham WT, Adamson PB, Bourge RC, et al. Wireless pulmonary artery haemodynamic monitoring in chronic heart failure: a randomised controlled trial. *Lancet (London, England)*. 2011;377(9766):658-666. doi:10.1016/S0140-6736(11)60101-3

60. Adamson PB, Abraham WT, Bourge RC, et al. Wireless pulmonary artery pressure monitoring guides management to reduce decompensation in heart failure with preserved ejection fraction. *Circ Heart Fail*. 2014;7(6):935-944. doi:10.1161/CIRCHEARTFAILURE.113.001229

61. Cleland JGF, Swedberg K, Follath F, et al. The EuroHeart Failure survey programme-- a survey on the quality of care among patients with heart failure in Europe. Part 1: patient characteristics and diagnosis. *Eur Heart J*. 2003;24(5):442-463. doi:10.1016/S0195-668X(02)00823-0

62. Bhatia RS, Tu J V., Lee DS, et al. Outcome of heart failure with preserved ejection fraction in a population-based study. *N Engl J Med*. 2006;355(3):260-269. doi:10.1056/NEJMOA051530

63. Owan TE, Redfield MM. Epidemiology of diastolic heart failure. *Prog Cardiovasc Dis*. 2005;47(5):320-332. doi:10.1016/J.PCAD.2005.02.010

64. Liao L, Jollis JG, Anstrom KJ, et al. Costs for heart failure with normal vs reduced ejection fraction. *Arch Intern Med*. 2006;166(1):112-118. doi:10.1001/ARCHINTE.166.1.112

65. Hillege HL, Nitsch D, Pfeffer MA, et al. Renal function as a predictor of outcome in a broad spectrum of patients with heart failure. *Circulation*.

2006;113(5):671-678. doi:10.1161/CIRCULATIONAHA.105.580506

66. Felker GM, Allen LA, Pocock SJ, et al. Red cell distribution width as a novel prognostic marker in heart failure: data from the CHARM Program and the Duke Databank. *J Am Coll Cardiol*. 2007;50(1):40-47. doi:10.1016/J.JACC.2007.02.067

67. Carson PE, Anand IS, Win S, et al. The Hospitalization Burden and Post-Hospitalization Mortality Risk in HeartFailure With Preserved EjectionFraction: Results From the I-PRESERVE Trial (Irbesartan in HeartFailureand Preserved Ejection Fraction). *JACC Hear Fail*. 2015;3(6):429-441. doi:10.1016/J.JCHF.2014.12.017/SUPPL_FILE/MMC1.PDF

68. Cauley E, Wang X, Dyavanapalli J, et al. Neurotransmission to parasympathetic cardiac vagal neurons in the brain stem is altered with left ventricular hypertrophy-induced heart failure. *Am J Physiol Circ Physiol*. 2015;309(8):H1281-H1287. doi:10.1152/ajpheart.00445.2015

69. Bishu K, Deswal A, Chen HH, et al. Biomarkers in acutely decompensated heart failure with preserved or reduced ejection fraction. *Am Heart J*. 2012;164(5). doi:10.1016/J.AHJ.2012.08.014

70. Farris SD, Moussavi-Harami F, Stempien-Otero A. Heart failure with preserved ejection fraction and skeletal muscle physiology. *Heart Fail Rev*. 2017;22(2):141-148. doi:10.1007/s10741-017-9603-x

71. Persson H, Lonn E, Edner M, et al. Diastolic dysfunction in heart failure with preserved systolic function: need for objective evidence:results from the

CHARM Echocardiographic Substudy-CHARMES. *J Am Coll Cardiol*. 2007;49(6):687-694. doi:10.1016/J.JACC.2006.08.062

72. Aurigemma GP, Gaasch WH. Clinical practice. Diastolic heart failure. *N Engl J Med*. 2004;351(11):1097-1105. doi:10.1056/NEJMCP022709

73. Aurigemma GP, Zile MR, Gaasch WH. Contractile behavior of the left ventricle in diastolic heart failure: with emphasis on regional systolic function. *Circulation*. 2006;113(2):296-304. doi:10.1161/CIRCULATIONAHA.104.481465

74. Baicu CF, Zile MR, Aurigemma GP, Gaasch WH. Left ventricular systolic performance, function, and contractility in patients with diastolic heart failure. *Circulation*. 2005;111(18):2306-2312. doi:10.1161/01.CIR.0000164273.57823.26

75. Borbély A, Van Der Velden J, Papp Z, et al. Cardiomyocyte stiffness in diastolic heart failure. *Circulation*. 2005;111(6):774-781. doi:10.1161/01.CIR.0000155257.33485.6D

76. Van Heerebeek L, Borbély A, Niessen HWM, et al. Myocardial structure and function differ in systolic and diastolic heart failure. *Circulation*. 2006;113(16):1966-1973. doi:10.1161/CIRCULATIONAHA.105.587519

77. Lam CSP, Roger VL, Rodeheffer RJ, et al. Cardiac structure and ventricular-vascular function in persons with heart failure and preserved ejection fraction from Olmsted County, Minnesota. *Circulation*. 2007;115(15):1982-1990. doi:10.1161/CIRCULATIONAHA.106.659763

78. Melenovsky V, Borlaug BA, Rosen B, et al. Cardiovascular features of heart

failure with preserved ejection fraction versus nonfailing hypertensive left ventricular hypertrophy in the urban Baltimore community: the role of atrial remodeling/dysfunction. *J Am Coll Cardiol*. 2007;49(2):198-207. doi:10.1016/J.JACC.2006.08.050

79. Kato S, Saito N, Kirigaya H, et al. Prognostic significance of quantitative assessment of focal myocardial fibrosis in patients with heart failure with preserved ejection fraction. *Int J Cardiol*. 2015;191:314-319.

80. Su MYM, Lin LY, Tseng YHE, et al. CMR-Verified Diffuse Myocardial Fibrosis Is Associated With Diastolic Dysfunction in HFpEF. *JACC Cardiovasc Imaging*. 2014;7(10):991-997. doi:10.1016/j.jcmg.2014.04.022

81. Mohammed SF, Hussain S, Mirzoyev SA, Edwards WD, Maleszewski JJ, Redfield MM. Coronary microvascular rarefaction and myocardial fibrosis in heart failure with preserved ejection fraction. *Circulation*. 2015;131(6):550-559. doi:10.1161/CIRCULATIONAHA.114.009625

82. Zile MR, Baicu CF, Gaasch WH. Diastolic heart failure--abnormalities in active relaxation and passive stiffness of the left ventricle. *N Engl J Med*. 2004;350(19):1953-1959. doi:10.1056/NEJMOA032566

83. Zile MR. Heart failure with preserved ejection fraction: is this diastolic heart failure? *J Am Coll Cardiol*. 2003;41(9):1519-1522. doi:10.1016/S0735-1097(03)00186-4

84. MR Z, WH G, JD C, et al. Heart failure with a normal ejection fraction: is measurement of diastolic function necessary to make the diagnosis of diastolic heart failure? *Circulation*. 2001;104(7):72-75. doi:10.1161/HC3201.094226

85. Borlaug BA, Olson TP, Lam CSP, et al. Global cardiovascular reserve dysfunction in heart failure with preserved ejection fraction. *J Am Coll Cardiol*. 2010;56(11):845-854. doi:10.1016/j.jacc.2010.03.077

86. Borlaug BA, Melenovsky V, Russell SD, et al. Impaired chronotropic and vasodilator reserves limit exercise capacity in patients with heart failure and a preserved ejection fraction. *Circulation*. 2006;114(20):2138-2147. doi:10.1161/CIRCULATIONAHA.106.632745

87. Borlaug BA. Mechanisms of exercise intolerance in heart failure with preserved ejection fraction. *Circ J*. 2014;78(1):20-32. doi:10.1253/CIRCJ.CJ-13-1103

88. Borlaug BA. The pathophysiology of heart failure with preserved ejection fraction. *Nat Rev Cardiol*. 2014;11(9):507-515. doi:10.1038/NRCARDIO.2014.83

89. Olson TP, Johnson BD, Borlaug BA. Impaired Pulmonary Diffusion in Heart Failure With Preserved Ejection Fraction. *JACC Heart Fail*. 2016;4(6):490-498. doi:10.1016/J.JCHF.2016.03.001

90. Mohammed SF, Hussain I, AbouEzzeddine OF, et al. Right ventricular function in heart failure with preserved ejection fraction: a community-based study. *Circulation*. 2014;130(25):2310-2320. doi:10.1161/CIRCULATIONAHA.113.008461

91. Cheitlin MD, Armstrong WF, Aurigemma GP, et al. ACC/AHA/ASE 2003 guideline update for the clinical application of echocardiography: Summary article. *J Am Soc Echocardiogr*. 2003;16(10):1091-1110. doi:10.1016/S0894-

7317(03)00685-0

92. Hasselberg NE, Haugaa KH, Sarvari SI, et al. Left ventricular global longitudinal strain is associated with exercise capacity in failing hearts with preserved and reduced ejection fraction. *Eur Heart J Cardiovasc Imaging*. 2015;16(2):217-224. doi:10.1093/ehjci/jeu277

93. Bajraktari G, Batalli A, Poniku A, et al. Left ventricular markers of global dyssynchrony predict limited exercise capacity in heart failure, but not in patients with preserved ejection fraction. *Cardiovasc Ultrasound*. 2012;10(1):1-8. doi:10.1186/1476-7120-10-36

94. Kosmala W, Rojek A, Przewlocka-Kosmala M, Mysiak A, Karolko B, Marwick TH. Contributions of nondiastolic factors to exercise intolerance in heart failure with preserved ejection fraction. *J Am Coll Cardiol*. 2016;67(6):659-670. doi:10.1016/j.jacc.2015.10.096

95. Bhella PS, Prasad A, Heinicke K, et al. Abnormal haemodynamic response to exercise in heart failure with preserved ejection fraction. *Eur J Heart Fail*. 2011;13(12):1296-1304. doi:10.1093/eurjhf/hfr133

96. Haykowsky MJ, Brubaker PH, John JM, Stewart KP, Morgan TM, Kitzman DW. Determinants of exercise intolerance in elderly heart failure patients with preserved ejection fraction. *J Am Coll Cardiol*. 2011;58(3):265-274. doi:10.1016/j.jacc.2011.02.055

97. Haykowsky M, Brubaker P, Kitzman D. Role of physical training in heart failure with preserved ejection fraction. *Curr Heart Fail Rep*. 2012;9(2):101-106. doi:10.1007/s11897-012-0087-7

98. Kitzman DW, Nicklas B, Kraus WE, et al. Skeletal muscle abnormalities and exercise intolerance in older patients with heart failure and preserved ejection fraction. *Am J Physiol - Hear Circ Physiol*. 2014;306(9):1364-1370. doi:10.1152/ajpheart.00004.2014

99. Kitzman DW, Brubaker PH, Morgan TM, Kathryn P, Little WC, Carolina N. Exercise Training in Older Patients with Heart Failure and Preserved Ejection Fraction: A Randomized, Controlled, Single-Blinded Trial. *Circ Hear Fail*. 2010;3(6):659-667. doi:10.1161/CIRCHEARTFAILURE.110.958785.Exercise

100. Haykowsky MJ, Kouba EJ, Brubaker PH, Nicklas BJ, Eggebeen J, Kitzman DW. Skeletal muscle composition and its relation to exercise intolerance in older patients with heart failure and preserved ejection fraction. *Am J Cardiol*. 2014;113(7):1211-1216. doi:10.1016/j.amjcard.2013.12.031

101. De Sousa E, Veksler V, Bigard X, Bing PM, Ventura-Clapier R. Heart failure affects mitochondrial but not myofibrillar intrinsic properties of skeletal muscle. *Circulation*. 2000;102(15):1847-1853. doi:10.1161/01.CIR.102.15.1847

102. Bowen TS, Rolim NPL, Fischer T, et al. Heart failure with preserved ejection fraction induces molecular, mitochondrial, histological, and functional alterations in rat respiratory and limb skeletal muscle. *Eur J Heart Fail*. 2015;17(3):263-272. doi:10.1002/ejhf.239

103. Bowen TS, Herz C, Rolim NPL, et al. Effects of Endurance Training on Detrimental Structural, Cellular, and Functional Alterations in Skeletal Muscles of Heart Failure With Preserved Ejection Fraction. *J Card Fail*.

2018;24(9):603-613. doi:10.1016/J.CARDFAIL.2018.08.009

104. Kehat I, Molkentin JD. Molecular pathways underlying cardiac remodeling during pathophysiologic stimulation. *Circulation*. 2010;122(25):2727-2735. doi:10.1161/CIRCULATIONAHA.110.942268

105. Redfield MM, Jacobsen SJ, Borlaug BA, Rodeheffer RJ, Kass DA. Age- and gender-related ventricular-vascular stiffening: A community-based study. *Circulation*. 2005;112(15):2254-2262. doi:10.1161/CIRCULATIONAHA.105.541078

106. JT W, JD W, PK W, et al. A Randomized Trial of Intensive versus Standard Blood-Pressure Control. *N Engl J Med*. 2015;373(22):2103-2116. doi:10.1056/NEJMOA1511939

107. Furberg CD, Wright JT, Davis BR, et al. Major outcomes in high-risk hypertensive patients randomized to angiotensin-converting enzyme inhibitor or calcium channel blocker vs diuretic: The Antihypertensive and Lipid-Lowering Treatment to Prevent Heart Attack Trial (ALLHAT). *JAMA*. 2002;288(23):2981-2997. doi:10.1001/JAMA.288.23.2981

108. Beckett NS, Peters R, Fletcher AE, et al. Treatment of hypertension in patients 80 years of age or older. *N Engl J Med*. 2008;358(18):1887-1898. doi:10.1056/NEJMOA0801369

109. Tam MC, Lee R, Cascino TM, Konerman MC, Hummel SL. Current Perspectives on Systemic Hypertension in Heart Failure with Preserved Ejection Fraction. *Curr Hypertens Rep*. 2017;19(2):12. doi:10.1007/S11906-017-0709-2

110. Conceição G, Heinonen I, Lourenço AP, Duncker DJ, Falcão-Pires I. Animal models of heart failure with preserved ejection fraction. *Netherlands Hear J*. 2016;24(4):275-286. doi:10.1007/s12471-016-0815-9

111. Overton JM, VanNess JM, Takata HJ. Effects of chronic exercise on blood pressure in Dahl salt-sensitive rats. *Am J Hypertens*. 1998;11(1 Pt 1):73-80. doi:10.1016/S0895-7061(97)00308-7

112. Fediuc S. Effect of voluntary wheel running on circadian corticosterone release and on HPA axis responsiveness to restraint stress in Sprague-Dawley rats. *J Appl Physiol*. 2006;100(6):1867-1875. doi:10.1152/japplphysiol.01416.2005

113. Leite S, Oliveira-Pinto J, Tavares-Silva M, et al. Echocardiography and invasive hemodynamics during stress testing for diagnosis of heart failure with preserved ejection fraction: An experimental study. *Am J Physiol - Hear Circ Physiol*. 2015;308(12):H1556-H1563. doi:10.1152/ajpheart.00076.2015

114. Miranda-Silva D, Wüst RCI, Conceição G, et al. Disturbed cardiac mitochondrial and cytosolic calcium handling in a metabolic risk-related rat model of heart failure with preserved ejection fraction. *Acta Physiol*. 2020;228(3):1-17. doi:10.1111/apha.13378

115. Leite S, Cerqueira RJ, Ibarrola J, et al. Arterial Remodeling and Dysfunction in the ZSF1 Rat Model of Heart Failure With Preserved Ejection Fraction. *Circ Hear Fail*. 2019;12(7). doi:10.1161/CIRCHEARTFAILURE.118.005596

116. Lygate C. Surgical models of hypertrophy and heart failure: Myocardial infarction and transverse aortic constriction. *Drug Discov Today Dis Model*. 2006;3(3):283-290. doi:10.1016/j.ddmod.2006.10.002

117. Harris DA, Das AM. Control of mitochondrial ATP synthesis in the heart. *Biochem J*. 1991;280(Pt 3):561. doi:10.1042/BJ2800561

118. Jennings RB, Reimer KA, Hill ML, Mayer SE. Total ischemia in dog hearts, in vitro. 1. Comparison of high energy phosphate production, utilization, and depletion, and of adenine nucleotide catabolism in total ischemia in vitro vs. severe ischemia in vivo. *Circ Res*. 1981;49(4):892-900. doi:10.1161/01.RES.49.4.892

119. Unitt JF, McCormack JG, Reid D, MacLachlan LK, England PJ. Direct evidence for a role of intramitochondrial Ca2+ in the regulation of oxidative phosphorylation in the stimulated rat heart. Studies using31P n.m.r. and ruthenium red. *Biochem J*. 1989;262(1):293-301. doi:10.1042/BJ2620293

120. Walweel K, Laver DR. Mechanisms of SR calcium release in healthy and failing human hearts. *Biophys Rev*. 2015;7(1):33. doi:10.1007/S12551-014-0152-4

121. Robert V, Gurlini P, Tosello V, et al. Beat-to-beat oscillations of mitochondrial [Ca2+] in cardiac cells. *EMBO J*. 2001;20(17):4998. doi:10.1093/EMBOJ/20.17.4998

122. Glancy B, Balaban RS. Role of mitochondrial Ca 2+ in the regulation of cellular energetics. *Biochemistry*. 2012;51(14):2959-2973. doi:10.1021/bi2018909

123. Willis WT, Jackman MR, Messer JI, Kuzmiak-Glancy S, Glancy B. A Simple Hydraulic Analog Model of Oxidative Phosphorylation. *Med Sci Sports Exerc*. 2016;48(6):990-1000. doi:10.1249/MSS.0000000000000884

124. Hansford RG. Physiological role of mitochondrial Ca2+ transport. *J Bioenerg Biomembr*. 1994;26(5):495-508. doi:10.1007/BF00762734

125. Jouaville LS, Pinton P, Bastianutto C, Rutter GA, Rizzuto R. Regulation of mitochondrial ATP synthesis by calcium: evidence for a long-term metabolic priming. *Proc Natl Acad Sci U S A*. 1999;96(24):13807-13812. doi:10.1073/PNAS.96.24.13807

126. Glancy B, Willis WT, Chess DJ, Balaban RS. Effect of calcium on the oxidative phosphorylation cascade in skeletal muscle mitochondria. *Biochemistry*. 2013;52(16):2793-2809. doi:10.1021/bi3015983

127. Territo PR, Mootha VK, French SA, Balaban RS. Ca2+ activation of heart mitochondrial oxidative phosphorylation: Role of the FoF1 ATPase. *Am J Physiol*. 2000;278:C423-C435.

128. Murphy E, Eisner DA. Regulation of Intracellular and Mitochondrial Sodium in Health and Disease. *Circ Res*. 2009;104(3):292-303. doi:10.1161/CIRCRESAHA.108.189050

129. Despa S, Islam MA, Weber CR, Pogwizd SM, Bers DM. Intracellular Na+ concentration is elevated in heart failure but Na/K pump function is unchanged. *Circulation*. 2002;105(21):2543-2548. doi:10.1161/01.CIR.0000016701.85760.97

130. Vaughan-Jones RD, Villafuerte FC, Swietach P, Yamamoto T, Rossini A, Spitzer KW. pH-Regulated Na(+) influx into the mammalian ventricular myocyte: the relative role of Na(+)-H(+) exchange and Na(+)-HCO Co-transport. *J Cardiovasc Electrophysiol*. 2006;17 Suppl 1(SUPPL. 1).

doi:10.1111/J.1540-8167.2006.00394.X

131. Takewaki S ichi, Kuro-o M, Hiroi Y, et al. Activation of Na+-H+ Antiporter (NHE-1) gene expression during growth, hypertrophy and proliferation of the rabbit cardiovascular system. *J Mol Cell Cardiol*. 1995;27(1):729-742. doi:10.1016/S0022-2828(08)80063-6

132. Baartscheer A, Schumacher CA, Borren MMGJ Van, Belterman CNW, Coronel R, Fiolet JWT. Increased Na+/H+-exchange activity is the cause of increased [Na+]i and underlies disturbed calcium handling in the rabbit pressure and volume overload heart failure model. *Cardiovasc Res*. 2003;57:1015-1024. file:///C:/Users/Sarah Clancy/AppData/Local/Mendeley Ltd./Mendeley Desktop/Downloaded/Baartscheer et al. - 2003 - Increased NaH-exchange activity is the cause of increased Nai and underlies disturbed calcium handling in th.pdf.

133. Barcenas-Ruiz L, Wier WG. Voltage dependence of intracellular [Ca2+]i transients in guinea pig ventricular myocytes. *Circ Res*. 1987;61(1):148-154. doi:10.1161/01.RES.61.1.148

134. Bers DM, Despa S, Bossuyt J. Regulation of Ca2+ and Na+ in normal and failing cardiac myocytes. *Ann N Y Acad Sci*. 2006;1080:165-177. http://www.ncbi.nlm.nih.gov/entrez/query.fcgi?cmd=Retrieve&db=PubMed&dopt=Citation&list_uids=17132783.

135. Sipido KR, Volders PGA, Vos MA, Verdonck F. Altered Na/Ca exchange activity in cardiac hypertrophy and heart failure: a new target for therapy? *Cardiovasc Res*. 2002;53(4):782-805. doi:10.1016/S0008-6363(01)00470-9

136. Hobai IA, O'Rourke B. Decreased sarcoplasmic reticulum calcium content is responsible for defective excitation-contraction coupling in canine heart failure. *Circulation*. 2001;103(11):1577-1584. doi:10.1161/01.CIR.103.11.1577

137. McDonough AA, Velotta JB, Schwinger RHG, Philipson KD, Farley RA. The cardiac sodium pump: structure and function. *Basic Res Cardiol*. 2002;97 Suppl 1(1):19-24. doi:10.1007/S003950200024

138. Murphy E, Imahashi KI, Steenbergen C. Bcl-2 regulation of mitochondrial energetics. *Trends Cardiovasc Med*. 2005;15(8):283-290. doi:10.1016/J.TCM.2005.09.002

139. Jung DW, Apel LM, Brierley GP. Transmembrane gradients of free Na+ in isolated heart mitochondria estimated using a fluorescent probe. *Am J Physiol*. 1992;262(4 Pt 1). doi:10.1152/AJPCELL.1992.262.4.C1047

140. Palty R, Silverman WF, Hershfinkel M, et al. NCLX is an essential component of mitochondrial Na+/Ca 2+ exchange. *Proc Natl Acad Sci U S A*. 2010;107(1):436-441. doi:10.1073/PNAS.0908099107/SUPPL_FILE/PNAS.200908099SI.PDF

141. Zhao Q, Wang S, Li Y, et al. The role of the mitochondrial calcium uniporter in cerebral ischemia/reperfusion injury in rats involves regulation of mitochondrial energy metabolism. *Mol Med Rep*. 2013;7(4):1073-1080. doi:10.3892/MMR.2013.1321

142. Crompton M, Ellinger H, Costi A. Inhibition by cyclosporin A of a Ca2+-dependent pore in heart mitochondria activated by inorganic phosphate and

oxidative stress. *Biochem J*. 1988;255(1):357. /pmc/articles/PMC1135230/?report=abstract. Accessed April 26, 2022.

143. Griffiths EJ, Halestrap AP. Further evidence that cyclosporin A protects mitochondria from calcium overload by inhibiting a matrix peptidyl-prolyl cis-trans isomerase. Implications for the immunosuppressive and toxic effects of cyclosporin. *Biochem J*. 1991;274 (Pt 2)(Pt 2):611-614. doi:10.1042/BJ2740611

144. Griffiths EJ, Halestrap AP. Protection by Cyclosporin A of ischemia/reperfusion-induced damage in isolated rat hearts. *J Mol Cell Cardiol*. 1993;25(12):1461-1469. doi:10.1006/JMCC.1993.1162

145. Liu T, Takimoto E, Dimaano VL, et al. Inhibiting mitochondrial Na+/Ca2+ exchange prevents sudden death in a Guinea pig model of heart failure. *Circ Res*. 2014;115(1):44-54. doi:10.1161/CIRCRESAHA.115.303062

146. Cox DA, Matlib MA. A role for the mitochondrial Na+-Ca2+ exchanger in the regulation of oxidative phosphorylation in isolated heart mitochondria. *J Biol Chem*. 1993;268(2):938-947. doi:10.1016/s0021-9258(18)54024-2

147. Baysal K, Jung DW, Gunter KK, Gunter TE, Brierley GP. Na(+)-dependent Ca2+ efflux mechanism of heart mitochondria is not a passive Ca2+/2Na+ exchanger. *Am J Physiol*. 1994;266(3 Pt 1). doi:10.1152/AJPCELL.1994.266.3.C800

148. Dash RK, Beard DA. Analysis of cardiac mitochondrial Na+-Ca2+ exchanger kinetics with a biophysical model of mitochondrial Ca2+ handling suggests a 3:1 stoichiometry. *J Physiol*. 2008;586(13):3267-3285.

doi:10.1113/JPHYSIOL.2008.151977

149. Liu T, O'Rourke B. Enhancing mitochondrial Ca2+ uptake in myocytes from failing hearts restores energy supply and demand matching. *Circ Res*. 2008;103(3):279-288. doi:10.1161/CIRCRESAHA.108.175919

150. Carafoli E. The interplay of mitochondria with calcium: an historical appraisal. *Cell Calcium*. 2012;52(1):1-8. doi:10.1016/J.CECA.2012.02.007

151. Allen DG, Blinks JR. Calcium transients in aequorin-injected frog cardiac muscle. *Nature*. 1978;273(5663):509-513. doi:10.1038/273509A0

152. Rizzuto R, Brini M, Murgia M, Pozzan T. Microdomains with high Ca2+ close to IP3-sensitive channels that are sensed by neighboring mitochondria. *Science*. 1993;262(5134):744-747. doi:10.1126/SCIENCE.8235595

153. Denton RM, McCormack JG. On the role of the calcium transport cycle in heart and other mammalian mitochondria. *FEBS Lett*. 1980;119(1):1-8. doi:10.1016/0014-5793(80)80986-0

154. Peoples JN, Saraf A, Ghazal N, Pham TT, Kwong JQ. Mitochondrial dysfunction and oxidative stress in heart disease. *Exp Mol Med 2019 5112*. 2019;51(12):1-13. doi:10.1038/s12276-019-0355-7

155. Kornfeld OS, Hwang S, Disatnik M-H, Chen C-H, Qvit N, Mochly-Rosen D. Mitochondrial Reactive Oxygen Species at the Heart of the Matter: New Therapeutic Approaches for Cardiovascular Diseases. *Circ Res*. 2015;116(11):1783-1799. doi:10.1161/CIRCRESAHA.116.305432

156. Korshunov SS, Skulachev VP, Starkov AA. High protonic potential actuates a mechanism of production of reactive oxygen species in mitochondria. *FEBS*

Lett. 1997;416(1):15-18. doi:10.1016/S0014-5793(97)01159-9

157. Kohlhaas M, Nickel AG, Maack C. Mitochondrial energetics and calcium coupling in the heart. *J Physiol*. 2017;595(12):3753-3763. doi:10.1113/JP273609

158. Balaban RS, Nemoto S, Finkel T. Mitochondria, oxidants, and aging. *Cell*. 2005;120(4):483-495.

159. Turrens JF. Mitochondrial formation of reactive oxygen species. *J Physiol*. 2003;552(Pt 2):335-344. doi:10.1113/JPHYSIOL.2003.049478

160. Moris D, Spartalis M, Spartalis E, et al. The role of reactive oxygen species in the pathophysiology of cardiovascular diseases and the clinical significance of myocardial redox. *Ann Transl Med*. 2017;5(16). doi:10.21037/ATM.2017.06.27

161. Starkov AA, Fiskum G. Regulation of brain mitochondrial H2O2 production by membrane potential and NAD(P)H redox state. *J Neurochem*. 2003;86:1101-1107.

162. Kohlhaas M, Liu T, Knopp A, et al. Elevated cytosolic Na+ increases mitochondrial formation of reactive oxygen species in failing cardiac myocytes. *Circulation*. 2010;121(14):1606-1613. doi:10.1161/CIRCULATIONAHA.109.914911

163. Armoundas AA, Hobai IA, Tomaselli GF, Winslow RL, O'Rourke B. Role of sodium-calcium exchanger in modulating the action potential of ventricular myocytes from normal and failing hearts. *Circ Res*. 2003;93(1):46-53. doi:10.1161/01.RES.0000080932.98903.D8

164. Weber CR, Piacentino V, Houser SR, Bers DM. Dynamic Regulation of Sodium/Calcium Exchange Function in Human Heart Failure. *Circulation*. 2003;108(18):2224-2229. doi:10.1161/01.CIR.0000095274.72486.94

165. Crompton M. The role of Ca2+ in the function and dysfunction of heart mitochondria. In: Langer G, ed. *Calcium and the Heart*. New York: Raven Press; 1990:167-198.

166. McCormack JG, Halestrap AP, Denton RM. Role of calcium ions in regulation of mammalian intramitochondrial metabolism. *Physiol Rev*. 1990;70(2):391-425. http://www.ncbi.nlm.nih.gov/pubmed/2157230.

167. Glancy B, Wt W, Dj C, Rs B. Effect of calcium on the oxidative phosphorylation cascade in skeletal muscle mitochondria . PubMed Commons. 2013. doi:10.1021/bi3015983.

168. Cox DA, Matlib MA. A Role for the Mitochondrial Na+ -Ca2+ Exchanger in the Regulation of Oxidative Phosphorylation in Isolated Heart Mitochondria. *J Biol Chem*. 1993;2:938-947. file:///C:/Users/Sarah Clancy/AppData/Local/Mendeley Ltd./Mendeley Desktop/Downloaded/Cox, Matlib - 1993 - A Role for the Mitochondrial Na -Ca2 Exchanger in the Regulation of Oxidative Phosphorylation in Isolated Heart Mit.pdf.

169. Maack C, Cortassa S, Aon MA, Ganesan AN, Liu T, O'Rourke B. Elevated cytosolic Na+ decreases mitochondrial Ca2+ uptake during excitation-contraction coupling and impairs energetic adaptation in cardiac myocytes. *Circ Res*. 2006;99(2):172-182. doi:10.1161/01.RES.0000232546.92777.05

170. Garnier A, Fortin D, Deloménie C, Momken I, Veksler V, Ventura-Clapier R.

Depressed mitochondrial transcription factors and oxidative capacity in rat failing cardiac and skeletal muscles. *J Physiol*. 2003;551(2):491-501. doi:10.1113/jphysiol.2003.045104

171. Molina AJA, Bharadwaj MS, Van Horn C, et al. Skeletal Muscle Mitochondrial Content, Oxidative Capacity, and Mfn2 Expression Are Reduced in Older Patients With Heart Failure and Preserved Ejection Fraction and Are Related to Exercise Intolerance. *JACC Hear Fail*. 2016;4(8):636-645. doi:10.1016/j.jchf.2016.03.011

172. Pohjoismäki JL, Goffart S. The role of mitochondria in cardiac development and protection. *Free Radic Biol Med*. 2017;106(November 2016):345-354. doi:10.1016/j.freeradbiomed.2017.02.032

173. Sharov VG, Todor A V, Silverman N, Goldstein S, Sabbah HN. Abnormal Mitochondrial Respiration in Failed Human Myocardium. 2000;2367:2361-2367. doi:10.1006/jmcc.2000.1266

174. Jarreta D, Orus J, Barrientos A, et al. Mitochondrial function in heart muscle from patients with idiopathic dilated cardiomyopathy. 2000;45:860-865.

175. Sebastiani M, Giordano C, Nediani C, et al. Induction of Mitochondrial Biogenesis Is a Maladaptive Mechanism in Mitochondrial Cardiomyopathies. *J Am Coll Cardiol*. 2007;50(14):1362-1369. doi:10.1016/j.jacc.2007.06.035

176. Rosca MG, Vazquez EJ, Kerner J, et al. Cardiac mitochondria in heart failure : decrease in respirasomes and oxidative phosphorylation. 2008:30-39. doi:10.1093/cvr/cvn184

177. Sun CK, Chang LT, Sheu JJ, et al. Losartan preserves integrity of cardiac gap

junctions and PGC-1α gene expression and prevents cellular apoptosis in remote area of left ventricular myocardium following acute myocardial infarction. *Int Heart J*. 2007;48(4):533-546. doi:10.1536/ihj.48.533

178. Rosca MG, Hoppel CL. Mitochondria in heart failure. *Cardiovasc Res*. 2010;88(1):40-50. doi:10.1093/cvr/cvq240

179. Piña IL, Apstein CS, Balady GJ, et al. Exercise and heart failure: A statement from the American Heart Association Committee on exercise, rehabilitation, and prevention. *Circulation*. 2003;107(8):1210-1225. http://www.ncbi.nlm.nih.gov/pubmed/12615804.

180. Braunwald E. Biomarkers in Heart Failure. *http://dx.doi.org/101056/NEJMra0800239*. 2009;358(20):2148-2159. doi:10.1056/NEJMRA0800239

181. Maack C, Cortassa S, Aon MA, Ganesan AN, Liu T, O'Rourke B. Elevated cytosolic Na+ decreases mitochondrial Ca2+ uptake during excitation-contraction coupling and impairs energetic adaptation in cardiac myocytes. *Circ Res*. 2006;99(2):172-182. doi:10.1161/01.RES.0000232546.92777.05

182. Schramm M, Klieber HG, Daut J. The energy expenditure of actomyosin-ATPase, Ca2+-ATPase and Na+,K+-ATPase in guinea-pig cardiac ventricular muscle. *J Physiol*. 1994;481.3:647-662. http://www.pubmedcentral.nih.gov/articlerender.fcgi?artid=1155908&tool=pmcentrez&rendertype=abstract.

183. Boyman L, Williams GSB, Khananshvili D, Sekler I, Lederer WJ. NCLX: The Mitochondrial Sodium Calcium Exchanger. *J Mol Cell Cardiol*. 2013;59:205.

doi:10.1016/J.YJMCC.2013.03.012

184. McMillin-Wood J, Wolkowicz PE, Chu A, Tate CA, Goldstone MA, Entman ML. Calcium uptake by two preparations of mitochondria from heart. *Biochim Biophys Acta*. 1980;591:251-265.

185. Hayat LH, Crompton M. Evidence for the existence of regulatory sites for Ca2+ on the Na+/Ca2 + carrier of cardiac mitochondria. *Biochem J*. 1982;202:509-518. file:///C:/Users/Sarah Clancy/AppData/Local/Mendeley Ltd./Mendeley Desktop/Downloaded/Hayat, Crompton - 1982 - Evidence for the existence of regulatory sites for Ca2 on the NaCa2 carrier of cardiac mitochondria.pdf.

186. Tsai CW, Wu Y, Pao PC, et al. Proteolytic control of the mitochondrial calcium uniporter complex. *Proc Natl Acad Sci U S A*. 2017;114(17):4388-4393. doi:10.1073/PNAS.1702938114/-/DCSUPPLEMENTAL

187. Vais H, Payne R, Paudel U, Li C, Foskett JK. Coupled transmembrane mechanisms control MCU-mediated mitochondrial Ca2+uptake. *Proc Natl Acad Sci U S A*. 2020;117(35):21731-21739. doi:10.1073/pnas.2005976117

188. Kostic M, Katoshevski T, Sekler I. Allosteric Regulation of NCLX by Mitochondrial Membrane Potential Links the Metabolic State and Ca2+ Signaling in Mitochondria. *Cell Rep*. 2018;25(12):3465-3475.e4. doi:10.1016/J.CELREP.2018.11.084/ATTACHMENT/8EC41F63-648F-49C2-A292-BF1F4955FF16/MMC1.PDF

189. Kim B, Matsuoka S. Cytoplasmic Na+-dependent modulation of mitochondrial Ca2+ via electrogenic mitochondrial Na+-Ca2+ exchange. *J Physiol*.

2008;586(6):1683-1697. doi:10.1113/JPHYSIOL.2007.148726

190. Pogwizd S, Sipido KR, Verdonck F, Bers DM. Intracellular Na in animal models of hypertrophy and heart failure: contractile function and arrhythmogenesis. *Cardiovasc Res*. 2003;57:887-896. doi:10.1016/S0008-6363(02)00735-6

191. Bers DM, Despa S. Cardiac Myocytes Ca2+ and Na+ Regulation in Normal and Failing Hearts. *J Pharmacol Sci*. 2006;100(5):315-322. doi:10.1254/jphs.CPJ06001X

192. Jelicks LA, Siri FM. Effects of hypertrophy and heart failure on [Na+] in pressure-overloaded guinea pig heart. *Am J Hypertens*. 1995;8:934-943. file:///C:/Users/Sarah Clancy/AppData/Local/Mendeley Ltd./Mendeley Desktop/Downloaded/Jelicks, Siri - 1995 - Effects of hypertrophy and heart failure on Na in pressure-overloaded guinea pig heart.pdf.

193. Babsky A, Doliba N, Doliba N, Savchenko A, Wehrli S, Osbakken M. Na+ Effects on Mitochondrial Respiration and Oxidative Phosphorylation in Diabetic Hearts. *Exp Biol Med*. 2001;226(6).

194. Crompton M, Moser R, Ludi H, Carafoli E. The Interrelations between the Transport of Sodium and Calcium in Mitochondria of Various Mammalian Tissues. *Eur J Biochem*. 1978;82(1):25-31. doi:10.1111/j.1432-1033.1978.tb11993.x

195. Crompton M, Kunzi M, Carafoli E. The Calcium-Induced and Sodium-Induced Effluxes of Calcium from Heart Mitochondria. *Eur J Biochem*. 1977;79:549-558.

196. Kuzmiak S, Glancy B, Sweazea KL, Willis WT. Mitochondrial function in sparrow pectoralis muscle. *J Exp Biol*. 2012;215(Pt 12):2039-2050. doi:10.1242/jeb.065094

197. Kuzmiak-Glancy S, Willis WT. Skeletal muscle fuel selection occurs at the mitochondrial level. *JEB*. 2014;217:1993-2003. file:///C:/Users/Sarah Clancy/AppData/Local/Mendeley Ltd./Mendeley Desktop/Downloaded/Kuzmiak-Glancy, Willis - 2014 - Skeletal muscle fuel selection occurs at the mitochondrial level.pdf.

198. Chess DJ, Billings E, Covian R, et al. Optical spectroscopy in turbid media using an integrating sphere: Mitochondrial chromophore analysis during metabolic transitions. *Anal Biochem*. 2013;439(2):161-172. doi:10.1016/J.AB.2013.04.017

199. Fisher-Wellman KH, Davidson MT, Narowski TM, Lin C Te, Koves TR, Muoio DM. Mitochondrial Diagnostics: A Multiplexed Assay Platform for Comprehensive Assessment of Mitochondrial Energy Fluxes. *Cell Rep*. 2018;24(13):3593-3606.e10. doi:10.1016/j.celrep.2018.08.091

200. Ying W. NAD+/NADH and NADP+/NADPH in cellular functions and cell death: regulation and biological consequences. *Antioxid Redox Signal*. 2007;10. doi:https://doi.org/10.1089/ars.2007.1672

201. Heart Physiology: From Cell to Circulation - Google Books. https://books.google.com/books?hl=en&lr=&id=CPVSg69CPMsC&oi=fnd&pg=PR9&ots=D2eDHhjbBX&sig=obY3K0p8kN9DeEBIxZMO5_VZo2c#v=onepage&q&f=false. Accessed April 24, 2022.

202. Cordero-Reyes AM, Gupte A a., Youker K a., et al. Freshly isolated mitochondria from failing human hearts exhibit preserved respiratory function. *J Mol Cell Cardiol*. 2014;68:98-105. doi:10.1016/j.yjmcc.2013.12.029

203. Balaban RS. Domestication of the cardiac mitochondrion for energy conversion. *J Mol Cell Cardiol*. 2009;46(6):832-841. doi:10.1016/J.YJMCC.2009.02.018

204. Balaban RS. The role of Ca(2+) signaling in the coordination of mitochondrial ATP production with cardiac work. *Biochim Biophys Acta*. 2009;1787(11):1334-1341. doi:10.1016/J.BBABIO.2009.05.011

205. Pogwizd SM, Qi M, Yuan W, Samarel AM, Bers DM. Upregulation of Na+/Ca2+ exchanger expression and-function in an arrhythmogenic rabbit model of heart failure. *Circ Res*. 1999;85(11):1009-1019. doi:10.1161/01.RES.85.11.1009

206. Kuzmiak S, Glancy B, Sweazea KL, Willis WT. Mitochondrial function in sparrow pectoralis muscle. *J Exp Biol*. 2012;215(12):2039-2050. doi:10.1242/jeb.065094

207. Chidsey CA, Weinbach EC, Pool PE, Morrow AG. Biochemical studies of energy production in the failing human heart. *J Clin Invest*. 1966;45(1):40. doi:10.1172/JCI105322

208. Rosca MG, Vazquez EJ, Kerner J, et al. Cardiac mitochondria in heart failure: decrease in respirasomes and oxidative phosphorylation. *Cardiovasc Res*. 2008;80(1):30-39. doi:10.1093/CVR/CVN184

209. Montgomery C, Hamilton N, Ianuzzo CD. Energy status of the rapidly paced

canine myocardium in congestive heart failure. *J Appl Physiol*. 1992;73(6):2363-2367. doi:10.1152/JAPPL.1992.73.6.2363

210. Mariappan N, Elks CM, Haque M, Francis J. Interaction of TNF with angiotensin II contributes to mitochondrial oxidative stress and cardiac damage in rats. *PLoS One*. 2012;7(10). doi:10.1371/JOURNAL.PONE.0046568

211. Doenst T, Pytel G, Schrepper A, et al. Decreased rates of substrate oxidation ex vivo predict the onset of heart failure and contractile dysfunction in rats with pressure overload. *Cardiovasc Res*. 2010;86(3):461-470. doi:10.1093/cvr/cvp414

212. Sharov VG, Todor A V., Imai M, Sabbah HN. Inhibition of Mitochondrial Permeability Transition Pores by Cyclosporine A Improves Cytochrome c Oxidase Function and Increases Rate of ATP Synthesis in Failing Cardiomyocytes. *Hear Fail Rev 2006 104*. 2006;10(4):305-310. doi:10.1007/S10741-005-7545-1

213. Sharov VG, Todor A, Khanal S, Imai M, Sabbah HN. Cyclosporine A attenuates mitochondrial permeability transition and improves mitochondrial respiratory function in cardiomyocytes isolated from dogs with heart failure. *J Mol Cell Cardiol*. 2007;42(1):150-158. doi:10.1016/J.YJMCC.2006.09.013

214. Smeir E, Leberer S, Blumrich A, et al. Depletion of cardiac cardiolipin synthase alters systolic and diastolic function. *iScience*. 2021;24(11). doi:10.1016/J.ISCI.2021.103314

215. Zhang H, Alder NN, Wang W, Szeto H, Marcinek DJ, Rabinovitch PS. Reduction of elevated proton leak rejuvenates mitochondria in the aged

cardiomyocyte. *Elife*. 2020;9:1-18. doi:10.7554/ELIFE.60827

216. Goh KY, Qu J, Hong H, et al. Editor's choice: Impaired mitochondrial network excitability in failing guinea-pig cardiomyocytes. *Cardiovasc Res*. 2016;109(1):79. doi:10.1093/CVR/CVV230

217. Ide T, Tsutsui H, Hayashidani S, et al. Mitochondrial DNA Damage and Dysfunction Associated With Oxidative Stress in Failing Hearts After Myocardial Infarction. *Circ Res*. 2001;88(5):529-535. doi:10.1161/01.RES.88.5.529

218. Ide T, Tsutsui H, Kinugawa S, et al. Mitochondrial Electron Transport Complex I Is a Potential Source of Oxygen Free Radicals in the Failing Myocardium. *Circ Res*. 1999;85(4):357-363. doi:10.1161/01.RES.85.4.357

219. Ide T, Tsutsui H, Kinugawa S, et al. Direct Evidence for Increased Hydroxyl Radicals Originating From Superoxide in the Failing Myocardium. *Circ Res*. 2000;86(2):152-157. doi:10.1161/01.RES.86.2.152

220. Finkel T, Holbrook NJ. Oxidants, oxidative stress and the biology of ageing. *Nature*. 2000;408(6809):239-247. doi:10.1038/35041687

221. Mutlu-Türkoğlu Ü, Ilhan E, Öztezcan S, Kuru A, Aykaç-Toker G, Uysal M. Age-related increases in plasma malondialdehyde and protein carbonyl levels and lymphocyte DNA damage in elderly subjects. *Clin Biochem*. 2003;36(5):397-400. doi:10.1016/S0009-9120(03)00035-3

222. Limberaki E, Eleftheriou PH, Vagdatli E, Kostoglou V, Petrou CH. Serum antioxidant status among young, middle-aged and elderly people before and after antioxidant rich diet. *Hippokratia*. 2012;16(2):118.

/pmc/articles/PMC3738412/. Accessed May 24, 2022.

223. Tembo MC, Holloway-Kew KL, Bortolasci CC, et al. Total Antioxidant Capacity and Frailty in Older Men. *Am J Mens Health*. 2020;14(5). doi:10.1177/1557988320946592

224. Sharma K, Mok Y, Kwak L, et al. Predictors of mortality by sex and race in heart failure with preserved ejection fraction: Aric community surveillance study. *J Am Heart Assoc*. 2020;9(19):14669. doi:10.1161/JAHA.119.014669

225. Dolgin M, Fox A, Gorlin R, Levin R. Diseases of the Heart and Blood Vessels. In: *Nomenclature and Criteria for Diagnosis*. ; 1994.

226. Valero-Muñoz M, Backman W, Sam F. Murine Models of Heart Failure With Preserved Ejection Fraction: A "Fishing Expedition." *JACC Basic to Transl Sci*. 2017;2(6):770-789. doi:10.1016/j.jacbts.2017.07.013

227. Richards DA, Bao W, Rambo M V., Burgert M, Jucker BM, Lenhard SC. Examining the relationship between exercise tolerance and isoproterenol-based cardiac reserve in murine models of heart failure. *J Appl Physiol*. 2013;114(9):1202-1210. doi:10.1152/japplphysiol.00556.2012

228. Wranne B, Woodson R. A graded treadmill test for rats: maximal work performance in normal and anemic animals. *J Appl Physiol*. 1973;34(5).

229. Craig JC, Colburn TD, Caldwell JT, et al. Central and peripheral factors mechanistically linked to exercise intolerance in heart failure with reduced ejection fraction. *Am J Physiol - Hear Circ Physiol*. 2019;317(2):H434-H444. doi:10.1152/ajpheart.00164.2019

230. Choi SY, Chang HJ, Choi S Il, et al. Long-Term Exercise Training Attenuates

Age-Related Diastolic Dysfunction: Association of Myocardial Collagen Cross-Linking. *J Korean Med Sci*. 2009;24(1):32-39. doi:10.3346/JKMS.2009.24.1.32

231. Kadoguchi T, Kinugawa S, Takada S, et al. Angiotensin II can directly induce mitochondrial dysfunction, decrease oxidative fibre number and induce atrophy in mouse hindlimb skeletal muscle. *Exp Physiol*. 2015;100(3):312-322. doi:10.1113/EXPPHYSIOL.2014.084095

232. Bai B, Yang W, Fu Y, et al. Seipin Knockout Mice Develop Heart Failure With Preserved Ejection Fraction. *JACC Basic to Transl Sci*. 2019;4(8):924-937. doi:10.1016/J.JACBTS.2019.07.008/SUPPL_FILE/MMC1.PDF

233. Tamaki M, Miyashita K, Wakino S, Mitsuishi M, Hayashi K, Itoh H. Chronic kidney disease reduces muscle mitochondria and exercise endurance and its exacerbation by dietary protein through inactivation of pyruvate dehydrogenase. *Kidney Int*. 2014;85(6):1330-1339. doi:10.1038/KI.2013.473

234. Morris GS, Fitzsimons DP, Baldwin KM, Barnard RJ. Exercise capacity of rats remains unaffected by a chronic pressure overload. *Cardiovasc Res*. 1993;27(7):1346-1349. doi:10.1093/CVR/27.7.1346

235. The UFAW Handbook on the Care and Management of Laboratory and Other ... - Google Books. https://books.google.com/books?hl=en&lr=&id=Wjr9u1AAht4C&oi=fnd&pg=PA206&dq=rodent+running+negative+or+positive+reinforcement+punishment+more+effective&ots=OVjYReCCTu&sig=dE7W60-3EYgGni3dTXTywoPnjPw. Accessed May 23, 2022.

236. Li YH, Reddy AK, Taffet GE, Michael LH, Entman ML, Hartley CJ. Doppler evaluation of peripheral vascular adaptations to transverse aortic banding in mice. *Ultrasound Med Biol*. 2003;29(9):1281-1289. doi:10.1016/S0301-5629(03)00986-4

237. Bekfani T, SICA-HF on behalf of, Valentova M, et al. Body composition in patients with diastolic dysfunction and heart failure with preserved ejection fraction and its effect on muscle strength and exercise capacity. *Eur Heart J*. 2013;34(suppl_1):P2441-P2441. doi:10.1093/EURHEARTJ/EHT308.P2441

238. Sparrow CT, Nassif ME, Andruska A, et al. Muscle Wasting in Patients with Heart Failure with Preserved Ejection Fraction and Its Impact on Muscle Strength and Functional Capacity during Exercise. *J Card Fail*. 2014;20(8):S3. doi:10.1016/J.CARDFAIL.2014.06.013

239. Sarma S, Howden E, Lawley J, Samels M, Levine BD. Central Command and the Regulation of Exercise Heart Rate Response in Heart Failure With Preserved Ejection Fraction. *Circulation*. 2021;143(8):783-789. doi:10.1161/CIRCULATIONAHA.120.048338

240. Schauer A, Draskowski R, Jannasch A, et al. ZSF1 rat as animal model for HFpEF: Development of reduced diastolic function and skeletal muscle dysfunction. *ESC Hear Fail*. 2020;7(5):2123-2134. doi:10.1002/EHF2.12915

241. Owan TE, Hodge DO, Herges RM, Jacobsen SJ, Roger VL, Redfield MM. Trends in Prevalence and Outcome of Heart Failure with Preserved Ejection Fraction. *http://dx.doi.org/101056/NEJMoa052256*. 2009;355(3):251-259. doi:10.1056/NEJMOA052256

242. Sotomi Y, Hikoso S, Nakatani D, et al. Sex differences in heart failure with preserved ejection fraction. *J Am Heart Assoc*. 2021;10(5):1-20. doi:10.1161/JAHA.120.018574

243. Tibrewala A, Yancy CW. Heart Failure with Preserved Ejection Fraction in Women. *Heart Fail Clin*. 2019;15(1):9-18. doi:10.1016/J.HFC.2018.08.002

244. Giordano FJ. Oxygen, oxidative stress, hypoxia, and heart failure. *J Clin Invest*. 2005;115(3):500-508. doi:10.1172/JCI24408

245. Nakamura R, Egashira K, Machida Y, et al. Probucol attenuates left ventricular dysfunction and remodeling in tachycardia-induced heart failure: roles of oxidative stress and inflammation. *Circulation*. 2002;106(3):362-367. doi:10.1161/01.CIR.0000021430.04195.51

246. Picard M, Taivassalo T, Gouspillou G, Hepple RT. Mitochondria: isolation, structure and function. *J Physiol*. 2011;589(Pt 18):4413. doi:10.1113/JPHYSIOL.2011.212712

247. Picard M, Taivassalo T, Ritchie D, et al. Mitochondrial Structure and Function Are Disrupted by Standard Isolation Methods. *PLoS One*. 2011;6(3):e18317. doi:10.1371/JOURNAL.PONE.0018317

248. Kirkwood SP, Munn EA, Brooks GA. Mitochondrial reticulum in limb skeletal muscle. *Am J Physiol*. 1986;251(3 Pt 1). doi:10.1152/AJPCELL.1986.251.3.C395

249. Ogata T, Yamasaki Y. Ultra-High-Resolution Scanning Electron Microscopic Studies on the Sarcoplasmic Reticulum and Mitochondria of the Rat Intrafusal Muscle Fibers- Part I. The Capsular Sleeve Region. *Arch Histol Cytol*.

1991;54(5):471-496. doi:10.1679/aohc.54.471

250. Bleck CKE, Kim Y, Willingham TB, Glancy B. Subcellular connectomic analyses of energy networks in striated muscle. *Nat Commun 2018 91*. 2018;9(1):1-11. doi:10.1038/s41467-018-07676-y

251. Ghosh S, Tran K, Delbridge LMD, et al. Insights on the impact of mitochondrial organisation on bioenergetics in high-resolution computational models of cardiac cell architecture. *PLOS Comput Biol*. 2018;14(12):e1006640. doi:10.1371/JOURNAL.PCBI.1006640

252. Picard M, Ritchie D, Wright KJ, et al. Mitochondrial functional impairment with aging is exaggerated in isolated mitochondria compared to permeabilized myofibers. *Aging Cell*. 2010;9(6):1032-1046. doi:10.1111/J.1474-9726.2010.00628.X

253. Deisl C, Simonin A, Anderegg M, et al. Sodium/hydrogen exchanger NHA2 is critical for insulin secretion in β-cells. *Proc Natl Acad Sci U S A*. 2013;110(24):10004-10009. doi:10.1073/PNAS.1220009110/-/DCSUPPLEMENTAL

254. Alvarez B V., Villa-Abrille MC. Mitochondrial NHE1: A newly identified target to prevent heart disease. *Front Physiol*. 2013;4 JUN:152. doi:10.3389/FPHYS.2013.00152/BIBTEX

255. Velázquez D, Průša V, Masrati G, Sychrova H, Ben-Tal N, Zimmermannova O. Allosteric links between the hydrophilic N-terminus and transmembrane core of human Na+/H+ antiporter NHA2. *bioRxiv*. April 2022:2022.04.26.489501. doi:10.1101/2022.04.26.489501

256. Numata M, Petrecca K, Lake N, Orlowski J. Identification of a Mitochondrial Na+/H+Exchanger. *J Biol Chem*. 1998;273(12):6951-6959. doi:10.1074/JBC.273.12.6951

257. Allen DG, Xiao XH. Role of the cardiac Na+/H+ exchanger during ischemia and reperfusion. *Cardiovasc Res*. 2003;57(4):934-941. doi:10.1016/S0008-6363(02)00836-2/2/57-4-934-FIG2.GIF

258. Arjun S, Bell RM. SGLT2 inhibitors: reviving the sodium-hydrogen exchanger cardioprotection hypothesis? *Cardiovasc Res*. 2019;115(10):1454-1456. doi:10.1093/CVR/CVZ105

259. Baartscheer A, Hardziyenka M, Schumacher CA, et al. Chronic inhibition of the Na+/H+ - exchanger causes regression of hypertrophy, heart failure, and ionic and electrophysiological remodelling. *Br J Pharmacol*. 2008;154(6):1266-1275. doi:10.1038/BJP.2008.189

260. De Pascalis A, Cianciolo G, Capelli I, Brunori G, La Manna G. SGLT2 inhibitors, sodium and off-target effects: an overview. *J Nephrol*. 2021;34(3):673-680. doi:10.1007/S40620-020-00845-7/FIGURES/2

261. Conner JD, Wolden-Hanson T, Quinn LS. Assessment of Murine Exercise Endurance Without the Use of a Shock Grid: An Alternative to Forced Exercise. *J Vis Exp*. 2014;90(90):51846. doi:10.3791/51846